博士学位論文

Molecular Biological Studies on the Spatial and Temporal Regulation of mRNA Translation during Early Zebrafish Development
（ゼブラフィッシュ初期発生における mRNA 翻訳の時空間制御機構の分子生物学的研究）

佐　藤　圭　祐

北海道大学大学院生命科学院

令和 7 年 3 月

CONTENTS

ACKNOWLEDGMENTS

I express my sincere appreciation to Associate Prof. Tomoya Kotani for his invaluable advice and encouragement throughout the course of this study. I am also grateful to Drs. Yoshinao Katsu, Atsushi Kimura, and Katsueki Ogiwara for helpful suggestions, discussion and practical guidance. I would also like to thank all members of the Kotani laboratory and laboratories of Reproductive and Developmental Biology for their cooperation and encouragement.

ABBREVIATIONS

BSA, bovine serum albumin

CHX, cycloheximide

Ddx3xb, DEAD-box helicase 3 X-linked b

DDW, double distilled water

DIG, digoxigenin

DMSO, dimethyl sulfoxide

DNA, deoxyribonucleic acid

DNP, dinitrophenyl

EB, extraction buffer

E. coli, escherichia coli

EWS, ewing sarcoma

EGTA, ethylene glycol tetraacetic acid

Emi2, early meiotic inhibitor 2

FITC, fluorescein isothiocyanate

FISH, fluorescence *in situ* hybridization

GFP, green fluorescent protein

His, histidine

hnRNP, heterogeneous nuclear ribonucleoprotein

HRP, horseradish peroxidase

Igf2bp3, insulin like growth factor 2 mRNA binding protein 3

IP, immunoprecipitation

mRNA, messenger RNA

miRNA, micro-RNA

MO, morpholino oligo nucleotide

ORF, open reading frame

PAT, poly(A) test

PCR, polymerase chain reaction

PBS, phosphate buffered saline

PFA, paraformaldehyde

Pou5f3, POU domain, class 5, transcription factor 3

Rbm14, RNA binding motif protein 14

RNA, ribonucleic acid

Rpl11, ribosomal protein l11

RT, room temperature

RT-PCR, reverse transcription-PCR

SDS, sodium dodecyl sulfate

SDS-PAGE, SDS-polyacrylamide gel electrophoresis

SIM, structured illumination microscopy

SSC, saline-sodium Citrate

Syncrip, synaptotagmin binding cytoplasmic RNA interacting protein

TBS, tris-buffered saline

UTR**,** untranslated region

UV, ultraviolet

WISH, whole mount *in situ* hybridization

GENERAL INTRODUCTION

Gene expression is regulated in a highly controlled manner at many levels, ranging from chromatin accessibility to post-translational modification of proteins. Translation is a process through which ribosomes decode the genetic information contained in mRNA into proteins. They directly connect various biological processes including the early development of animals. Because transcription is silent shortly before fertilization until zygotic genome activation at around the 1000-cell stage in zebrafish (Kane and Kimmel, 1993; Harvey et al., 2013), timely and spatially controlled protein synthesis after fertilization is achieved by translational activation of mRNAs which are stored in eggs. When and where these mRNAs are translated after fertilization are crucial for promoting early developmental processes. However, spatial and temporal translational regulation of individual mRNAs after fertilization remain largely unresolved.

Eukaryotic mRNA consists of the coding region that is translated into protein and the untranslated regions (UTRs) at their 5' and 3' ends. A cap structure is added to the 5' UTR, and poly(A) tail is added to the 3' UTR. Since 3' UTR is a repository of regulatory elements for mRNA stability, intracellular localization and translation, 3' UTRs are known to play crucial roles in various stages of the mRNA life cycle from the nucleus to cytoplasm (Mayr, 2018). RNA-binding proteins (RBPs) are typically thought of as proteins that bind RNA through one or multiple globular RNA-binding domains (RBDs) and change the fate, function or translational activity of the bound RNAs (Corley et al., 2020). Translation is thought to be regulated through interactions between cis-acting elements of mRNAs and trans-acting factors such as RBPs. They form a subcellular unit called RNA granule (Mitchell and Parker, 2014). RNA granules are membrane-less aggregates and observed in many types of eukaryotic cells

(Anderson and Kedersha, 2006; Hirose at al., 2022). Previous research showed that global changes in interactions between mRNA 3' UTR and RBP are important for the progression of early zebrafish development by UV mRNA-protein linking followed by mass spectrometry analysis (Despic et al., 2017). However, the function of individual RBPs binding to the 3' UTR of target mRNA in translational regulation is not well understood.

The temporal control of translation has been most extensively studied in oocyte maturation. Fully grown vertebrate oocytes accumulate thousands of translationally repressed mRNAs in the cytoplasm (Kotani et al., 2017; Winata and Korzh, 2018). Translational activation of the dormant mRNAs, including cyclin B1, has been shown to be regulated by the cytoplasmic polyadenylation of mRNAs, which is mediated by the cytoplasmic polyadenylation element (CPE) in their 3′ UTR (McGrew et al., 1989; Sheets et al., 1994). The CPE-binding protein 1 (CPEB1) functions in both repression and direction of the cytoplasmic polyadenylation (Barkoff et al., 2000; Tay et al., 2000). Although many dormant mRNAs contain CPEs, they are translated in different periods during oocyte maturation.

Cytoplasmic RNA granules such as stress granules and processing bodies (P-bodies) are assembled in many types of cells of organisms ranging from yeast to mammals. They are thought to function as sites of storage and/or degradation of translationally repressed mRNAs (Buchan and Parker, 2009; Ivanov et al., 2019). Our laboratory previously showed that zebrafish and mouse oocytes possess cytoplasmic RNA granules consisting of translationally repressed *cyclinB1*, *mos*, *mad2*, or *emi2* mRNA (Horie and Kotani, 2016; Kotani et al., 2013; Kotani et al., 2017; Takei et al., 2020; Takei et al., 2021). These granules disassembled at different timings after initiation of meiosis, coinciding with the translational activation of assembled mRNA. Collectively,

the results of most studies have suggested that cytoplasmic RNA granules function as sites of storage, cargo, transportation, and localization of dormant mRNAs within cells. However, the role of RNA granules in translational regulation after fertilization and during embryogenesis remains unclear.

Previous research showed that intrinsically disordered regions (IDRs) of RBPs drive intracellular liquid-liquid phase separation (LLPS) to form membrane-less organelles such as RNA granules (Kato et al., 2012; Wang et al., 2018). Intrinsically disordered regions account for only a few percent of the protein domains in prokaryotes, but in eukaryotes they account for more than 30% (Ward et al., 2004). IDRs are defined by an amino acid sequence that are not likely to form a stable three-dimensional structure (Holehouse and Kragelund, 2024). The amino acid composition within the IDR is biased, which leads to biases in physical properties such as charge and hydrophobicity, and the weak intermolecular interactions between IDRs induce LLPS. IDR is a key for understanding the function of RNA granules.

To elucidate the molecular mechanisms of translation after fertilization, I performed molecular and cellular analyses using zebrafish eggs and embryos. Because biochemical, cell biological, imaging and developmental approaches are available for zebrafish, this model animal provides a powerful experimental system to investigate the mechanisms of translational control during early development. In chapter I, I investigated the molecular mechanism of *pou5f3* mRNA translation. Since Pou5f3 is one of the key transcriptional factors in early zebrafish development (Lee et al., 2013), I set the analysis of *pou5f3* as a starting point for elucidating the translational control of individual mRNAs during early development. I showed that *pou5f3* mRNA formed granules in eggs and the mRNA translation was activated after fertilization while maintaining granular structures. These *pou5f3* "embryonic" RNA granules changed the

state from solid-like to liquid-like during early development and their changes into liquid droplets were linked to translational activation. In chapter II, I investigated the functions of two RBPs, Syncrip and Ewsr1b, which were thought to interact with *pou5f3* mRNA 3' UTR and to be involved in translational regulation of *pou5f3* mRNA. The functional analysis of Syncrip revealed that Syncrip repressed translation of *pou5f3* mRNA. The functional analysis of Ewsr1b showed that Ewsr1b was involved in translational activation of *pou5f3* mRNA and in post-translational regulation of Pou5f3 protein. Furthermore, I found that two transcript variants of *ewsr1b* that have different lengths of 3' UTR were expressed in zebrafish embryo, and the functions of Ewsr1b were regulated by the translational control of these variants.

Chapter I

Analysis of the spatial and temporal regulation of *pou5f3* mRNA translation in early zebrafish development

ABSTRACT

Fertilized eggs begin to translate mRNAs at appropriate times and placements to control development, but how the translation is regulated remains unclear. In zebrafish, Pou5f3 protein synthesis from *pou5f3* mRNA is important for various developmental processes, such as zygotic genome activation, ventral specification, and endoderm formation. Previous research in our laboratory showed that *pou5f3* mRNA formed granular structures in embryos and that these granules were maintained during early development. I showed that although the number of *pou5f3* granules remained constant, Pou5f3 protein was accumulated after fertilization. Intriguingly, translational sites of polysomes became colocalized with *pou5f3* RNA granules during the cleavage stage and, moreover, nascent Pou5f3 was shown to be synthesized in the granules. This functional change in translational activity of granules was accompanied by changes in the state of granules from solid-like to liquid-like. Dissolution of the granules reduced the rate of protein synthesis. These results suggest that RNA granules function as activation sites of translation after changing the physical properties.

INTRODUCTION

Protein syntheses at appropriate times and placements direct various biological processes in almost all organisms including the development of animals. Since transcription is silent shortly before fertilization until zygotic genome activation at around the 1000-cell stage in zebrafish and the 2-cell stage in mouse (Hamatani et al., 2004; Harvey et al., 2013; Kane and Kimmel, 1993), timely and spatially controlled protein synthesis after fertilization is achieved by translational activation of the dormant mRNAs stored in eggs. Comprehensive analyses of gene expression demonstrated that zebrafish and mouse eggs accumulate more than eight thousand mRNAs during oogenesis (Aanes et al., 2011; Chen et al., 2011; Harvey et al., 2013). Of these mRNAs, more than two thousand mRNAs are stored as a translationally repressed form (Chen et al., 2011; Luong et al., 2020; Winata and Korzh, 2018). Although when and where distinct mRNAs are translated remain largely unknown, the temporal and spatial control of global translation has been shown to be crucial for the proper promotion of developmental processes including zygotic genome activation, formation of embryonic axes, and cell differentiation (Aoki et al., 2003; Kumari et al., 2013; Sun et al., 2018; Wang and Latham, 1997; Winata and Korzh, 2018; Winata et al., 2018; Zaucker et al., 2020). However, the mechanisms by which translation of the dormant mRNAs is temporally and spatially controlled after fertilization remain largely unresolved.

pou5f3 mRNA encodes the Pou-domain transcription factor Pou5f3 (also known as Pou2/Pou5f1), a homolog of mammalian Oct4/Pou5f1 (Takeda et al., 1994), and was identified as one of the mRNAs extensively translated in polysomes of zebrafish embryos at the cleavage stage (Lee et al., 2013). Identification of *pou5f3* mutants in zebrafish that possess the maternally expressed *pou5f3* transcript but are deficient in

zygotically expressed *pou5f3* demonstrated that Pou5f3 is essential for brain morphogenesis (Belting et al., 2001). Moreover, generation and analyses of maternal and zygotic *pou5f3* mutants demonstrated that Pou5f3 is essential in early embryogenesis for differentiation of endoderm cells and specification of dorsal-ventral regions (Belting et al., 2001; Hauptmann et al., 2002; Lunde et al., 2004; Reim et al., 2004; Reim and Brand, 2006; Lachnit et al., 2008; Onichtchouk et al.,2010; Belting et al., 2011; Perez-Camps et al., 2016). In addition, Pou5f3 has been shown to trigger zygotic genome activation cooperatively with Nanog and Sox19b, which are also extensively translated in cleavage-stage embryos (Lee et al., 2013; Leichsenring et al., 2013). These studies demonstrated the importance of Pou5f3 synthesis from maternally stored mRNAs after fertilization for directing diverse developmental processes. However, how the translation of *pou5f3* mRNA is controlled during embryogenesis remains unknown. Since there are more than two thousand mRNAs that may be important for early development, I decided to focus on the analysis of *pou5f3* as a first step.

Previous research in our laboratory showed that *pou5f3* mRNA assembled into cytoplasmic RNA granules in a translationally repressed form in zebrafish oocytes. The granular structure of *pou5f3* mRNA persisted after fertilization until, at least, the gastrulation stage. In this study, I showed an increase in Pou5f3 protein during zebrafish development by generating anti-Pou5f3 antibodies. Visualization of translating ribosomes indicated that translation sites were not colocalized with *pou5f3* RNA granules in fertilized eggs but became colocalized in later stages. Moreover, nascent Pou5f3 polypeptides translated in polysomes were detected within *pou5f3* RNA granules. The state of granules was found to be changed after fertilization, and their change into liquid droplets was shown to be important for effective translation. These findings provide a model in which RNA granules, termed embryonic RNA granules, function as both

repression and activation sites of translation for directing developmental processes.

MATERIALS AND METHODS

Animals

All animal experiments in this study were approved by the Committee on Animal Experimentation, Hokkaido University. Zebrafish were maintained and bred under artificial lighting (14 hours in the light period, 10 hours in the dark period) at 28℃.

Production of antibodies

The DNA sequence encoding a part of zebrafish Pou5f3 (residues 1-122) was amplified by PCR using primer sets specific for the target region (*pou5f3*-ORF-f1; *pou5f3*-ORF-r1) and ligated into the pET21 vector with appropriate restriction enzymes (EcoRI and HindIII) to produce a His-tagged protein. The recombinant protein was expressed in *E. coli* (BL21) and purified by SDS-PAGE, followed by electroelution in Tris-glycine buffer without SDS. The purified protein was dialyzed against 1 mM HEPES (pH 7.5), lyophilized, and used for injection into two mice and one rabbit. The obtained antisera were affinity-purified with recombinant Pou5f3-His protein electroblotted onto a membrane (Immobilon; EMD Millipore, IPVH00010).

Immunoblotting

Zebrafish oocytes were manually isolated from ovaries in zebrafish Ringer's solution (116 mM NaCl, 2.9 mM KCl, 1.8 mM $CaCl_2$, and 5 mM HEPES; pH 7.2) using forceps under a dissecting microscope. Oocyte maturation was induced by treatment with 17α, 20β-dihydroxy-4-pregnen-3-one (1 μg/ml), a maturation-inducing hormone in fish. Embryos were obtained via natural spawning and staged according to the time post fertilization and morphological criteria. Oocytes and embryos were homogenized with an

equal volume of ice-cold extraction buffer [EB; 100 mM β-glycerophosphate, 20 mM HEPES, 15 mM $MgCl_2$, 5 mM EGTA, 1 mM dithiothreitol, 100 μM (*p*-amidinophenyl) methanesulfonyl fluoride, and leupeptin (3 μg/ml); pH 7.5]. After centrifugation at 15,000 rpm for 10 min at 4°C, the supernatant was collected and used as crude extracts. Crude extracts from oocytes and embryos at appropriate time points were separated by SDS-PAGE, blotted onto the Immobilon membrane, and probed with the mouse and rabbit anti-Pou5f3 antibody (this study; 1:100). Rpl11 was detected by immunoblotting crude extracts with rabbit anti-Rpl11 antibody (Abcam, ab79352; 1:2000). The antibodies were diluted in blocking buffer (4% skim-milk, 0.1% Tween 20 in TBS).

MO injection

The sequences of MOs (Gene Tools, LLC) are presented in Table 1. The Pou5f3-ATG-MO (ATG-MO) targets the start codon of *pou5f3* mRNA, whereas the Pou5f3-5mm-MO (5mm-MO) contains 5-nt mismatches. Using Femtojet (Eppendorf), 1nl of mixture containing 4 ng MOs was injected into fertilized eggs.

DIG-labelled *pou5f3* RNA probe synthesis

The DNA sequence encoding a full length of zebrafish *pou5f3* mRNA was amplified by PCR using primer sets specific for the target region (*pou5f3*-f1; *pou5f3*-3' UTR-r1) and ligated into the pGEM-T easy vector. The plasmid was linearized with appropriate restriction enzymes (antisense: Apa I, sense: Spe I) at 37˚C for 2 hours. Primer sequences are presented in Table 1. The RNA probes were synthesized using SP6 (antisense) or T7 (sense) RNA polymerase and DIG RNA Labeling Mix (total 20 μL reaction) at 37˚C for 2 hours. After purification, the RNA probes were diluted (50 ng/μL) with Hybridization Buffer (HYB+; 50% formamide, 5× SSC, 5 mg/ml torula RNA, 50 μg/ml heparin, and

0.1% Tween 20) and stored at -20˚C.

Whole mount *in situ* hybridization

Zebrafish embryos at appropriate time points were fixed with 4% PFA/PBS overnight at 4℃. The chorions of fixed embryos were removed with forceps in PBS and the embryos were treated with 100% methanol overnight at -20℃. After rehydration and washing with PBS containing 0.1% Tween 20, the embryos were incubated with hybridization buffer - (HYB-) (50% formamide, 5× SSC, 0.1% Tween 20) for 5 min at 55℃. The samples were then prehybridized with HYB+ (5 mg/ml torula RNA, 50 μg/ml heparin in HYB-) for 1 hour at 55℃ and hybridized with the antisense *pou5f3* RNA probe in HYB+ overnight at 65℃. The embryos were washed once with HYB- for 30 min at 65˚C, twice with 2× SSCT for 30 min at 65 ˚C, and twice with 0.2x SSCT for 30 min at 65˚C. The embryos were then incubated with Maleic acid buffer (150 mM Maleic acid, 100 mM NaCl; pH 7.5) containing 0.1% Tween 20 (MBST) for 5 min and with 2% Blocking reagent (Roche, 10447200) in MBST for 5 hours. The embryos were incubated with anti-DIG-HRP antibody (1:700 dilution) overnight at 4℃. After washing, embryos were incubated with tyramide-DNP (PerkinElmer, NEL746A) according to the manufacturer's instructions, followed by incubation with the anti-DNP-Alexa 488 antibody. After being mounted with VECTASHIELD Mounting Medium containing DAPI (Vector Laboratories, Inc, H1200), the samples were observed under the LSM 5 LIVE confocal microscope. The number of *pou5f3* granules was quantified using ImageJ software.

Poly(A) test (PAT) assay

RNA ligation–coupled RT-PCR was performed according to a previously reported

procedure (Kotani et al., 2013). 2 μg of total RNA extracted from pools of 50 zebrafish embryos was ligated to 0.4 μg of P1 anchor primer in a 10-μl reaction mixture using T4 RNA ligase (New England Biolabs) for 30 min at 37°C. The ligase was inactivated for 5 min at 92°C. Overall, 4.75 μl of the reaction mixture was used in a 10-μl reverse transcription reaction using FastGene Scriptase II cDNA synthesis kit with a P1' primer. Then, 2 μl of the cDNA was used for the first round of PCR in a total volume of 25 μl with a P1' primer and a primer specific for *pou5f3* (*pou5f3*-PAT-f1) for 20 cycles. Subsequently, 1 μl of the first-round PCR product was used for second-round PCR in a total volume of 25 μl with a P1' primer and a primer specific for *pou5f3* (*pou5f3*-PAT-f2) for 35 cycles. Primer sequences are presented in Table 1.

Ribopuromycylation

The chorions of embryos at 0, 3, and 6 hours post fertilization (hpf) were removed with forceps and the embryos were pretreated with 355 μM cycloheximide or 40 μM anisomycin for 15 min in E3 solution (5 mM NaCl, 0.17 mM KCl, 0.33 mM $CaCl_2$, 0.33 mM $MgSO_4$). The embryos were then incubated with 2 μM puromycin (Invitrogen, ant-pr-1) and 355 μM cycloheximide for 5 min in E3 solution. The embryos were incubated for 2 min with permeabilization buffer (50 mM Tris-HCl, 5 mM $MgCl_2$, 25 mM KCl, 0.015% digitonin; pH 6.8) containing 355 μM cycloheximide or 40 μM anisomycin, 1 mM dithiothreitol, 100 μM (p-amidinophenyl) methanesulfonyl fluoride, 3 μg/ml leupeptin, and 8 U/ml RNasin Plus RNase Inhibitor (Promega, N2611). The embryos were fixed with 4% PFA/PBS for 1 hour and then washed with PBS overnight at 4°C. The embryos were incubated for 15 min with Blocking buffer (0.05% saponin, 10 mM glycine in PBS) containing 5% newborn calf serum (Sigma, N4762). The embryos were then incubated with mouse anti-Puromycin antibody (Kerafast, 3RH11) (1:300 dilution in

Blocking buffer) for 1 hour. After washing, the embryos were incubated with anti-mouse IgG-Alexa 546 antibody (Molecular probes) (1:200 dilution in Blocking buffer) for 1 hour. After being mounted with VECTASHIELD Mounting Medium containing DAPI, the samples were observed under the LSM 5 LIVE confocal microscope. The number of translating sites was quantified using ImageJ software.

Simultaneous detection of translating sites and *pou5f3* RNA granules was performed as follows. After hybridization with the DIG-labeled antisense *pou5f3* RNA probe, the translating sites were detected with anti-Puromycin antibody as described above. After washing, the embryos were incubated with anti-DIG-HRP antibody, and the signals were detected as described in whole mount *in situ* hybridization. The samples were mounted and observed under the N-SIM super-resolution microscope (Nikon). The number and volume of individual signals and the number of colocalizations of both signals were analyzed by AIVIA software.

Puro-PLA

The proximity ligation assay (PLA) was performed according to the manufacturer's instructions (Sigma). Briefly, after ribopuromycylation stimulation and fixation with PFA/PBS, the embryos were incubated with Duolink Blocking Solution (Sigma) for 1 hour. The embryos were then incubated with mouse anti-Puromycin antibody (1:300) and affinity-purified rabbit anti-Pou5f3 antibody (1:50) diluted in Duolink Antibody Diluent (Sigma) for 90 min. After washing with Wash Buffer A (10 mM Tris-HCl, 0.15M NaCl, 0.05% Tween 20; pH 6.8), the embryos were incubated with Duolink PLA Probes (mouse PLUS and rabbit MINUS; Sigma, DUO092001 and DUO09002) diluted in Duolink Antibody Diluent (1:5) for 1 hour at 37°C. After washing with Wash Buffer A, the embryos were incubated with a Ligase (Sigma, DUO092013) diluted in Ligation Buffer

(1:40) (Sigma, DUO092013) for 30 min at 37℃. Amplification and binding of the FarRed-labeled probe were performed with a Polymerase (Sigma, DUO092013) diluted in Amplification Buffer (1:80) (Sigma, DUO092013) for 100 min at 37℃. Amplification was stopped by washing with Wash Buffer B (0.2 M Tris-HCl, 0.1 M NaCl; pH 6.8), followed by washing with PBS. After being mounted with VECTASHIELD Mounting Medium containing DAPI, the samples were observed under the LSM 5 LIVE confocal microscope. The number of translating sites was quantified using ImageJ software.

Simultaneous detection of *pou5f3*-translating sites and *pou5f3* RNA granules was performed as follows. After hybridization with the DIG-labeled antisense *pou5f3* RNA probe, the *pou5f3*-translating sites were detected as described above. After washing, the embryos were incubated with anti-DIG-HRP antibody, and the signals were detected as described in whole mount in situ hybridization. The samples were mounted and observed under the N-SIM super-resolution microscope. The number and volume of individual signals and the number of colocalizations of both signals were analyzed by AIVIA software.

Rpl11-Pou5f3 PLA

After fixation of embryos with 4% PFA/PBS and removal of the chorions, the PLA of Rpl11 and Pou5f3 proteins was performed with the rabbit anti-Rpl11 antibody (1:200 dilution) and mouse anti-Pou5f3 antibody (1:50 dilution) as described above. Simultaneous detection of Rpl11-Pou5f3 PLA sites and *pou5f3* RNA granules was performed as follows. After hybridization with the DIG-labeled antisense *pou5f3* RNA probe, Rpl11-Pou5f3 sites were detected. After washing, the embryos were incubated with anti-DIG-HRP antibody, and the signals were detected as described in whole mount *in situ* hybridization. The samples were mounted and observed under the N-SIM

super-resolution microscope. The number of individual signals and the number of colocalizations of both signals were analyzed by AIVIA software.

Immunofluorescence

Zebrafish embryos were fixed with 4% PFA/PBS overnight at 4˚C. After removing the chorions, the embryos were incubated with blocking buffer (4% skim-milk, 0.1% Tween 20 in TBS) for 1 hour. The embryos were then incubated with affinity-purified rabbit anti-Pou5f3 antibody (1:50 dilution) overnight at room temperature, followed by incubation with anti-rabbit IgG Alexa-546 antibody (1:200 dilution) for 1 hour. Fixation and immunofluorescence of mouse embryos were performed according to the procedure reported previously (Takada et al., 2020). After being mounted, the samples were observed under the LSM 5 LIVE confocal microscope.

Hexanediol treatment

To dissociate lipid droplets, embryos were treated with 1,6-hexanediol (10% w/v in E3 solution) for 20 min at 28℃. As a control, embryos were treated with 1,2,3-hexanetriol (10% w/v in E3 solution) for 20 min at 28℃. Hexanediol and hexanetriol were dissolved in E3 solution as stocks and diluted in E3 solution before use. After fixation with 4% PFA/PBS overnight at 4˚C, the embryos were analyzed by whole mount in situ hybridization. Puro-PLA was performed after hexanediol and hexanetriol treatment as described above.

Image analyses

Single confocal optical images (Fig. 2A, 3B, 3C, 5B, 7B, 8C, 8E, and 8H) were acquired by the confocal microscopes, LSM 5 LIVE and LSM 980, and analyzed by

Image J software. Z-stack images (Fig. 4A, 6A, and 7D) were acquired by the N-SIM super-resolution microscope and were analyzed by AIVIA software after reconstruction of 3D images with intensities in binary 16-bit type. The number and volume of signals of FISH, ribopuromycylation, immunofluorescence and PLA were quantified using the 3D Object Analysis recipe in AIVIA.

Statistical analyses

All the results were expressed as mean ± standard deviations. Statistical analysis comparing two samples was performed using Student's *t*-test, and that comparing multiple groups was performed using Tukey-Kramer test as indicated in the figure legends. Significance was defined as $p < 0.05$ ($****p < 0.0001$, $***p < 0.001$, $**p < 0.01$, $*p < 0.05$).

RESULTS

Zebrafish embryos accumulate Pou5f3 protein during the early stages of development

To confirm the synthesis of Pou5f3 protein during zebrafish oogenesis and embryogenesis, I produced antibodies against the N-terminus region of zebrafish Pou5f3 (amino acids 1-122; Fig. 1A). Both affinity-purified mouse antibodies recognized mainly a protein with a molecular mass of ~55 kDa and slightly recognized a protein with ~62 kDa in immunoblots (Fig. 1B and C). The intensities of both signals were significantly reduced when the translation of *pou5f3* mRNA was inhibited with the antisense MO (Fig. 1D and E), confirming that the antibodies specifically recognize Pou5f3. The protein with a higher molecular mass may be a phosphorylated form of Pou5f3 as shown in a previous study (Lippok et al., 2014). Time course analysis of oocytes and embryos showed that the amount of Pou5f3 was significantly increased from 0 to 6 hpf (Fig. 1C and F). No statistical significance was shown between immature and mature oocytes (Fig. 1F), and the amount of Pou5f3 was slightly increased between immature oocytes and fertilized eggs (0 hpf). These results suggest that *pou5f3* mRNA is actively translated after fertilization and that the activity increases during early development.

Visualization of translating sites during early development

I confirmed the previous results of our laboratory that the *pou5f3* mRNA formed granular structures in eggs and these granules persisted during early stages of development (Fig. 2A and B). In addition, I confirmed the elongation of poly(A) tails of *pou5f3* mRNA after fertilization by poly(A) test (PAT) assay (Fig. 2C). From these results, I speculated that the *pou5f3* mRNA is translated within granular structures. To

assess this possibility, I used the ribopuromycylation method (David et al., 2012) in embryos. This method is based on properties of the translational inhibitor puromycin, which enters into the ribosome A-site and is subsequently incorporated into the nascent chain C-terminus by the peptidyl-transferase activity of ribosomes (David et al., 2012). Incubation with cycloheximide (CHX) before and during puromycin stimulation stabilizes translating ribosomes on mRNAs and detection of puromycin with an anti-puromycin antibody visualizes the sites of mRNA translation (Fig. 3A) (David et al., 2012; Moissoglu et al., 2019). This method has been developed using cultured cells but has not been applied to vertebrate embryos.

Zebrafish embryos at the cleavage stage were stimulated with CHX and puromycin after preincubation with CHX and the embryos were then washed with PBS containing CHX to remove free puromycin. Many spots in the cytoplasm of embryonic cells stimulated with CHX and puromycin were detected by immunofluorescence with the anti-puromycin antibody, whereas no signal was detected in cells stimulated with CHX but not puromycin (Fig. 3B). In addition, the spots of puromycin were significantly reduced when embryos were stimulated with puromycin after preincubation with anisomycin, which also stabilizes polysomes but prevents puromycylation by entering into the ribosome A-site and interfering with the peptidyl-transferase activity (David et al., 2012), confirming that the signals indeed show the actively translating polysomes (Fig. 3B). Time course analysis of ribopuromycylation showed that the numbers of translation sites were similar in embryos at 0, 3 and 6 hpf (Fig. 3C and D). Intriguingly, however, the sizes of translation sites were increased in embryos at 3 and 6 hpf (Fig. 3E). Although these results are basically consistent with the results obtained using *Xenopus* embryonic extracts, in which the percentage of ribosomes in polysome fractions increased after fertilization (Woodland, 1974), my observations show an increase in the

level of translational activity during early development at the subcellular level.

Translating sites in embryos become colocalized with *pou5f3* RNA granules during early development

I then examined the relationship between *pou5f3* RNA granules and translation sites in embryos by super-resolution microscopy (structured illumination microscopy, SIM) with z-stack imaging, which allows a better resolution (<120 nm) than that of conventional confocal microscopy. In this experiment, I focused on the differences between 0 and 3 hpf, since Pou5f3 appeared to be significantly accumulated between 0 to 3 hpf (Fig. 1C and F). Three-dimensional (3D) images of SIM showed that *pou5f3* RNA granules rarely colocalized with translating sites of polysomes in embryos at 0 hpf, whereas they became colocalized with the translating sites in embryos at 3 hpf (Fig. 4A). Quantitative analyses of 3D images showed that the number of *pou5f3* RNA granules and the number of translation sites were not changed in embryos at 0 and 3 hpf (Fig. 4A and B). In contrast, the number of *pou5f3* RNA granules colocalizing with translating sites became increased in embryos at 3 hpf (722 ± 143 granules; average of 18.0% of total granules) compared with the number in embryos at 0 hpf (288 ± 91.6 granules; average of 6.9% of total granules) (Fig. 4C). These results demonstrate that *pou5f3* mRNA is translationally dormant in fertilized eggs and becomes selectively translated during the cleavage stage within granules.

Visualization of *pou5f3*-translating sites during early development

To more directly assess the translational activation of *pou5f3* mRNA within granules, I performed puromycylation followed by a proximity ligation assay (Puro-PLA) (tom Dieck et al., 2015) in embryos. Nascent Pou5f3 protein synthesized in polysomes can be

visualized by Puro-PLA, since, only when the anti-puromycin and anti-Pou5f3 antibodies are in proximity (<40 nm), linker oligonucleotides fused with secondary antibodies make a circle by a ligase, which is amplified and is finally detected with fluorescently labeled probes (Fig. 5A). Antibodies recognizing the N-terminal, but not C-terminal, region of proteins allow detection of translating sites with high sensitivity (tom Dieck et al., 2015). For Puro-PLA, I produced rabbit antibody against the N-terminus region (amino acids 1-122) of zebrafish Pou5f3. The affinity-purified rabbit antibody recognized a protein with a molecular mass of ~55 kDa, a protein with ~62 kDa and proteins with ~72kDa in immunoblots (Fig. 5B). Proteins around 72kDa, which were not detected when using the mouse antibodies (Fig. 1B), were clearly detected. Proteins around 72 kDa are also considered to be the Pou5f3 proteins that have been modified as phosphorylation. I believe that there are two main causes in the difference of detection between mouse and rabbit antibody. First is the improved detection due to the use of rabbit antibody and second is the difference of SDS-PAGE gels due to the new acrylamide.

I stimulated zebrafish embryos with puromycin in a way similar to ribopuromycylation. After fixation, the embryos were incubated with mouse anti-puromycin antibody and rabbit anti-Pou5f3 N-terminus antibody followed by incubation with the secondary antibodies. The sites of proximity ligation were labeled with fluorescence probes. Confocal images of Puro-PLA showed many spots in the cytoplasm of embryonic cells at 3 hpf and a few spots in the blastdiscs of fertilized eggs (Fig. 5C and D). No spot was detected when the embryos were stimulated with CHX but not puromycin or when the puromycin-stimulated embryos were incubated with the secondary antibodies but not with the primary antibodies (Fig. 5C and D). The significant increase in the number of *pou5f3*-translating sites from 0 to 3 hpf (Fig. 5C and D) is consistent with the results of immunoblots (Fig. 1C and F).

Embryos start to translate *pou5f3* mRNAs at the sites of granules, termed embryonic RNA granules, during the mitotic cleavage stage

The *pou5f3*-translating sites and *pou5f3* RNA granules were simultaneously detected by Puro-PLA followed by FISH. Three-dimensional images of SIM showed that only a few *pou5f3* RNA granules were overlapped with *pou5f3*-translating sites in fertilized eggs (Fig. 6A and B), whereas the number of *pou5f3* RNA granules overlapped with *pou5f3*-translating sites was increased in embryos at 3 hpf (Fig. 6A and B). Conformation analysis between the *pou5f3*-RNA granules, which was detected with the full-length RNA probe, and *pou5f3*-translating sites showed that both signals were partially overlapped and exhibited a direction from RNA granules to translating sites (Fig. 6C). These observations suggest the organization of highly ordered structures in the complexes of RNA granules and polysomes, in which coding regions of mRNAs are aligned at the one side of granules and translating ribosomes assemble there, extending synthesized Pou5f3 peptides into the opposite direction. I further assessed the translational activation of *pou5f3* mRNA within granules by simultaneously detecting one of the ribosomal proteins, Rpl11 with Pou5f3. I performed PLA using anti-Rpl11 rabbit antibody and anti-Pou5f3 mouse antibody (Fig. 7A). Rpl11-Pou5f3 PLA detected few spots in embryos at 0 hpf and many spots at 3 hpf (Fig. 7B and C). Simultaneous detection of Rpl11-Pou5f3 PLA with *pou5f3* mRNA demonstrated that nascent Pou5f3 peptides synthesized in ribosomes were found within *pou5f3* RNA granules with a direction from RNA granules to Rpl11-Pou5f3 PLA sites (Fig. 7D). The number of Rpl11-Pou5f3 PLA sites colocalized with *pou5f3* RNA granules was significantly increased in embryos at 3 hpf (Fig. 7E). Altogether, my results demonstrate that *pou5f3* mRNA assembles into granular structures that are translationally dormant in fertilized eggs and are translationally activated through persisting granular structures from the cleavage stage. I termed this

type of granule “embryonic RNA granule”.

The state of *pou5f3* RNA granules is changed during early development

In the quantitative analysis of *pou5f3* RNA granules, I noticed that the volume of granules increased after fertilization (Fig. 8A and B). I speculated that this change was caused by a change in the phase of granules from solid-like to liquid-like, since the RNA-binding protein Pumilio1 changes its phase from solid-like to liquid-like prior to translational activation of target mRNAs (Takei et al., 2020). To address the molecular nature of temporal control of mRNA translation in embryonic RNA granules, I analyzed the phase of granules in embryos at 0 and 3 hpf. Cytoplasmic granules such as P-granules in *C. elegance* embryos and stress granules in many types of cells have been shown to form liquid droplets, which are generated by liquid-liquid phase separation (Shin and Brangwynne, 2017). These droplets are important for concentrating certain molecules and facilitating spatial and temporal regulation of cellular functions. Treatment of cells with 1,6-hexanediol (hexanediol) dissociates these liquid droplets but does not affect assemblies in a solid-like state (Kroschwald et al., 2015; Updike et al., 2011). I treated zebrafish embryos with hexanediol at 0 and 3 hpf for 20 min and fixed them. As a control, embryos were treated with hexanetriol, a less effective chemical (Updike et al., 2011). FISH analysis showed that neither hexanediol nor hexanetriol affected the assembly of *pou5f3* RNA granules at 0 hpf (Fig. 8C and D), whereas approximately half of the *pou5f3* RNA granules were dissociated by treatment with hexanediol but not by treatment with hexanetriol at 3 hpf (Fig. 8E and F). These results suggest that *pou5f3* RNA granules exhibit a solid-like property in fertilized eggs, whereas they become liquid droplets during the mitotic cleavage stage.

To assess whether the assembly of *pou5f3* mRNAs into liquid droplets affects the

translational efficiency of mRNAs, I examined *pou5f3*-translating sites by Puro-PLA. Hexanediol treatment did not affect global mRNA translation, since puromycylated peptides detected by immunoblotting were equivalent in both control and hexanediol-treated embryos (Fig. 8G). Interestingly, the number of *pou5f3*-translating sites was significantly reduced in embryos treated with hexanediol but not with hexanetriol (Fig. 8H and I). The percentage of reduction in *pou5f3*-translating sites (79.5%) was higher than that of reduction in *pou5f3* RNA granules (47.5%, Fig. 8F), suggesting that *pou5f3* mRNA is effectively translated within liquid-state granules. Since treatment with hexanediol for more than 30 min causes reassembly of liquid droplets due to unknown side effects (Kroschwald et al., 2017), I could not examine the changes in the total amount of Pou5f3 in embryos by treatment with hexanediol. However, the results of Puro-PLA strongly suggest that assembly of liquid droplet RNA granules promotes translational efficiency of assembled mRNAs.

DISCUSSION

Translational control of dormant mRNAs during early stages of development

Timings of translational activation and the mechanisms of temporally regulated translation of dormant mRNAs have been extensively analyzed in a period of oocyte maturation using *Xenopus* oocytes (MacNicol et al., 2015; Mendez and Richter, 2001; Richter, 2007). Compared to the regulation in oocyte maturation, little is known about timings and mechanisms of translational control of mRNAs after fertilization. Mitotic cell cycles after fertilization were shown to be promoted by temporally controlled translation of *cyclin B1* mRNA through timely regulated polyadenylation in *Xenopus* embryos (Groisman et al., 2000; Groisman et al., 2002). A previous study showed the global changes in mRNAs that were incorporated into polysomes during zebrafish embryogenesis and the involvement of polyadenylation in promoting translation of widespread mRNAs (Winata et al., 2018). Previous research in our laboratory showed that poly(A) tail of *pou5f3* mRNA was elongated after fertilization. I confirmed the results in this study (Fig. 2C). Pou5f3 was accumulated after fertilization (Fig. 1C and F). Furthermore, *pou5f3*-translating sites increased from 0 to 3 hpf (Fig. 5C and D). These results demonstrate that *pou5f3* mRNA translation is activated from 0 to 3 hpf. However, observations in this research also showed that not all *pou5f3* RNA granules are translationally activated at 3 hpf (Fig. 4A-C). These results suggest that recruitment of ribosomes to embryonic granules is spatially regulated. It will be interesting to address the relationship between polyadenylation of *pou5f3* mRNA and recruitment of ribosomes in temporal and spatial control of mRNA translation.

Translational control within subcellular compartments, embryonic RNA granules

Extensive microscopic studies have suggested that membrane-less compartments such as stress granules, P-bodies and neuronal granules are involved in translational control of assembled mRNAs. Stress granules are assembled in response to cellular stresses in many types of cells and are thought to be sites of storage of mRNAs (Ivanov et al., 2019). A recent study using live imaging of single mRNA translation demonstrated that mRNAs assembled into stress granules are indeed translationally repressed and that these mRNAs are translated after disassembly of the granules (Moon et al., 2019). In neurons, many translationally repressed mRNAs are packaged into neuronal granules and are transported to their final destinations. These granules disassemble in response to neuronal activity, resulting in translational activation of the mRNAs (Thomas et al., 2014). In *Drosophila* oocytes, translationally repressed *bcd* mRNA was shown to be assembled into P-bodies, and the mRNA became translated after disassembly of P-bodies on fertilization (Weil et al., 2012). In zebrafish and mouse oocytes, translationally repressed mRNAs such as *cyclin B1*, *mos*, *mad2* and *emi2* mRNAs were shown to be assembled into granular structures. These oocyte RNA granules disassembled at the time of translational activation of distinct mRNAs during oocyte maturation (Horie and Kotani, 2016; Kotani et al., 2013; Takei et al., 2020; Takei et al., 2021). Collectively, many types of cytoplasmic RNA granules have been shown to act as repression sites of translation. The assembled mRNAs are translated after dissolution from the granules.

Only a few RNA granules have been demonstrated to act as activation sites of translation. In cultured fibroblast cells, Fus, an RNA-binding protein, directs translation of mRNAs assembled in adenomatous polyposis coli (APC) granules (Yasuda et al., 2013). In yeast, cytoplasmic granules called translation factor mRNA granules actively translate mRNAs assembled into the granules (Pizzinga et al., 2019). mRNA translation

continuously occurs in these granules even while they are transported to their final destination (Moissoglu et al., 2019). Embryonic RNA granules found in this study act as repression sites of translation at 0 hpf, whereas they become activation sites during early stages of embryogenesis without disassembling their granular structure (Figs. 2-6). Thereby, embryonic RNA granules are a novel type of cytoplasmic granules, and my findings provide a novel mode of translational regulation via formation and maintenance of granular structures in temporal and spatial control of mRNA translation. Future studies such as analysis of other mRNAs required for early development are needed to address whether the regulation of mRNAs in embryonic RNA granules is universal or not.

Functional changes in embryonic RNA granules

How do embryonic RNA granules regulate translational activity while maintaining their granular structures? The repression type of embryonic RNA granules exhibited a solid-like property since treatment with hexanediol did not affect the granular structures in embryos at 0 hpf (Fig. 8C and D). A recent study demonstrated that the solid-like state of RNA-binding proteins promotes translational repression of mRNAs (Shiina, 2019). A previous study in our laboratory showed that Pumilio1 in a solid-like state stably represses translation of target mRNAs and that the phase change into a liquid-like state promotes translational activation of them (Takei et al., 2020). My findings in this study support the notion that RNA granules in a solid-like state effectively repress the translation of assembled mRNAs in the cell cytoplasm. In this state, granular compartments effectively sequester the assembled mRNAs from translational machinery such as ribosomes.

In contrast to oocyte RNA granules such as *cyclin B1*, *mos*, *mad2* and *emi2* RNA granules, embryonic RNA granules did not disassemble and rather the state was changed

from solid-like to liquid-like, resulting in granules of liquid droplets (Fig. 8). The changes in the state and internal structure may be induced by post-translational modifications or changes in trans-acting factors binding to and/or assembling with the mRNAs (Nosella and Forman-Kay, 2021). These issues need to be addressed in future studies. What then is the role of liquid-state granules in mRNA regulation? My results demonstrated that dissolution of liquid-state *pou5f3* RNA granules by treatment with hexanediol significantly decreased the rate of translation (Fig. 8H and I). Therefore, one of the functions of liquid-state embryonic granules would be to promote translational efficiency of assembled mRNAs by colocalizing mRNAs, trans-acting factors and ribosomes in a highly concentrated state. Another possibility is that assembly of mRNAs into liquid droplets allows stable synthesis of the encoded proteins during a long period of development. In this regard, it should be noted that zygotic *pou5f3* mutants develop until tail-bud stages without obvious defects except for a defect in brain morphology (Belting et al., 2001). This implies that maternally deposited *pou5f3* mRNA can produce sufficient amounts of Pou5f3 protein to promote diverse developmental processes including progression of gastrulation, specification of endodermal cells, and dorsal-ventral development of embryos, all of which are defective in the maternal and zygotic *pou5f3* mutants (Lunde et al., 2004; Reim et al., 2004; Reim and Brand, 2006), until the tail-bud stage. Liquid-state *pou5f3* RNA granules may function to prevent degradation of maternal mRNAs for long durations to safely promote development. My finding that certain fractions, but not all, of *pou5f3* RNA granules were actively translated in embryos at 3 hpf (Figs. 4-7) supports this notion. The remaining granules would be stocks for synthesizing a large amount of Pou5f3 in later stages.

In summary, I discovered the existence of a novel type of embryonic RNA granules which is important for translational regulation after fertilization. My findings improve the

understanding of how embryos regulate mRNA translation to properly control development and how cells locally and temporally regulate mRNA translation through assembling and changing the properties of membrane-less compartments.

Chapter II

Functional analysis of Syncrip and Ewsr1b in translational regulation during early zebrafish development

ABSTRACT

Translational regulation of maternal transcripts is crucial for promoting early development. However, the translational regulation of maternal mRNAs after fertilization remains unclear. Because mRNA translation is mainly regulated by interactions between *cis*-acting elements of mRNAs and *trans*-acting factors such as RNA-binding proteins (RBPs), the functions of RBPs are important for understanding translational regulation. In this chapter II, I investigated the function of Syncrip and Ewsr1b, candidate RBPs that bind to *pou5f3* mRNA and are involved in translation. In chapter I, I showed that the state of *pou5f3* RNA granules changed when translation was activated. I hypothesized that intrinsically disordered regions (IDRs) of RBPs were a key for the change. Syncrip and Ewsr1b contain IDRs. The amount of Syncrip was decreased during the early stages of development. Notably, over-expression of Syncrip inhibited the Pou5f3 protein synthesis and the elongation of poly (A) tail of *pou5f3* mRNA. These results suggest that Syncrip is a key factor for translational repression of target mRNAs in early embryo. Ewsr1b was accumulated after fertilization and colocalized with *pou5f3* RNA granules. Knockdown of Ewsr1b attenuated the Pou5f3 protein synthesis. These results suggest that Ewsr1b is involved in translational activation of *pou5f3* mRNA and functional regulation of Pou5f3. Furthermore, I found that two transcript variants of *ewsr1b* mRNA were expressed in zebrafish embryo. In these variants, the length of 3' UTR was different. Surprisingly, the localization and function of synthesized proteins from these variants were different. These results suggest that Ewsr1b plays various roles in a cell, and the functions of Ewsr1b are regulated by the translational control according to the length of its 3' UTR.

INTRODUCTION

Since embryos in the early developmental stages are transcriptionally quiescent, production of proteins that are necessary for embryogenesis depends on translational regulation of maternally stored mRNAs. The regulatory mechanisms of maternal transcripts that are translationally activated during oocyte maturation have been well studied (Kotani et al., 2013; Horie and Kotani., 2016; Conti and Kunitomi, 2023). On the other hand, translational regulation after fertilization has been little studied. In chapter I, I showed that the state of *pou5f3* RNA granules changed from solid-like to liquid-like, and this change linked with translational activation. Because RNA granules mainly consist of mRNAs and RBPs (Anderson and Kedersha, 2009), the proteins that compose RNA granules play an important role in translational regulation. I hypothesized that intrinsically disordered regions (IDRs) of RBPs were involved in the change of state of *pou5f3* RNA granules. To investigate the molecular mechanism of translational regulation in more detail, I focused on two RNA-binding proteins, Syncrip and Ewsr1b. These proteins contain IDRs that are important for the regulation of RNA granules and liquid-liquid phase separation within a cell. In this chapter II, by investigating the roles of these proteins, I uncovered the molecular mechanism of translational repression and translational activation of maternal mRNAs.

Our laboratory found that the 3' end sequences of *pou5f3* mRNA were shortened after fertilization and that this shortening triggered translational activation (Takada et al. 2023). In total, 383 proteins were identified as candidates that bind to long and short 3' UTR of *pou5f3* mRNA, respectively, by RNA pull-down followed by mass spectrometry assay (Takada et al., 2023). As a result of more detailed analysis, 129 proteins were isolated as proteins specifically binding to the long 3' UTR, 191 proteins

specifically binding to the short 3' UTR, and 63 proteins binding to both long and short 3' UTR. I focused on proteins that specifically bind to long 3' UTR as proteins involved in translational repression, and proteins that specifically bind to short 3' UTR as proteins involved in translational activation. Among the former, I focused on Syncrip, which has been previously studied as being involved in translational control, and among the latter, I focused on Ewsr1b, which has been previously studied as being involved in phase separation. The fact that these two proteins have IDRs strongly prompted me to investigate their functions.

IDRs in proteins play a central role in the formation of liquid-liquid phase separation within cells (Oldfield and Dunker, 2014; Holehouse and Kragelund, 2024). IDRs are defined as regions that are composed mainly of a limited number of amino acids, cannot form a regular three-dimensional structure, and fluctuate like strings. The bias in amino acid composition leads to bias in physical properties (charge, hydrophobicity, etc.), which, combined with the fluctuating structure, induces LLPS. Naturally disordered regions with different properties repel each other like oil and water, while regions with affinity will mix and form liquid droplets. In this way, the necessary molecular groups gather locally through LLPS, creating membrane-less molecular condensates including RNA granules.

Syncrip, a member of the cellular heterogenous nuclear ribonucleoprotein (hnRNP) family, also known as hnRNP Q, regulates various aspects of neuronal development and plasticity (Mizutani et al., 2000; Bannai et al., 2004). Previous research showed that cytoplasmic Syncrip binds mostly to the 3' UTR of mRNAs and plays a key role in the post-transcriptional regulation of neuronal mRNAs (Duning et al., 2008; Khudayberdiev et al., 2020). However, the function of Syncrip during early development is unknown.

EWS RNA-binding protein 1 (Ewsr1) belongs to a FET family of proteins, which includes Fused in Sarcoma (Fus), TATA-box binding protein Associated Factor 15 (Taf15) and Ewsr1. The amino acid sequences of these proteins share high homology (~70%) and are evolutionarily conserved from fish to human (Morohoshi et al., 1998). A major characteristic of these proteins is that they are composed of IDRs. FET proteins are expressed in most cell and tissue types, and predominantly reside in the nucleus (Andresson et al., 2008). Importantly, previous studies have shown that mutations in FET family genes are closely linked to certain neurodegenerative disorders such as amyotrophic lateral sclerosis (ALS) (Tan and Manley, 2009; Kapeli et al., 2017; Kanekura and Kuroda, 2022). However, the function of FET proteins on translational regulation and early development remains unknown.

The most-studied cellular function of EWSR1 is the regulation of transcription. Previous research showed that EWSR1 forms higher-order assemblies near the promoters and transcription start sites of genes and recruit RNA polymerase II through interactions with the C-terminal domain (Bertolotti et al., 1996; Yang et al., 2000; Kwon et al., 2013). In addition, EWSR1 activates the transcriptional activity of transcriptional factors such as Oct4, CBP and HNF4α through direct binding (Araya et al., 2003; Lee et al., 2005).

To elucidate the function of Syncrip and Ewsr1b after fertilization, I investigated how these proteins were involved in translational regulation of *pou5f3* mRNA. I showed that the amount of Syncrip decreased during early development. Furthermore, over-expression of Syncrip reduced the amount of Pou5f3 and suppressed poly(A) tail extension of *pou5f3* mRNA. These results suggest that Syncrip is one of the key factors in translational repression of target mRNAs. The amount of Ewsr1b was increased at an earlier stage than Pou5f3 accumulation after fertilization. Ewsr1b became

colocalized with *pou5f3* RNA granules during early stages of development. Furthermore, knockdown of Ewsr1b decreased the amount of Pou5f3. These results suggest that Ewsr1b is important for translational activation of *pou5f3* mRNA. Ewsr1b was localized in both the nucleus and cytoplasm in a cell. Ewsr1b was colocalized with Pou5f3 in the nucleus, suggesting that Ewsr1b was also involved in the post-translational regulation of Pou5f3. RNA-seq analysis of the 3' UTR lengths of mRNAs in embryos revealed that *ewsr1b* mRNA possessed two transcript variants with different length of 3' UTR, that is short or long type. I found that Ewsr1b plays various roles in a cell, including translational regulation, and that the timings and functions of Ewsr1b are regulated by the translational control according to the length of 3' UTR.

MATERIALS AND METHODS

Production of antibodies

The DNA sequence encoding a part of zebrafish Ewsr1b (residues 1-329) was amplified by PCR using primer sets specific for the target region (*ewsr1b*-ORF-f1; *ewsr1b*-ORF-r2) and ligated into the pET21 vector with appropriate restriction enzymes sites (EcoRI and HindIII) to produce a His-tagged protein. The recombinant protein was expressed in *E. coli* (BL21) and purified by SDS-PAGE, followed by electroelution in Tris-glycine buffer without SDS. The purified protein was dialyzed against 1 mM HEPES (pH 7.5), lyophilized, and used for injection into two mice and one rabbit. The obtained antisera were affinity-purified with recombinant Ewsr1b-His protein electroblotted onto a membrane (Immobilon; EMD Millipore, IPVH00010). Primer sequences are presented in Table 1.

Immunoblotting

Crude extracts from wild-type zebrafish embryos were prepared using a method similar to that described in Chapter 1 (p10-11). The crude extracts from zebrafish embryos were separated by SDS-PAGE, blotted onto an Immobilon membrane, and probed with mouse anti-Syncrip antibody (hnRNP Q; Santa Cruz Biotechnology, I8E4; sc-56703; 1:1000), rabbit anti-Syncrip antibody (Proteintech, 14024-1-AP; 1:1000), rabbit anti-Rpl11 antibody (Abcam, ab79352; 1:2000), mouse anti-GFP antibody (Roche, 11814460001; 1:1000), mouse anti-Ewsr1b antibody (this study: 1:100), rabbit anti-Pou5f3 antibody (this study; 1:200), or rabbit anti-Importin beta-1 antibody (Proteintech, 10077-1-AP; 1:1000). The antibodies were diluted in blocking buffer (4% skim-milk,

0.1% Tween 20 in TBS). Quantification of relative amounts was performed using ImageJ software.

DIG- and FITC- labeled RNA probe synthesis

The DNA sequence encoding ORF and 3' UTR of zebrafish *ewsr1b* mRNA and GFP was amplified by PCR using primer sets specific for the target region (*ewsr1b* ORF: *ewsr1b*-ORF-f1; *ewsr1b*-ORF-r1, *ewsr1b* 3' UTR: *ewsr1b*-ORF-f2; *ewsr1b*-3' UTR-r1, GFP: *gfp*-f1; *gfp*-r1) and ligated into the pGEM-T easy vector. The plasmid was linearized with appropriate restriction enzymes (antisense: Apa I, sense: Spe I) at 37˚C for 2 hours. Primer sequences are presented in Table 1. The RNA probes were synthesized using SP6 (antisense) or T7 (sense) RNA polymerase and DIG (*ewsr1b* ORF and GFP) or FITC (*ewsr1b* 3' UTR) RNA Labeling Mix (total 20 µL reaction; Roche) at 37˚C for 2 hours. After purification, the RNA probes were diluted (50 ng/µL) with HYB+ and stored at -20˚C.

Double whole mount *in situ* hybridization (WISH)

Double WISH of *ewsr1b* ORF and *ewsr1b* 3' UTR was performed as follows. After hybridization with the FITC-labeled antisense RNA probe for *ewsr1b* 3' UTR and the DIG-labeled antisense RNA probe for *ewsr1b* ORF, the embryos were incubated with anti-Fluorescein-HRP antibody (1:300 dilution) for 3 hours, followed by incubation with tyramide-Cy3 (Akoya Biosciences, NEL704A001KT) according to the manufacturer's instructions. The embryos were then incubated with 1% H_2O_2 in methanol for 30 min for inactivating HRP. After rehydration and washing with PBS, the embryos were incubated with anti-DIG-HRP antibody (1:700 dilution) for 3 hours, followed by incubation with tyramide-Fluorescein (Akoya Biosciences,

NEL701A001KT) according to the manufacturer's instructions. After being mounted with VECTASHIELD Mounting Medium (Funakoshi), the samples were observed under the ZEISS LSM980 confocal microscope. The distance from the center of the nucleus to signals of *ewsr1b* mRNA was quantified using ImageJ software.

Immunofluorescence

Whole-mount immunofluorescence was performed according to a previously reported procedure (Shen et al., 2022). Zebrafish embryos were collected at desired stages and fixed with 4% paraformaldehyde in PBS overnight at 4°C. Then embryonic chorion was removed in PBS, replaced with 100% methanol, and stored overnight at -20°C. Immunostaining assay began with rehydration in 50% methanol in PBS and PBS, followed by washing in PBTD (0.1% Tween-20, 1% DMSO in PBS) for two times for 5 min each. Embryos were blocked in blocking buffer (1% BSA, 10% new-born calf serum, 0.3M glycine in PBTD) for 1 hour at RT and incubated with primary antibody diluted in blocking buffer overnight at 4°C. Primary antibodies included rabbit anti-Syncrip (1:200), mouse anti-GFP (1:200), rabbit anti-Pou5f3 (1:50), mouse anti-Ewsr1b (this study; 1:50), and rabbit anti-Importin beta-1 (1:200). Next day, embryos were rinsed in PBTD two times for 5 min each. Thereafter, embryos were incubated in fluorochrome-conjugated secondary antibodies diluted in blocking buffer at 1:200 for 2 hours at RT and all processes would be kept in dark after this step. After washing with PBTD two times for 5 min, embryos were mounted with VECTASHIELD Mounting Medium. The mounted samples were observed under the ZEISS LSM980 confocal microscope. The intensities and number of signals of Ewsr1b and Pou5f3 were quantified using ImageJ software.

To detect simultaneously GFP and Pou5f3 (Fig. 11C) or Ewsr1b and Pou5f3 (Fig.

14F), primary antibodies and secondary antibodies for the two proteins were diluted simultaneously in blocking buffer and used for the reactions.

Simultaneous detection of Syncrip, Ewsr1b or Ewsr1b, Pou5f3 and *pou5f3* RNA granules (Fig. 10A; Fig. 14C; Fig. 14E) was performed as follows. After hybridization with the DIG-labeled antisense *pou5f3* RNA probe, the proteins were detected as described above. After washing, the embryos were incubated with anti-DIG-HRP antibody, and the signals of *pou5f3* were detected as described in whole mount *in situ* hybridization. The number of colocalization sites of Syncrip or Ewsr1b and *pou5f3* RNA granules was quantified using ImageJ software.

To detect simultaneously *gfp* mRNA and GFP protein (Fig. 17F) and *ewsr1b* mRNA 3' UTR and Importin beta-1 (Fig. 19C), the same procedure as above was performed using the DIG-labeled antisense *gfp* RNA probe and the fluorescein-labeled *ewsr1b* 3' UTR RNA probe, respectively.

Immunoprecipitation followed by RT-PCR (IP/RT-PCR)

The crude extracts of zebrafish embryos were incubated with mouse anti-Syncrip, mouse anti-GFP, rabbit anti-Rpl11, or rabbit anti-Importin beta-1 and protein A Mag Sepharose (GE Healthcare) overnight at 4℃. The same volume of mouse IgG or rabbit IgG was used as a control. After washing, mRNAs were extracted from the beads using TRIzol reagent (Invitrogen) and reverse transcription was performed with FastGene Scriptase II cDNA synthesis kit (FastGene) using oligo (dT) primer. RT-PCR was performed using primer sets specific for *pou5f3* (*pou5f3*-3'UTR-f1; *pou5f3*-3'UTR-r1), *α-tubulin* (*α-tubulin*-f1; *α-tubulin*-r1), *ewsr1b* ORF (*ewsr1b*-ORF-f1; *ewsr1b*-ORF-r3), *ewsr1b* 3' UTR (*ewsr1b*-ORF-f2; *ewsr1b*-3' UTR-r1). Primer sequences are presented in Table 1.

Immunoprecipitation followed by mass spectrometry

After immunoprecipitation with anti-Syncrip antibody, the samples were separated by SDS-PAGE, and the SDS-PAGE gel were stained by silver staining with the Silver Stain MS kit (Wako Pure Chemical Industries, Ltd) to visualize the proteins associated with Syncrip. Each sample lane was divided into five regions and subjected to a mass spectrometric analysis with Orbitrap Exploris 240 (Thermo Fisher Scientific). For protein identification, Sequest HT (Thermo Fisher Scientific) with Proteome Discoverer 3.0 software (Thermo Fisher Scientific) was used for database searching against the zebrafish (*D. rerio*) section of the UniProtKB database (2024-1-24, 3314 sequences, 1619742 residues) and validated with the Percolator based on q-value. The number of peptides identical to the proteins was more than one. Gene ontology (GO) analysis was performed using the DAVID Knowledgebase v2023q4 (https://david.ncifcrf.gov/).

RT-PCR

Total RNA from oocytes and embryos was extracted by using TRIzol reagent according to the manufacturer's instructions. Reverse transcription was performed with FastGene Scriptase II cDNA synthesis kit using oligo (dT) primer. RT-PCR was performed using primer sets specific for *ewsr1a*, (*ewsr1a*-ORF-f1; *ewsr1a*-ORF-r1) *ewsr1b* (*ewsr1b*-ORF-f1; *ewsr1b*-ORF-r2) and *β-actin* (*β-actin*-ORF-f1; *β-actin*-ORF-r1). Primer sequences are presented in Table 1.

Quantitative PCR

Total RNA from oocytes and embryos was extracted by using TRIzol reagent.

Reverse transcription was performed with HiScript III All-in-one RT SuperMix Perfect for qPCR (Vazyme). The transcripts were amplified with the cDNA and primer sets specific for *ewsr1a* (*ewsr1a*-ORF-f1; *ewsr1a*-ORF-r2) and *ewsr1b* mRNA (*ewsr1b*-ORF-f1; *ewsr1b*-ORF-r4) and quantified using a real-time PCR system with SYBR green PCR Master Mix (Applied Biosystems) according to the manufacturer's instructions. Primer sequences are presented in Table 1.

Proximity ligation assay (PLA)

The proximity ligation assay (PLA) was performed according to the manufacturer's instructions (Sigma) and methods described in chapter I. Embryos were incubated with mouse anti-Ewsr1b antibody (1:50) and rabbit anti-Pou5f3 antibody (1:50) or mouse anti-Ewsr1b antibody (1:50) and rabbit anti-Importin beta-1 antibody (1:200). The number of PLA signals was quantified using ImageJ software.

MO injection

The sequences of MOs (Gene Tools, LLC) are presented in Table 1. The Ewsr1b-ATG-MO (ATG-MO) targets the start codon of *ewsr1b* mRNA, whereas the Ewsr1b-5mm-MO (5mm-MO) contains 5-nt mismatches. Ewsr1b-3' UTR-MO (3' UTR-MO) targets the 3' end sequences of *ewsr1b* mRNA. Using Femtojet (Eppendorf), 1nl of mixture containing 4 ng MOs was injected into fertilized eggs.

PAT assay

RNA ligation–coupled RT-PCR was performed according to a previously reported procedure (Kotani et al., 2013). 2 μg of total RNA extracted from pools of 50 zebrafish embryos was ligated to 0.4 μg of P1 anchor primer in a 10-μl reaction mixture using T4

RNA ligase (New England Biolabs) for 30 min at 37°C. The ligase was inactivated for 5 min at 92°C. Overall, 4.75 µl of the reaction mixture was used in a 10-µl reverse transcription reaction using FastGene Scriptase II cDNA synthesis kit with a P1′ primer. Then, 2 µl of the cDNA was used for the first round of PCR in a total volume of 25 µl with a P1′ primer and a primer specific for *pou5f3* (*pou5f3*-PAT-f1), *ewsr1b* 3' UTR-Long (*ewsr1b* 3' UTR-Long-PAT-f1), or *ewsr1b* 3' UTR-Short (*ewsr1b* 3' UTR-Short-PAT-f1) for 20 cycles. Subsequently, 1 µl of the first-round PCR product was used for second-round PCR in a total volume of 25 µl with a P1′ primer and a primer specific for *pou5f3* (*pou5f3*-PAT-f2), *ewsr1b* 3' UTR-Long (*ewsr1b* 3' UTR-Long-PAT-f2), or *ewsr1b* 3' UTR-Short (*ewsr1b* ORF-f2) for 35 cycles. Primer sequences are presented in Table 1. The PCR products were then cloned into a pGEM-T vector (Promega), transformed into XL-1 cells, and sequenced.

GFP-tagged mRNA synthesis, mRNA injection, Live imaging, and FRAP

For plasmid construction of GFP-Ewsr1b 3' UTR-Long and GFP-Ewsr1b 3' UTR-Short, these regions were amplified by PCR using specific primer sets (Long: *ewsr1b*-ORF-f1; *ewsr1b*-ORF-r3, Short: *ewsr1b*-ORF-f1; *ewsr1b*-ORF-r1). GFP-tagged mRNA was synthesized using the mMESSAGE mMACHINE SP6 Transcription Kit (Ambion) and dissolved in nuclease-free distilled water. 1 nl of 200 ng/µl mRNA was injected into fertilized eggs. For live imaging, the injected embryos were mounted and observed under the ZEISS LSM980 confocal microscope. FRAP measurements were performed under the ZEISS LSM980 confocal microscope. A small area (approximately 5 µm diameter circle) was positioned in a region of the embryo cytoplasm and bleached using 100% 488 nm laser for 1 second. Images were then collected using 1.0% laser power every 1.0 second for 10 seconds.

MG132 injection

1 nl of mixture containing 10 μM proteasomal inhibitor MG132 (Wako Pure Chemical Industries, Ltd) in DMSO or the same amount of DMSO was injected into fertilized eggs. The mixture was made by diluting the 0.1M MG132 in DMSO stock solution.

Statistical analyses

All results were expressed as mean ± standard deviations. Statistical analysis comparing two samples was performed using Student's *t*-test, and that comparing multiple groups was performed using Tukey-Kramer test as indicated in the figure legends. Significance was defined as $p < 0.05$ ($****p < 0.0001$, $***p < 0.001$, $**p < 0.01$, $*p < 0.05$).

RESULTS

The amount of Syncrip is decreased during the early stages of zebrafish development

Syncrip was isolated as the candidate protein that predominantly binds to the *pou5f3* mRNA 3' UTR with full-length 3' end (Takada et al., 2023). Syncrip is a highly conserved RNA-binding protein that has three sequence-specific RNA-binding domains (Fig. 9A). I first evaluated the specificity of mouse and rabbit anti-Syncrip antibody. The antibodies recognized a protein with a molecular mass of ~74 kDa in immunoblots (Fig. 9B). To elucidate the function of Syncrip, I investigated the amount of Syncrip in zebrafish early embryo. Time course analysis showed that Syncrip was expressed in eggs and the amount of Syncrip was decreased from 0 to 6 hours post fertilization (hpf) (Fig. 9C and D). Immunofluorescence using rabbit anti-Syncrip antibody showed that Syncrip was expressed in the cytoplasm at 0 hpf. The signals of Syncrip decreased in embryos at 3 and 6 hpf (Fig. 9E).

Syncrip binds to *pou5f3* mRNA in embryos

Based on the results above, I predicted that Syncrip is involved in the translational repression of *pou5f3* mRNA. To analyze the relationship between Syncrip and *pou5f3* mRNA, I performed the double staining of Syncrip protein and *pou5f3* mRNA. Syncrip and *pou5f3* mRNA granules were colocalized in embryos at 0 hpf (Fig. 10A). The colocalization was decreased in embryos at 3 hpf (Fig. 10A and B). Immunoprecipitation followed by RT-PCR analysis (IP/RT-PCR) showed that Syncrip bound to *pou5f3* mRNA but not *α-tubulin* mRNA (Fig. 10C).

Over-expression of Syncrip represses *pou5f3* mRNA translation

To figure out whether Syncrip is involved in the translational repression of *pou5f3* mRNA, I performed GFP-Syncrip over-expression experiment. I prepared the *gfp-syncrip* mRNA and injected it into fertilized eggs. Immunoblotting analysis showed that the amount of Pou5f3 at 6 hpf was decreased by over-expression of Syncrip but not GFP alone (Fig. 11A and B). Double immunostaining of GFP-Syncrip and Pou5f3 in embryos at 6 hpf showed that GFP-Syncrip was localized in the cytoplasm and over-expression of GFP-Syncrip, but not GFP, reduced the amount of Pou5f3 (Fig. 11C). Furthermore, analysis of the poly(A) tail lengths of *pou5f3* mRNA by poly(A) tail (PAT) assay showed that over-expression of GFP-Syncrip inhibited the elongation of poly(A) tail of *pou5f3* mRNA (Fig. 11D). I confirmed GFP-Syncrip interacted with *pou5f3* mRNA by IP/RT-PCR analysis (Fig. 11E). These results suggest that Syncrip represses *pou5f3* mRNA translation by inhibiting polyadenylation.

Syncrip interacts with various proteins involved in translational regulation

To isolate proteins interacting with Syncrip, I performed immunoprecipitation of Syncrip followed by mass spectrometry analysis. After immunoprecipitation (Fig. 12A), I carried out silver staining and detected some specific bands in the sample in which Syncrip was immunoprecipitated (Fig. 12B). Mass spectrometry analysis identified 87 proteins that bound to Syncrip (Table 2). Gene ontology analysis showed that proteins involved in translational control were precipitated with Syncrip (Fig. 12C), including the Ccr4-Not complex subunit 1 (Cnot1; Fig. 12D), which is known to be involved in mRNA translation. These results provide a possibility that Syncrip regulates translation of target mRNAs by interacting with some proteins.

Ewsr1b is increased during the early stages of development and localized in the nucleus and cytoplasm

Ewsr1b was also isolated as a candidate protein that predominantly binds to the *pou5f3* mRNA 3' UTR with shortened 3' end. Ewsr1b is one of the FET family proteins. They have similar domain structures, serine-tyrosine-glycine-glutamine-rich domain (SYGQ-rich), arginine-glycine-glycine-rich domain (RGG), RNA recognition domain (RRM), zinc finger domain (ZnF), and nuclear localization signal (NLS) (Fig. 13A). In zebrafish, two genes as homologues (orthologous) of human *EWSR1*, *ewsr1a* and *ewsr1b*, have been identified (Azuma et al., 2007). Comparison of the amino acid sequences of Ewsr1a and Ewsr1b illustrated that they share most of amino acids (396) in the entire region (Fig. 13A). I first analyzed the expression level of *ewsr1a* and *ewsr1b* in oocytes and embryos. RT-PCR and quantitative PCR analyses showed that the expression level of *ewsr1a* was significantly low compared to *ewsr1b* in both oocytes and embryos (Fig. 13B and C). From these results, I decided to focus on *ewsr1b*. To confirm the synthesis of Ewsr1b protein during zebrafish embryogenesis, I produced antibodies against the N-terminus region of zebrafish Ewsr1b (amino acids 1-329). The affinity-purified mouse antibody recognized mainly a protein with a molecular mass of ~62 kDa that is around the predicted molecular weight (60.6 kDa; Fig. 13D). To analyze the synthesis and localization of Ewsr1b protein in embryos, I performed time course analysis of Ewsr1b by immunoblotting and immunofluorescence. As a result, I found that the amount of Ewsr1b was increased from 0 to 6 hpf, especially from 0 to 3 hpf (Fig. 13E and F). An increase of Ewsr1b was also observed from 0 to 6 hpf by immunofluorescence (Fig. 13G). Particularly, Ewsr1b was localized in both the nucleus and cytoplasm at 6 hpf (Fig. 13G). This result suggests that Ewsr1b functions in both the nucleus and cytoplasm.

Ewsr1b would regulate *pou5f3* mRNA translation and Pou5f3 protein function

To investigate whether Ewsr1b is involved in translational activation of *pou5f3* mRNA, I performed time course analysis of Ewsr1b in shorter intervals of early developmental stages. To compare the changes in accumulation of Ewsr1b and Pou5f3, I quantified the intensities of immunoblotting at 0, 1, 2, and 3 hpf. The amount of Ewsr1b was increased at the stage earlier than Pou5f3, which started at 1 hpf (Fig. 14A and B). Double staining of *pou5f3* mRNA and Ewsr1b protein showed that *pou5f3* RNA granules co-localizing with Ewsr1b increased from 0 to 3 hpf (Fig. 14C and D). Furthermore, I simultaneously stained *pou5f3* mRNA, Ewsr1b, and Pou5f3 in embryos at 3 hpf. Pou5f3 was synthesized at the sites where *pou5f3* mRNA and Ewsr1b were colocalized (Fig. 14E). I also found that Ewsr1b was colocalized with Pou5f3 in the nucleus and cytoplasm (Fig. 14F). To explore this result, I performed proximity ligation assay analysis (PLA) between Ewsr1b and Pou5f3. The signals of PLA began to be detected from 2 hpf, throughout the cell, but strong signals were detected in the nucleus at 3 hpf (Fig. 14G and H). These results provide a possibility that Ewsr1b would be involved in not only *pou5f3* mRNA translation but also changing physical properties of *pou5f3* RNA granules and functional regulation of Pou5f3 protein.

Ewsr1b is required for the progression of early zebrafish development

To assess whether Ewsr1b plays a role in the regulation of *pou5f3* mRNA and progression of early development, I conducted a knockdown experiment of Ewsr1b by using a morpholino oligonucleotide (MO) that targets the start codon of *ewsr1b* mRNA (ATG-MO). A control MO containing 5-nt mismatches (5mm-MO) was also used. Interestingly, in embryos deficient for Ewsr1b by injection with ATG-MO, the amount of Pou5f3 was also decreased (Fig. 15A and B). This result suggests that Ewsr1b is

involved in translational activation of *pou5f3* mRNA or in stabilization of Pou5f3 protein. Injection with ATG-MO, but not 5mm-MO, caused severe developmental defects, including delayed epiboly from 6 hpf and shrinkage of entire embryo at 24 hpf (Fig. 15C). Embryos showing these phenotypes were observed in approximately 60% of the embryos injected with ATG-MO (Fig. 15D). These results suggest that the function of Ewsr1b is crucial for driving early development.

Two transcript variants of *ewsr1b* mRNA are expressed in zebrafish embryo

From the results so far, Ewsr1b was shown to be involved in translational regulation of *pou5f3* mRNA, regulation of Pou5f3 protein, and embryogenesis. My question was what molecular mechanisms underpin these various functions of Ewsr1b. I focused on the results of 3'- end RNA sequences of *ewsr1b* mRNA (Takada et al., 2023). I found that two transcript variants of *ewsr1b* mRNA with different lengths of 3' UTR were expressed in zebrafish embryo, which is 3' UTR-Long and 3' UTR-Short mRNAs (Fig. 16A). The length of 3' UTR of Long mRNA is 302 bases and that of Short mRNA is 16 bases. To check the sequences and changes of poly(A) tail lengths of each endogenous transcript, I performed a PAT assay. PAT assay analysis revealed that the poly(A) tail of 3' UTR-Long mRNA was gradually elongated from 0 to 3 hpf (Fig. 16B). On the other hand, the poly(A) tail of 3' UTR-Short mRNA was rapidly elongated after fertilization, from 0 to 1 hpf (Fig. 16B). This result suggests that the timing and mechanism of translational activation of 3' UTR-Long mRNA and 3' UTR-Short mRNA are different. To further examine this result, I performed immunoprecipitation of Rpl11 followed by RT-PCR for *ewsr1b* mRNA at 1 and 3 hpf. Since Rpl11 binds to translationally activated mRNAs, it is possible to specifically detect translationally activated mRNAs by RT-PCR. When both 3' UTR-Long and Short mRNAs were detected by amplifying ORF of

ewsr1b, the signals were observed in embryos at 1 and 3 hpf (Fig. 16C). However, when only the 3’ UTR-Long mRNA was detected, the signals were not observed in embryos at 1 hpf but were detected in embryos at 3 hpf (Fig. 16C). These results indicate that the 3’ UTR-Short mRNA translation is activated at an earlier stage of development than the 3’ UTR-Long mRNA translation. The signals of *pou5f3* mRNA were not detected in embryos at 1 hpf but were detected at 3 hpf (Fig. 16C), suggesting translational activation during early development. I attempted to distinguish and label endogenous 3’ UTR-Long mRNA and 3’ UTR-Short mRNA in FISH analysis. I synthesized an RNA probe to label the ORF (green) and an RNA probe to label the 3' UTR (red), respectively (Fig. 16D). The green signal alone is 3’ UTR-Short mRNA, and the colocalized signal of green and red is 3’ UTR-Long mRNA (Fig. 16D). Double *in situ* hybridization using these probes could label 3’ UTR-Long mRNA and 3’ UTR-Short mRNA at 0 and 3 hpf (Fig. 16E). I speculated that there would be differences in the intracellular localization between 3’ UTR-Long mRNA and 3’ UTR-Short mRNA. To address this hypothesis, I measured the distance from the center of the nucleus to the signals of 3’ UTR-Long mRNA and 3’ UTR-Short mRNA, respectively in embryos at 3 hpf (Fig. 16F). As a result of quantification, 3’ UTR-Short mRNA was localized farther from the center of the nucleus than 3’ UTR-Long mRNA (Fig. 16G). These results suggest that localization of 3’ UTR-Long and Short mRNA is different in a cell. Do such differences in the timing of translational activation and localization of mRNA between 3’ UTR-Long mRNA and 3’ UTR-Short mRNA affect the synthesized proteins?

The lengths of *ewsr1b* mRNA 3' UTR determine the protein localization and function

To investigate the differences in the localization and function of proteins synthesized

from 3’ UTR-Long mRNA and 3’ UTR-Short mRNA, I performed localization analysis of GFP-tagged proteins. I prepared GFP-Ewsr1b 3’ UTR-Long mRNA and GFP-Ewsr1b 3’ UTR-Short mRNA (Fig. 17A) and injected them into fertilized eggs. Due to the design of primer for PCR amplification and cloning, the length of 3’ UTR of GFP-Ewsr1b 3’ UTR-Long mRNA is 255 of 302 full lengths (Fig. 17A). Surprisingly, the protein synthesized from 3’ UTR-Long mRNA was localized in the nucleus, whereas the protein synthesized from 3’ UTR-Short mRNA was localized in the cytoplasm (Fig. 17B). To further explore this result, I performed immunoprecipitation of GFP-Ewsr1b protein followed by immunoblotting of Pou5f3 protein and RT-PCR for *pou5f3* mRNA. Immunoblotting of GFP-Ewsr1b protein showed that there was no obvious difference in molecular weight between the proteins synthesized from 3’ UTR-Long mRNA and 3’ UTR-Short mRNA (Fig. 17C). Surprisingly, Pou5f3 protein was detected in precipitates of GFP-Ewsr1b synthesized from 3’ UTR-Long, but not in Short mRNA (Fig. 17C), *pou5f3* mRNA was detected in precipitates of GFP-Ewsr1b synthesized from 3’ UTR-Short, but not Long mRNA (Fig. 17C). These results suggest that the protein synthesized from 3’ UTR-Long mRNA is localized in the nucleus and interacts with Pou5f3 protein, and the protein synthesized from 3’ UTR-Short mRNA is localized in the cytoplasm and interacts with *pou5f3* mRNA. To investigate the physical properties of GFP-Ewsr1b synthesized from 3’ UTR-Short mRNA, I performed the time lapse imaging in embryos at 6 hpf. As a result, the fusion of the two droplets of Ewsr1b protein was observed (Fig. 17D), suggesting that GFP-Ewsr1b synthesized from 3’ UTR-Short mRNA was in liquid droplet-like properties. To examine differences in the localization of injected 3’ UTR-Long mRNA and 3’ UTR-Short mRNA, the localization of injected RNA was visualized by *in situ* hybridization using an RNA probe against the GFP sequence (Fig. 17E). *In situ* hybridization revealed that GFP-3’ UTR Long mRNAs were localized at the periphery of

the nucleus, while GFP-3' UTR Short mRNAs were localized in the outside region of the cell (Fig. 17F). Measurement of the distance from the center of the nucleus revealed that the 3' UTR-Short mRNA was localized farther from the center of the nucleus than the 3' UTR-Long mRNA (Fig. 17G), similarly to the analysis of endogenous mRNA. These results indicate that the lengths of *ewsr1b* mRNA 3' UTR play important roles for determining the mRNA localization, which would link to the localization and function of synthesized protein.

Ewsr1b synthesized from 3' UTR-Long mRNA is important for proper protein localization in the nucleus

To investigate the function of endogenous *ewsr1b* mRNA 3' UTR, I knocked down the protein synthesis from *ewsr1b* 3' UTR-Long mRNA. I injected a MO that targets the 3' end of *ewsr1b* mRNA (3' UTR-MO; Fig. 18A). I performed double immunofluorescence of Ewsr1b and Pou5f3 and quantified the amount of each protein in the nucleus and cytoplasm, respectively. Injection with ATG-MO reduced the amount of Ewsr1b and Pou5f3 in both the nucleus and cytoplasm (Fig. 18B and C). In contrast, injection with 3' UTR-MO reduced the amount of Ewsr1b and Pou5f3 in the nucleus (Fig. 18B and C). In the cytoplasm, the amount of Ewsr1b was slightly decreased, and that of Pou5f3 was unchanged with 3' UTR-MO injection (Fig. 18B and C), suggesting that Ewsr1b synthesized from 3' UTR-Short mRNA was localized in the cytoplasm and promoted the Pou5f3 synthesis. Immunoblotting revealed that injection with ATG-MO inhibited the Ewsr1b and Pou5f3 synthesis, whereas injection with 3' UTR-MO did not (Fig. 18D and E). These results suggest that proteins synthesized from 3' UTR-Long mRNA are expressed in the nucleus and involved in the nuclear localization of target proteins, but the proteins are not involved in translational activation in the cytoplasm.

Importin beta-1 binds to *ewsr1b* mRNA 3' UTR and transports Ewsr1b to the nucleus

I then attempted to address how the Ewsr1b synthesized from mRNA with the long 3' UTR localizes in the nucleus. The function of nuclear transport proteins is crucial for proper localization of proteins in the nucleus (Yang et al., 2023). Karyopherin beta-1/Importin beta-1 is a highly conserved member of the superfamily of nuclear transport receptor, acting in protein nuclear import (Harel and Forbes, 2004; Chook and Suel, 2011; Kimura and Imamoto, 2014). Since FET family proteins have nuclear localization signal (NLS), the nuclear transport proteins may be important for regulating localization and function of these proteins. Previous studies showed that nuclear import proteins function as chaperone and regulate phase separation of Fus, a member of FET family proteins (Hofweber et al., 2018; Yoshizawa et al., 2018; Baade et al., 2021). Furthermore, previous research showed that EWSR1 is one of the Importin beta-1 interactors (Francesco et al., 2018). Importin beta-1 was localized in both the nucleus and cytoplasm in zebrafish embryo (Fig. 19A). IP/RT-PCR analysis revealed that Importin-beta-1 could bind to *ewsr1b* mRNA (Fig. 19B). Double staining of *ewsr1b* mRNA 3' UTR and Importin beta-1 protein also showed that Importin beta-1 would interact with *ewsr1b* mRNA 3' UTR (Fig. 19C). Furthermore, PLA analysis showed that Importin beta-1 interacted with Ewsr1b throughout the cell at 3 hpf and in the nucleus at 6 hpf (Fig. 19D). This result suggests that Ewsr1b synthesized in the cytoplasm interacts with Importin beta-1 and is transported to the nucleus. From these results, I propose a model that Importin beta-1 binds to *ewsr1b* mRNA 3' UTR and transports Ewsr1b synthesized from 3' UTR-Long mRNA to the nucleus.

Protein degradation after fertilization is involved in translational regulation

My next question was how the *ewsr1b* 3' UTR-Short mRNA translation is activated immediately after fertilization. Poly (A) tail of *ewsr1b* 3' UTR-Short mRNA was elongated immediately after fertilization, from 0 to 1 hpf (Fig. 16B). This result suggests that an event that occurs immediately after fertilization is involved in the translational regulation. Previous research showed that rapid protein degradation occurred by the 8-cell stage (1 hpf) and involved in proper progression of early zebrafish development (Dutta and Sinha, 2017). This result indicates that proper protein degradation after fertilization is crucial for embryogenesis. I predicted that this proteolysis also resulted in the degradation of proteins involved in translational repression and focused on the relationship between this proteolysis and translational activation of *ewsr1b* 3' UTR-Short mRNA immediately after fertilization. MG132 is a potent proteasome inhibitor and used as a tool for studying cellular degradation of the ubiquitin-proteasome pathway. I injected MG132 into fertilized eggs and found that this inhibitor did not prevent the progression of mitotic cleavage (Fig. 20A). However, immunoblotting and immunofluorescence analyses revealed that MG132 inhibited Ewsr1b protein synthesis at 1 hpf (Fig. 20B, C and D). Furthermore, MG132 also inhibited the poly(A) tail elongation of *ewsr1b* 3' UTR-Short mRNA at 1 hpf (Fig. 20E). These results suggest that proper proteolysis after fertilization is important for the translational regulation of *ewsr1b* 3' UTR-Short mRNA.

The state of Syncrip and Ewsr1b is different

My last question was whether the functions of Syncrip and Ewsr1b relate to the change of physical properties of *pou5f3* RNA granules described in chapter I. Syncrip and Ewsr1b contain IDRs that are important for functional regulation of membrane-less compartments including RNA granules (Fig. 21A). To analyze the physical properties of

Syncrip and Ewsr1b, I performed time-lapse imaging and fluorescence recovery after photobleaching analysis (FRAP) of GFP-Syncrip and GFP-Ewsr1b in the cytoplasm at 6 hpf. In time-lapse imaging, the fusion of two GFP-Ewsr1b droplets was observed, whereas the GFP-Syncrip droplets did not fuse and remained in place (Fig. 21B). In FRAP, GFP-Ewsr1b recovered fluorescence more quickly and strongly after fluorescence bleaching compared to GFP-Syncrip (Fig. 21C and D). These results suggest that GFP-Syncrip formed more solid-like aggregates, whereas GFP-Ewsr1b formed more liquid-like droplets, restictively. I found that Syncrip bound to *pou5f3* RNA granules and was involved in translational repression and that Ewsr1b bound to *pou5f3* RNA granules and was involved in translational activation. These results suggest that RBPs exhibit distinct dynamics within the cell and the properties of RBPs affect the state and translational activity of RNA granules.

DISCUSSION

Translational repression of dormant mRNAs by Syncrip in zebrafish embryo

Previous research showed that Syncrip represses translation of target neuronal mRNAs, which is mediated with specific miRNAs in mammals (Svitkin et al., 2013; Hobor et al., 2018; Khudayberdiev at al., 2020). However, the function of Syncrip during early development was unknown. I showed that the amount of Syncrip gradually decreased during early stages of development (Fig. 9). Syncrip was colocalized with *pou5f3* RNA granules at 0 hpf, but the colocalization sites were decreased at 3 hpf (Fig. 10). Interestingly, over-expression of Syncrip repressed *pou5f3* mRNA translation (Fig. 11). Furthermore, immunoprecipitation followed by mass spectrometry analysis revealed that Syncrip interacted with various proteins involved in translational regulation such as Ccr4-Not complex protein (Cnot1) and Igf2bp3 (Fig. 12D). The Ccr4-Not complex is a regulator of global mRNA metabolism in eukaryotic cells that is most well-known to repress translation by deadenylation (Collart et al., 2023). Since over-expression of Syncrip inhibited poly(A) tail elongation of *pou5f3* mRNA (Fig. 11D), Syncrip would interact with Ccr4-Not complex and repress translation of target mRNAs by deadenylation. Previous research showed that Igf2bp3 is an important regulator of maternal mRNA stability in zebrafish (Ren et al., 2020). These results suggest that Syncrip is a crucial RBP for the regulation of mRNA translation in early embryos. Furthermore, recent research showed that Syncrip is one of the key factors in mRNA-RBP interactions through the mRNA life cycle (Choi et al., 2024). Future studies such as the interactions between Syncrip, miRNA and Ccr4-Not complex or other partner proteins will be interesting to approach the more detailed mechanism of translational regulation.

Diverse functions of Ewsr1b on translational regulation, protein function, and early development

Ewsr1b is one of the FET family proteins that is related to diverse cellular processes such as DNA repair, RNA splicing, and cellular signal transduction (Schwartz et al., 2015; Lee et al., 2018). Previous research showed that EWSR1 binds to 3' UTR of target mRNAs (Hoell et al., 2011). However, the role of Ewsr1b in translational regulation and early embryogenesis was unclear. I found that Ewsr1b was localized in both the nucleus and cytoplasm (Fig. 13G). Since previous research showed that EWSR1 was normally expressed in the nucleus (Andresson et al., 2008), this was an intriguing result. In the cytoplasm, Ewsr1b was colocalized with *pou5f3* RNA granules (Fig. 14C and E) and formed liquid-like assemblies in the cytoplasm (Fig. 17D). Protein-RNA interactions are important for liquid-liquid phase separation (Maharana et al., 2018; Zeke et al., 2022; Vries et al., 2024). These results indicate that the molecular property of Ewsr1b in the cytoplasm is involved in the changes of the state of RNA granules shown in chapter I. In the nucleus, Ewsr1b was colocalized with Pou5f3 protein (Fig. 14F-H). Previous research demonstrated that EWSR1 regulates the transcriptional activity of human Oct4, a homolog of zebrafish Pou5f3, in the nucleus (Araya et al., 2003; Lee et al., 2005; Kovar et al., 2011). My results suggest that Ewsr1b also plays a role in regulating the transcriptional activity of Pou5f3 in the nucleus of zebrafish embryos. Furthermore, knockdown of Ewsr1b induced abnormal embryogenesis (Fig. 15). Previous research reported that zebrafish *fus,* a member of FET family genes, morphants display defects in motoneurons and impaired locomotion (Armstrong and Drapeau, 2013). *Ewsr1b* morphants in this study also displayed significant neuronal abnormalities and impairment of locomotion (Fig. 15). Since the various mutations of FET family proteins are involved in neurodegenerative disease, phenotypes of morphants reflect neurodegeneration. These results indicate that

Ewsr1b is a multifunctional protein, which regulates translation, protein function, and early development. Future studies such as the analysis using conditional knockout lines of *ewsr1b* and analysis of other target mRNAs are needed to explore the function of Ewsr1b in translational regulation during early development.

Previous research showed that FET family proteins function in the nucleus and are primarily localized in the nucleus (Andresson et al., 2008; Tan and Manley, 2009). They are largely soluble in the nucleus but form solid pathological aggregates when mis-localized to the cytoplasm that has been linked to stress granule assembly and neurodegenerative diseases (Daigle et al., 2013; Patel et al., 2015; Molliex et al., 2015; Mateju et al., 2017). However, Ewsr1b was localized in both the nucleus and cytoplasm (Fig. 13G) in liquid-like state (Fig. 21). These results indicate that Ewsr1b performs novel functions in early zebrafish embryos.

Alternative 3' UTR of *ewsr1b* mRNA and multifunction of Ewsr1b

Ewsr1b and other FET family proteins are known to be expressed and function in the nucleus, so there have been many studies on their roles in the nucleus, such as transcriptional regulation, RNA splicing, and DNA damage responses (Schwartz et al., 2015; Shao et aal., 2023: Kim et al., 2024). Interestingly, Ewsr1b was expressed in both the nucleus and cytoplasm in early zebrafish embryos (Fig. 13F), suggesting the importance of their functions in a cell of embryos. I hypothesized that there would be the molecular mechanisms that enable Ewsr1b to exert its diverse functions. mRNA alternative 3' UTR is important in regulating the function of synthesized protein (Mayr, 2019; Mitschka and Mayr, 2022). About half of human genes generate mRNA transcripts that differ in the length of 3' UTRs, although these transcripts produce the same protein (Mayr and Bartel, 2009; Lianoglou et al., 2013). Alternative 3' UTRs can regulate the synthesis

and localizations of their encoded proteins through several mechanisms, including modulation of mRNA export, mRNA stability and mRNA translation rates (Navarro et al., 2021; Gasparski et al., 2023). RBPs and miRNAs can differentially bind and regulate transcripts with different lengths of 3' UTR. FUS and ELAV-like proteins target mRNA stability in a 3' UTR-dependent manner, resulting in the stable expression of alternative transcripts (Yokoi et al., 2017). The functions of the human ubiquitin ligase BIRC3 are regulated through 3' UTR-mediated protein complex formation (Lee et al., 2019).

3'-end RNA seq analysis in zebrafish embryo revealed that *ewsr1b* mRNA has two transcript variants with alternative 3' UTR: 3' UTR-Long mRNA and 3' UTR-Short mRNA (Fig. 16A). The timing of translational activation and mRNA localization in a cell are different between 3' UTR-Long mRNA and 3' UTR-Short mRNA (Figs. 16B-G and 17E-G). Furthermore, the protein synthesized from 3' UTR-Long mRNA was localized in the nucleus and interacted with Pou5f3 protein, whereas the protein synthesized from 3' UTR-Short mRNA was localized in the cytoplasm and bound to mRNA (Fig. 17B and C). These results indicate that the lengths of 3' UTR determine the timing of translation and the localization of mRNA and localization and function of synthesized protein. Furthermore, knockdown of 3' UTR-Long mRNA inhibited the Ewsr1b protein synthesis that localized in the nucleus (Fig. 18). In addition, I showed that Importin beta-1 bound to *ewsr1b* mRNA 3' UTR by IP/RT-PCR and double staining of 3' UTR and Importin beta-1 (Fig.19), although whether the binding is direct or via other molecules remains explored. Furthermore, PLA analysis revealed that Importin beta-1 interacted with Ewsr1b and transported it to the nucleus (Fig. 19). To understand the function of Importin beta-1 in more detail, further analysis such as functional inhibition of importin beta-1 is required. These results suggest that long 3' UTR of *ewsr1b* has function as a nurturing niche with recruited proteins for regulating the localization and function of nascent proteins. These

results also suggest that there are differences in proteins that bind to mRNA between 3' UTR-Long and Short mRNA.

Previous research showed that alternative 3' UTR isoforms are expressed in a highly gene-specific and cell-type-specific manner (Lianoglou et al., 2013) and associated with various phenomena such as cancer, T cell activation, and oocyte maturation (Mayr and Bartel, 2009; Yang et al., 2017; Chan et al., 2022; Blake et al., 2024; Wang et al., 2024). However, the function of alternative 3' UTR in translational regulation during early development is unknown. In this study, I found that translational regulation via the length of 3' UTR is also important during embryogenesis. The synthesis of proteins with different functions and localizations from mRNAs of a single gene that depends on the length of 3' UTR will be useful in controlling spatial, temporal, and stage- and tissue-specific gene expression in the embryo. Multi-UTR genes generate mRNA isoforms with short 3' UTRs or long 3' UTRs, such as the *ewsr1b* mRNA in this study. mRNA processing at proximal or distal polyadenylation sites in terminal exons generates mRNA isoforms with short 3' UTRs or long 3' UTRs. However, *ewsr1b* mRNA has only distal polyadenylation site, not proximal polyadenylation site to generate 3' UTR-Short mRNA (Fig. 16A). Future studies need to address what is the molecular mechanism by which 3' UTR-Long mRNA and 3' UTR-Short mRNA are produced and how many mRNAs have alternative 3' UTR.

Post-translational modifications (PTMs) are chemical changes that can direct protein localization. PTMs can occur at any time during protein synthesis and release from the ribosome, and can affect a protein's structure, dynamics, localization, and function (Zhong et al., 2023). For example, arginine methylation of FUS or EWSR1 causes it to accumulate in the cytoplasm and prevents its nuclear functions (Belyanskaya et al., 2003; Araya et al., 2005; Dormann et al., 2012; Tradewell et al., 2012; Scaramuzzino et al., 2013; Hofweber et al., 2018). My result illustrated that there was no significant difference in apparent

molecular weight between the proteins synthesized from the 3' UTR-Long and 3' UTR-Short mRNA (Fig. 17C). It remains unknown whether there are any differences in PTMs between synthesized proteins from 3' UTR-Long and Short mRNA. Previous research revealed the importance of RNA secondary structure in regulating RNA granule assembly, phase separation and translational activity (Langdon et al., 2018; Fernandez-Moya et al., 2021; Wang and Xu, 2024). Furthermore, previous research showed that dynamics in maternal mRNA 3' UTR structures regulate early zebrafish embryogenesis (Beaudoin et al., 2018; Shi et al., 2020). In these studies, the dynamic structural changes in the 3' UTR of maternal mRNAs were revealed, detecting an opening in the 3' UTR structure immediately after fertilization and a gradual close during cleavage stages, followed by a reopening after the zygotic genome activation. Are there any differences in secondary structure between 3' UTR-Long and Short mRNA? Future detailed studies such as analysis of proteins that bind to 3' UTR-Long and Short mRNA, molecular mechanism of production of alternative 3' UTR, PTMs of synthesized proteins, and RNA secondary structure are important for elucidating the functions of alternative 3' UTRs in translational regulation during early development.

Protein degradation after fertilization affect translational regulation

I found that the translation of *ewsr1b* 3' UTR-Short mRNA was activated immediately after fertilization (Fig. 16B and C), and my question was what mechanism activates translation. The oocyte-to-embryo transition (OET) is one of the most dynamic developmental transitions and regulated by maternal products stored in the oocyte. The protein degradation associated with OET was mediated via the embryonic ATP pathway and crucial for zebrafish embryogenesis (Dutta and Shinha, 2017). Previous research demonstrated that maternal mRNAs are remodeled during the zebrafish OET. The

solubility phase transition of maternal mRNAs occurred during OET (Hwang et al., 2023). One hypothesis is that protein degradation after fertilization results in the degradation of proteins involved in translational repression and *ewsr1b* 3' UTR-Short mRNA translation is activated. The injection of proteasome inhibitor MG132 did not inhibit mitotic cleavages but inhibited the Ewsr1b synthesis at 1 hpf (Fig. 20A-D) and the poly(A) tail elongation of *ewsr1b* 3' UTR-Short mRNA (Fig. 20E). These results suggest that the proper protein degradation after fertilization is important for translational regulation. Future studies such as RNA-seq analysis of mRNAs whose translational activity is affected by MG132 injection are needed to clarify the significance of protein degradation.

The importance of physical properties of molecules in translation

The functions and behavior of intracellular proteins are exerted by the cooperation of "structural domains" and "unstructured domains; intrinsically disordered regions (IDRs)." The role of unstructured domains was not understood for a long time, but in recent years, they have been brought into the spotlight after reports of liquid-liquid phase separation and the formation of RNA granules. IDRs are not "meaningless because they have no structure," but are important precisely because they have no structure. RNA granules have been proposed to assemble by forming solid RNA/protein aggregates or through phase separation into a liquid RNA/protein phase through IDRs (Tauber et al., 2020; Ripin and Parker, 2023). Previous research reported that zebrafish Rbm14 functions in RNP compartments through phase separation to regulate RNA metabolism and dorsoventral patterning (Xiao et al., 2019), and zebrafish Ddx3xb regulates maternal mRNA translation efficiency in a condensation-dependent manner (Shi et al., 2022). Since both Rbm14 and Ddx3xb contain IDRs and undergo phase separation, the physical properties of RBPs through their IDRs are important for zebrafish embryogenesis and translational regulation.

Furthermore, recent research showed that eukaryotic initiation factor eIF4B undergoes self-association through its IDRs and regulates its function in translation (Swain et al., 2024). Syncrip and Ewsr1b also contain IDRs (Fig. 21A). However, the physical properties of molecules were different (Fig. 21B and C). Syncrip is involved in translational repression, whereas Ewsr1b is involved in translational activation. Since the state of *pou5f3* RNA granules is changed from solid-like state to liquid-like state when translation is activated, the properties and functions of proteins that compose RNA granules are related to the properties and translational activity of RNA granules.

Previous studies showed that protein-RNA, RNA-RNA, and protein-protein interaction are crucial for regulating dynamics, phase separation and function of biomolecular condensates (Wang et al., 2018; Wadsworth et al., 2023; Vries et al., 2024; Wang and Xu, 2024; Trussina et al., 2025). Future studies on not only RNA-protein, but also RNA-RNA and protein-protein interactions are needed for a deeper understanding of the molecular properties and functions of RNA granules.

GENERAL DISCUSSION

The temporal and spatial control of global translation has been shown to be crucial for the proper promotion of processes before and after fertilization. Previous research on translational regulation during oocyte maturation showed that regulatory mechanism via assembly and disassembly of RNA granules is important for mRNA translation (Kotani et al., 2013; Horie and Kotani, 2016; Takei et al., 2021). However, the mechanisms by which translation of the dormant mRNAs is temporally and spatially controlled after fertilization remain largely unresolved.

In zebrafish, Pou5f3 protein synthesis from *pou5f3* mRNA is important for diverse developmental processes, such as zygotic genome activation, ventral specification, endoderm formation, and neurogenesis (Belting et al., 2001; Hauptmann et al., 2002; Reim and Brand, 2006; Lachnit et al., 2008; Onichtchouk et al.,2010; Lee et al., 2013; Veli et al., 2019; Inomata et al., 2020). However, how the translation of *pou5f3* mRNA is regulated during embryogenesis remains unknown. In chapter I, I analyzed the molecular mechanism of *pou5f3* mRNA translation. Previous research in our laboratory showed that *pou5f3* mRNA forms granular structures in oocytes and embryos. I found that Pou5f3 protein was accumulated after fertilization while maintaining RNA granular structures and that nascent Pou5f3 was synthesized in the RNA granules (Figs. 1-7). These results suggest that *pou5f3* embryonic RNA granules function as the site of translational activation and protein synthesis. Furthermore, I showed that the change in the state of RNA granules is linked to translational activity within RNA granules (Fig. 8). This *pou5f3* embryonic RNA granule functions as activation sites of translation after changing physical properties. These findings provide previously unknown molecular mechanisms by which the translation of dormant mRNAs is temporally and spatially

regulated.

mRNA translation is mainly regulated by interactions between *cis*-acting elements of mRNAs and *trans*-acting factors such as RNA-binding proteins (RBPs). The functions of RBPs are important for translational regulation. In chapter II, I focused on Syncrip and Ewsr1b as proteins involved in translational regulation of *pou5f3* mRNA described in chapter I and performed functional analysis. I found that the amount of Syncrip was decreased during early development and over-expression of Syncrip repressed *pou5f3* mRNA translation (Figs. 9-11). Furthermore, Syncrip interacted with other proteins involved in translational regulation such as Ccr4-Not complex protein (Fig. 12). These results suggest that Syncrip plays a key role in translational repression of *pou5f3* mRNA. Ewsr1b was accumulated during early stages of development and localized in the nucleus and cytoplasm (Fig. 13). Ewsr1b was colocalized with *pou5f3* RNA granules in the cytoplasm and Pou5f3 protein in the nucleus (Fig. 14). Knockdown of Ewsr1b reduced the amount of Pou5f3 protein and caused abnormal development (Fig. 15). These results indicate that Ewsr1b is involved in translational regulation of mRNA, functional regulation of protein, and embryogenesis. I investigated the underlying molecular mechanism that enables Ewsr1b to perform such diverse functions. Two transcript variants of *ewsr1b* mRNA with different lengths of 3' UTR were expressed in the zebrafish embryo: 3' UTR-Long mRNA and 3' UTR-Short mRNA (Fig.16). Surprisingly, the translational timing, the mRNA localization, and localizations and functions of synthesized proteins were different between 3' UTR-Long mRNA and 3' UTR-Short mRNA (Figs. 16-17). My results suggest that long 3' UTR of *ewsr1b* has function as a nurturing niche with recruited proteins for regulating the localization and function of nascent proteins (Figs. 18-19). These results reveal the importance of

alternative mRNA 3' UTR in translational regulation, proper protein localization, and protein function during early development. Surprisingly, proper protein degradation after fertilization is a crucial factor for translational activation of 3' UTR-Short mRNA (Fig. 20). Since mRNA with short 3' UTR greatly lacks regulatory elements in 3' UTR controlling translation, including sites for RBPs and miRNA binding, protein degradation system may be an important trigger for translational activation. Furthermore, the molecular properties of Syncrip and Ewsr1b in a cell were different (Fig. 21). This result indicates that the state and the translational activity of *pou5f3* embryonic RNA granules are regulated by the property and function of RBPs. RNA granules are composed of RNA and RBPs, and their crosstalk through co-phase separation regulates physical property, function and translation of RNA granules.

Protein synthesis from maternal transcripts in the early stage of embryos is essential for progression of embryo development (Aanes et al., 2011; Zhang et al., 2022; Yang et al., 2024). Although thousands of maternal transcripts were shown to be translated after fertilization (Winata et al., 2018), little is known about the mechanisms of translational regulation of each maternal mRNA during embryogenesis. Thus, the molecular mechanism of translational regulation described in this research (Fig. 22) will contribute to understanding the spatial and temporal regulatory mechanisms of mRNA translation during early development. Since membrane-less organelles including RNA granules are linked to various biological phenomena such as phase separation, memory, development, and disease (Buchan, 2011; Nakayama et al., 2017; Shiina, 2019; Tauber et al., 2020; Ripin and Parker, 2023), this research will contribute to a wide range of research. I revealed that the temporal regulation of translation that depends on the length of 3' UTR drives embryogenesis (Fig. 22). This finding provides a new

perspective on the function of mRNA 3' UTR and early development and will lead to the advancements in these research fields. Furthermore, EWSR1 is linked to neurodegenerative disease. I believe that this study will also contribute to elucidating the pathology of diseases and establishing treatment methods.

Copyright Licensing

REFERENCES

Aanes, H., Winata, C. L., Lin, C. H., Chen, J. P., Srinivasan, K. G., Lee, S. G. P., Lim, A. Y. M., Hajan, H. S., Collas, P., Bourque, G., Gong, Z., Korzh, V., Aleström, P., and Mathavan, S. (2011). Zebrafish mRNA sequencing deciphers novelties in transcriptome dynamics during maternal to zygotic transition. *Genome Research*, *21*, 1328–1338. https://doi.org/10.1101/gr.116012.110

Anderson, P., and Kedersha, N. (2009). RNA granules: post-transcriptional and epigenetic modulators of gene expression. *Nature Reviews Molecular Cell Biology*, *10*, 430-436. https://doi.org/10.1038/nrm2694

Andresson, M. K., Stahlberg, A., Arvidsson, A., Olofsson, A., Semb, H., Stenman, G., Nilsson, O., and Aman, P. (2008). The multifunctional FUS, EWS and TAF15 proto-oncoproteins show cell type-specific expression patterns and involvement in cell spreading and stress response. *BMC Cell Biology*, *9*, 37. https://doi.org/10.1186/1471-2121-9-37

Araya, N., Hiraga, H., Kako, K., Arao, Y., Kato, S., and Fukamizu, A. (2005). Transcriptional down-regulation through nuclear exclusion of EWS methylated by PRMT1. *Biochemical and Biophysical Research Communications*, *329*, 653-660. https://doi.org/10.1016/j.bbrc.2005.02.018

Araya, N., Hirota, K., Shimamoto, Y., Miyagishi, M., Yoshida, E., Ishida, J., Kaneko, S., Kaneko, M., Nakajima, T., and Fukamizu, A. (2003). Cooperative interaction of EWS with CREB-binding protein selectively activates hepatocyte nuclear factor 4-mediated transcription. *Journal of Biological Chemistry*, *278*, 5427-5432. https://doi.org/10.1074/jbc.M210234200

Azuma, M., Embree, L. J., Sabaawy, H., and Hickstein, D. D. (2007). Ewing Sarcoma Protein Ewsr1 Maintains Mitotic Integrity and Proneural Cell Survival in the Zebrafish Embryo. *PLoS ONE*, *2*, e979. https://doi.org/10.1371/journal.pone.0000979

Baade, I., Hutten, S., Sternburg, E. L., Pörschke, M., Hofweber, M., Dormann, D., and Kehlenbach, R. H. (2021). The RNA-binding protein FUS is chaperoned and imported into the nucleus by a network of import receptors. *Journal of Biological Chemistry*, *296*, 100659. https://doi.org/10.1016/j.jbc.2021.100659

Bannai, H., Fukatsu, K., Mizutani, A., Natsume, T., Iemura, S., Ikegami, T., Inoue, T., and Mikoshiba, K. (2004). An RNA-interacting protein, SYNCRIP (heterogeneous nuclear ribonuclear protein Q1/NSAP1) is a component of mRNA granule transported with inositol 1,4,5-trisphosphate receptor type 1 mRNA in neuronal dendrites. *Journal of Biological Chemistry*, *279*, 53427-53434. https://doi.org/10.1074/jbc.M409732200

Barkoff, A. F., Dickson, K. S., Gray, N. K. and Wickens, M. (2000). Translational control of cyclin B1 mRNA during meiotic maturation: coordinated repression and cytoplasmic polyadenylation. *Developmental Biology*, *220*, 97-109. https://doi.org/10.1006/dbio.2000.9613

Beaudoin, J., Novoa, E. M., Vejnar, C. E., Yartseva, V., Takacs, C. M., Kellis, M., and Giraldez, A. J. (2018). Analyses of mRNA structure dynamics identify embryonic gene regulatory programs. *Nature Structural and Molecular Biology*, 25, 677-686. https://doi.org/10.1038/s41594-018-0091-z

Belting, H.G., Hauptmann, G., Meyer, D., Abdelilah-Seyfried, S., Chitnis, A., Eschbach, C., Soll, I., Thisse, C., Thisse, B., Artinger, K.B., et al. (2001). S*piel*

ohne grenzen/*pou2* is required during establishment of the zebrafish midbrainhindbrain boundary organizer. *Development*, *128*, 4165–4176. https://doi.org/10.1242/dev.128.21.4165

Belting, H.G., Wendik, B., Lunde, K., Leichsenring, M., Mossner, R., Driever, W., and Onichtchouk, D. (2011). Pou5f1 contributes to dorsoventral patterning by positive regulation of vox and modulation of fgf8a expression. *Developmental Biology*, *356*, 323–336. https://doi.org/10.1016/j.ydbio.2011.05.660

Belyanskaya, L. L., Delattre, O., and Gehring, H. (2003). Expression and subcellular localization of Ewing sarcoma (EWS) protein is affected by the methylation process. *Experimental Cell Research*, *288*, 374-381. https://doi.org/10.1016/S0014-4827(03)00221-0

Blake, D., Gazzara, M. R., Breuer, I., Ferretti, M., and Lynch, K. W. (2024). Alternative 3′UTR expression induced by T cell activation is regulated in a temporal and signal dependent manner. *Scientific Reports*, *14*, 10987. https://doi.org/10.1038/s41598-024-61951-1

Buchan, J.R., and Parker, R. (2009). Eukaryotic stress granules: the ins and outs of translation. *Molecular Cell*, *36*, 932–941. https://doi.org/10.1016/j.molcel.2009.11.020

Buchan, J. R. (2011). mRNP granules: Assembly, function, and connections with disease. *RNA Biology*, *11*, 1-12. https://doi.org/10.4161/15476286.2014.972208

Buxbaum, A.R., Haimovich, G., and Singer, R.H. (2015). In the right place at the right time: visualizing and understanding mRNA localization. *Nature Reviews Molecular Cell Biology*, *16*, 95–109. https://doi.org/10.1038/nrm3918

Chan, J. J., Zhang, B., Chew, X. H., Salhi, A., Kwok, Z. H., Lim, C. Y., Desi, N.,

Subramaniam, N., Siemens, A., Kinanti, T., Ong, S., Sanchez-Mejias, A., Ly, P. T., An, O., Sundar, R., Fan, X., Wang, S., Siew, B. E., Lee, K. C., Chong, C. S., Lieske, B., Cheong, W., Goh, Y., Fam, W. N., Ooi, M. G., Koh, B., Lyer, S. G., Ling, W. H., Chen, J., Yoong, B., Chanwat, R., Bonney, G. K., Goh, B., Zhai, W., Fullwood, M. J., Wang, W., Tan, K., Chng, W. J., Dan, Y. Y., Pitt, J, J., Roca, X., Guccione, E., Vardy, L. H., Chen, L., Gao, X., Chow, P., Yang, H., and Tay, Y. (2022). Pan-cancer pervasive upregulation of 3′ UTR splicing drives tumourigenesis. *Nature Cell Biology*, *24*, 928-939. https://doi.org/10.1038/s41556-022-00913-z

Charlesworth, A., Cox, L.L., and MacNicol, A.M. (2004). Cytoplasmic polyadenylation element (CPE)- and CPE-binding protein (CPEB)-independent mechanisms regulate early class maternal mRNA translational activation in *Xenopus* oocytes. *Journal Biological Chemistry*, *279*, 17650–17659. https://doi.org/10.1074/jbc.m313837200

Chen, J., Melton, C., Suh, N., Oh, J.S., Horner, K., Xie, F., Sette, C., Blelloch, R., and Conti, M. (2011). Genome-wide analysis of translation reveals a critical role for deleted in azoospermia-like (Dazl) at the oocyte-to-zygote transition. *Genes and Development*, *25*, 755–766. https://doi.org/10.1101/gad.2028911

Choi, Y., Um, B., Na, Y., Kim, J., Kim, J. S., and Kim, V. N. (2024). Time-resolved profiling of RNA binding proteins throughout the mRNA life cycle. *Molecular Cell*, *84*, 1764-1782. https://doi.org/10.1016/j.molcel.2024.03.012

Chook, Y. M., and Süel, K. E. (2011). Nuclear import by karyopherin-βs: recognition and inhibition. *Biochimica et Biophysica Acta*, *1813*, 1593-1606. https://doi.org/10.1016/j.bbamcr.2010.10.014

Chouaib, R., Safieddine, A., Pichon, X., Imbert, A., Kwon, O.S., Samacoits, A., Traboulsi, A.M., Robert, M.C., Tsanov, N., Coleno, E., et al. (2020). A dual protein-mRNA localization screen reveals compartmentalized translation and widespread co-translational RNA targeting. *Developmental Cell*, *54*, 773–791. https://doi.org/10.1016/j.devcel.2020.07.010

Collart, M. A., Audebert, L., and Bushell, M. (2023). Roles of CCR4-Not complex in translation and dynamics of co-translation events. *WIREs RNA*, *15*, e2187. https://doi.org/10.1002/wrna.1827

Conti, M., and Kunitomi, C. (2023). A genome-wide perspective of the maternal mRNA translation program during oocyte development. *Seminars in Cell and Developmental Biology*, *154*, 88-98. https://doi.org/10.1016/j.semcdb.2023.03.003

Corley, M., Burns, M. C., and Yeo, G. W. (2020). How RNA-Binding Proteins Interact with RNA: Molecules and Mechanisms. *Molecular Cell*, *78*, 9-29. https://doi.org/10.1016/j.molcel.2020.03.011

Daigle, J. B., Lanson, N. A., Smith, R. B., Casci, I., Maltare, A., Monaghan, J., Nichols, C. D., Kryndushkin, D., Shewmaker, F., and Pandey, U. B. (2013). RNA-binding ability of FUS regulates neurodegeneration, cytoplasmic mislocalization and incorporation into stress granules associated with FUS carrying ALS-linked mutations. *Human Molecular Genetics*, *15*, 1193-1205. https://doi.org/10.1093/hmg/dds526

David, A., Dolan, B.P., Hickman, H.D., Knowlton, J.J., Clavarino, G., Pierre, P., Bennink, J.R., and Yewdell, J.W. (2012). Nuclear translation visualized by ribosome-bound nascent chain puromycylation. *Journal of Cell Biology*, *197*, 45–57. https://doi.org/10.1083/jcb.201112145

Despic, V., Dejung, M., Gu, M., Krishnan, J., Zhang, J., Herzel, L., Straube, K., Gerstein, M. B., Butter, F., and Neugebauer, K. M. (2017). Dynamic RNA-protein interactions underlie the zebrafish maternal-to-zygotic transition. *Genome Research*, *27*, 1184-1194. https://doi.org/10.1101/gr.215954.116

Dormann, D., Madl, T., Valori, C. F., Bentmann, E., Tahirovic, S., Abou-Ajram, C., Kremmer, E., Ansorge, Mackenzie, I., Neumann, M., and Haass, C. (2012). Arginine methylation next to the PY-NLS modulates Transportin binding and nuclear import of FUS. *EMBO Journal*, *31*, 4258-4275. https://doi.org/10.1038/emboj.2012.261

Duning, K., Buck, F., Barnekow, A., and Kremerskothen, J. (2008). SYNCRIP, a component of dendritically localized mRNPs, binds to the translation regulator BC200 RNA. *Journal of Neurochemistry*, *105*, 351-359. https://doi.org/10.1111/j.1471-4159.2007.05138.x

Dutta, A., and Sinha, D. K. (2017). Zebrafish lipid droplets regulate embryonic ATP homeostasis to power early development. *Open Biology*, *7*, 170063. https://doi.org/10.1098/rsob.170063

Enam, S.U., Zinshteyn, B., Goldman, D.H., Cassani, M., Livingston, N.M., Seydoux, G., and Green, R. (2020). Puromycin reactivity does not accurately localize translation at the subcellular level. *eLife*, *9*, e60303. https://doi.org/10.7554/elife.60303

Fernandez-Moya, S. M., Ehses, J., Bauer, K. E., Schieweck, R., Chakrabarti, A. M., Lee, F., Illig, C., Luscombe, N. M., Harner, M., Ule, J., and Kiebler, M. A. (2021). RGS4 RNA Secondary Structure Mediates Staufen2 RNP Assembly in Neurons. *International Journal of Molecular Sciences*, *22*, 13021.

https://doi.org/10.3390/ijms222313021

Francesco, L. D., Verrico, A., Asteriti, I. A., Rovella, P., Cirigliano, P., Guarguaglini, G., Schinina, M. E., and Lavia, P. (2018). Visualization of human karyopherin beta-1/importin beta-1 interactions with protein partners in mitotic cells by co-immunoprecipitation and proximity ligation assay. *Scientific Reports*, *8*, 1850. https://doi.org/10.1038/s41598-018-19351-9

Gasparski, A. N., Moissoglu, K., Pallikkuth, S., Meydan, S., Guydosh, N. R., and Mili, S. (2023). mRNA location and translation rate determine protein targeting to dual destinations. *Molecular Cell, 83*, 2726-2738. https://doi.org/10.1016/j.molcel.2023.06.036

Groisman, I., Huang, Y.S., Mendez, R., Cao, Q.P., Theurkauf, W., and Richter, J.D. (2000). *CPEB*, *Maskin*, and *cyclin B1* mRNA at the mitotic apparatus. *Cell*, *103*, 435–447. https://doi.org/10.1016/s0092-8674(00)00135-5

Groisman, I., Jung, M.Y., Sarkissian, M., Cao, Q., and Richter, J.D. (2002). Translational control of the embryonic cell cycle. *Cell*, *109*, 473–483. https://doi.org/10.1016/s0092-8674(02)00733-x

Harvey, S.A., Sealy, I., Kettleborough, R., Fenyes, F., White, R., Stemple, D., and Smith, J.C. (2013). Identification of the zebrafish maternal and paternal transcriptomes. *Development*, *140*, 2703–2710. https://doi.org/10.1242/dev.095091

Hauptmann, G., Belting, H., Wolke, U., Lunde, K., Soli, I., Abdelilah-Seyfried, S., Prince, V., and Driver, W. (2002). *spiel ohne grenzen/pou2* is required for zebrafish hindbrain segmentation. *Development*, *129*, 1645-1655. https://doi.org/10.1242/dev.129.7.1645

Hentze, M. W., Castello, A., Schwarzl, T., and Preiss, T. (2018). A brave new world of RNA-binding proteins. *Nature Reviews and Molecular Cell Biology*, *19*, 327–341. https://doi.org/10.1038/nrm.2017.130

Herei, A., and Forbes, D. J. (2004). Importin beta: conducting a much larger cellular symphony. *Molecular Cell*, *16*, 319-330. https://doi.org/10.1016/j.molcel.2004.10.026

Hirose, T., Ninomiya, K., Nakagawa, S., and Yamazaki, T. (2023). A guide to membraneless organelles and their various roles in gene regulation. *Nature Reviews Molecular Cell Biology*, *24*, 288-304. https://doi.org/10.1038/s41580-022-00558-8

Hobor, F., Dallmann, A., Ball, N. J., Cicchini, C., Battistelli, C., Ogrodowicz, R. W., Christodoulou, E., Martin, S. R., Castello, A., Tripodi, M., Taylor, I. A., and Ramos, A. (2018). A cryptic RNA-binding domain mediates Syncrip recognition and exosomal partitioning of miRNA targets. *Nature Communications*, *9*, 831. https://doi.org/10.1038/s41467-018-03182-3

Hobson, B.D., Kong, L., Hartwick, E.W., Gonzalez, R. L., and Sims, P.A. (2020). Elongation inhibitors do not prevent the release of puromycylated nascent polypeptide chains from ribosomes. *eLlife*, *9*, e60048. https://doi.org/10.7554/elife.60048

Hoell, J. I., Larsson, E., Runge, S., Nusbaum, J. D., Duggimpudi, S., Farazi, T. A., Hafner, M., Borkhardt, S., Sander, C., and Tuschl, T. (2011). RNA targets of wild-type and mutant FET family proteins. *Nature Structural and Molecular Biology*, *18*, 1428–1431. https://doi.org/10.1038/nsmb.2163

Hofweber, M., Hutten, S., Bourgeous, B., Spreitzer, E., Niedner-Boblenz, A.,

Schifferer, M., Ruepp, M., Simons, M., Niessing, D., Madl, T., and Dormann, D. (2018). Phase Separation of FUS Is Suppressed by Its Nuclear Import Receptor and Arginine Methylation. *Cell*, *173*, 706-719. https://doi.org/10.1016/j.cell.2018.03.004

Holehouse, A. S., and Kragelund, B. B. (2024). The molecular basis for cellular function of intrinsically disordered protein regions. *Nature Reviews Molecular Cell Biology*, *25*, 187-211. https://doi.org/10.1038/s41580-023-00673-0

Horie, M., and Kotani, T. (2016). Formation of *mos* RNA granules in the zebrafish oocyte that differ from *cyclin B1* RNA granules in distribution, density and regulation. *European Journal of Cell Biology*, *95*, 563–573. https://doi.org/10.1016/j.ejcb.2016.10.001

Howley, C., and Ho, R.K. (2000). mRNA localization patterns in zebrafish oocytes. *Mechanisms of Development*, *92*, 305–309. https://doi.org/10.1016/s0925-4773(00)00247-1

Hwang, H., Chen, S., Ma, M., Divyanshi., Fan, H., Borwick, E., Boke, E., Mei, W., and Yang, J. (2023). Solubility phase transition of maternal RNAs during vertebrate oocyte-to-embryo transition. *Developmental Cell*, *58*, 2776-2788. https://doi.org/10.1016/j.devcel.2023.10.005

Inomata, C., Yukikawa, T., Nakayama-Sadakiyo, Y., Kobayashi, K., Ikeda, M., Chiba, M., Konishi, C., Ishioka, A., Tsuda, S., and Yamasu, K. (2020). Involvement of an *Oct4*-related *PouV* gene, *pou5f3/pou2*, in neurogenesis in the early neural plate of zebrafish embryos. *Developmental Biology*, *457*, 30-42. https://doi.org/10.1016/j.ydbio.2019.09.002

Ivanov, P., Kedersha, N., and Anderson, P. (2019). Stress granules and processing

bodies in translational control. *Cold Spring Harbor Perspectives Biology*, *11*, a032813. https://doi.org/10.1101/cshperspect.a032813

Jain, S., Wheeler, J.R., Walters, R.W., Agrawal, A., Barsic, A., and Parker, R. (2016). ATPase modulated stress granules contain a diverse proteome and substructure. *Cell*, *164*, 487–498. https://doi.org/10.1016/j.cell.2015.12.038

Jambor, H., Surendranath, V., Kalinka, A.T., Mejstrik, P., Saalfeld, S., and Tomancak, P. (2015). Systematic imaging reveals features and changing localization of mRNAs in Drosophila development. *eLlife*, *4*, e05003. https://doi.org/10.7554/elife.05003

Jansova, D., Aleshkina, D., Jindrova, A., Iyyappan, R., An, Q., Fan, G., and Susor, A. (2021). Single molecule RNA localization and translation in the mammalian oocyte and embryo. *Journal of Molecular Biology*, *433*, 167166. https://doi.org/10.1016/j.jmb.2021.167166

Kane, D.A., and Kimmel, C.B. (1993). The zebrafish midblastula transition. *Development*, *119*, 447–456. https://doi.org/10.1242/dev.119.2.447

Kanekura, K., and Kuroda, M. (2022). How can we interpret the relationship between liquid-liquid phase separation and amyotrophic lateral sclerosis? *Laboratory Investigation*, *102*, 912–918. https://doi.org/10.1038/s41374-022-00791-x

Kapel, K., Martinez, F. J., and Yeo, W. Y. (2017). Genetic mutations in RNA-binding proteins and their roles in ALS. *Human Genetics*, *136*, 1193-1214. https://doi.org/10.1007/s00439-017-1830-7

Kato, M., Han, T. W., Xie, S., Shi, K., Du, X., Wu, L. C., Mirzaei, H., Goldsmith, E. J., Longgood, J., Pei, J., Grishin, N. V., Frantz, D. E., Schneider, J. W., Chen, S., Li, L., Sawaya, M. R., Eisenberg, D., Tycko, R., and Mcknight, S. L. (2012). Cell-free

formation of RNA granules: low complexity sequence domains form dynamic fibers within hydrogels. *Cell*, *149*, 753–767.

Khudayberdiev, S., Soutschek, M., Ammann, I., Heinze, A., Rust, M. B., Baumeister, S., and Schratt, G. (2020). The cytoplasmic SYNCRIP mRNA interactome of mammalian neurons. RNA Biology, 18, 1252-1264. https://doi.org/10.1080/15476286.2020.1830553

Kiebler, M.A., and Bassell, G.J. (2006). Neuronal RNA granules: movers and makers. *Neuron*, *51*, 685–690. https://doi.org/10.1016/j.neuron.2006.08.021.

Kim, Y. R., J, J., Lee, H. J., Kim, C., Park, J., Yu, Y. S., Kim, C. R., Lee, D, H., Cha, J., Kwon, H., Hanssen, K. M., Grunewald, T., Choi, M., Han, I., Bae, S., Jung, I., Shin, Y., and Baek, S. H. (2024). Prion-like domain mediated phase separation of ARID1A promotes oncogenic potential of Ewing's sarcoma. *Nature Communications*, *15*, 6569. https://doi.org/10.1038/s41467-024-51050-0

Kimura, M., and Imamoto, N. (2014). Biological significance of the importin-β family-dependent nucleocytoplasmic transport pathways. *Traffic*, *15*, 727-748. https://doi.org/10.1111/tra.12174

Kloc, M., Zearfoss, N.R., and Etkin, L.D. (2002). Mechanisms of subcellular mRNA localization. *Cell*, *108*, 533–544. https://doi.org/10.1016/s0092-8674(02)00651-7

Kondo, T., Kotani, T., and Yamashita, M. (2001). Dispersion of *cyclin B* mRNA aggregation is coupled with translational activation of the mRNA during zebrafish oocyte maturation. *Developmental Biology*, *229*, 421–431. https://doi.org/10.1006/dbio.2000.9990

Kotani, T., Maehata, K., and Takei, N. (2017). Regulation of translationally repressed mRNAs in zebrafish and mouse oocytes. *Results and Problems in Cell*

Differentiation, *63*, 297–324. https://doi.org/10.1007/978-3-319-60855-6_13

Kotani, T., Yasuda, K., Ota, R., and Yamashita, M. (2013). Cyclin B1 mRNA translation is temporally controlled through formation and disassembly of RNA granules. *Journal of Cell Biology*, *202*, 1041–1055. https://doi.org/10.1083/jcb.201302139

Kovar, H. (2011). Dr. Jekyll and Mr. Hyde: The Two Faces of the FUS/EWS/TAF15 Protein Family. *Sarcoma*, 837474. https://doi.org/10.1155/2011/837474

Kroschwald, S., Maharana, S., Mateju, D., Malinovska, L., Nuske, E., Poser, I., Richter, D., and Alberti, S. (2015). Promiscuous interactions and protein disaggregate determine the material state of stress-inducible RNP granules. *eLife*, *4*, e06807. https://doi.org/10.7554/elife.06807

Kroschwald, S., Maharana, S., and Simon, A. (2017). Hexanediol: a chemical probe to Investigate the material properties of membraneless compartments. *Matters*. https://doi.org/10.19185/matters.201702000010

Kumari, P., Gilligan, P.C., Lim, S., Tran, L.D., Winkler, S., Philp, R., and Sampath, K. (2013). An essential role for maternal control of Nodal signaling. *eLife*, *2*, e00683. https://doi.org/10.7554/elife.00683

Lachnit, M., Kur, E., and Driver, W. (2008). Alterations of the cytoskeleton in all three embryonic lineages contribute to the epiboly defect of Pou5f1/Oct4 deficient MZ*spg* zebrafish embryos. *Developmental Biology*, *315*, 1-17. https://doi.org/10.1016/j.ydbio.2007.10.008

Lecuyer, E., Yoshida, H., Parthasarathy, N., Alm, C., Babak, T., Cerovina, T., Hughes, T.R., Tomancak, P., and Krause, H.M. (2007). Global analysis of mRNA localization reveals a prominent role in organizing cellular architecture and

function. *Cell*, *131*, 174–187. https://doi.org/10.1016/j.cell.2007.08.003

Lee, J., Nguyen, P. T., Shim, H. S., Hyeon, S. J., Im, H., Choi, M., Chung, S., Kowall, N. W., Lee, S. B., and Ryu, H. (2018). EWSR1, a multifunctional protein, regulates cellular function and aging via genetic and epigenetic pathways. *Molecular Basis of Disease*, *1865*, 1938-1945. https://doi.org/10.1016/j.bbadis.2018.10.042

Lee, J., Rhee, B. K., Bae, G., Han, Y., and Kim, J. (2005). Stimulation of Oct-4 activity by Ewing's sarcoma protein. *Stem Cells*, *23*, 738-751. https://doi.org/10.1634/stemcells.2004-0375

Lee, M. T., Bonneau, A. R., Takacs, C. M., Bazzini, A. A., DiVito, K. R., Fleming, E. S., and Giraldez, A. J. (2013). Nanog, Pou5f1 and SoxB1 activate zygotic gene expression during the maternal-to-zygotic transition. *Nature*, *503*, 360–364. https://doi.org/10.1038/nature12632

Lee, S., and Mayr, C. (2019). Gain of Additional BIRC3 Protein Functions through 3'-UTR-Mediated Protein Complex Formation. *Molecular Cell*, *74*, 701-712. https://doi.org/10.1016/j.molcel.2019.03.006

Leichsenring, M., Maes, J., Mossner, R., Driever, W., and Onichtchouk, D. (2013). Pou5f1 transcription factor controls zygotic gene activation in vertebrates. *Science*, *341*, 1005–1009. https://doi.org/10.1126/science.1242527

Lippok, B., Song, S., and Driever, W. (2014). Pou5f1 protein expression and posttranslational modification during early zebrafish development. *Developmental Dynamics*, *243*, 468–477. https://doi.org/10.1002/ dvdy.24079

Lunde, K., Belting, H.G., and Driever, W. (2004). Zebrafish pou5f1/pou2, homolog of mammalian Oct4, functions in the endoderm specification cascade. *Current*

Biology, *14*, 48–55. https://doi.org/10. 1016/j.cub.2003.11.022

Luong, X.G., Daldello, E.M., Rajkovic, G., Yang, C.R., and Conti, M. (2020). Genome-wide analysis reveals a switch in the translational program upon oocyte meiotic resumption. *Nucleic Acids Research*, *48*, 3257–3276. https://doi.org/10.1093/nar/ gkaa010

MacNicol, M.C., Cragle, C.E., Arumugam, K., Fosso, B., Pesole, G., and MacNicol, A.M. (2015). Functional integration of mRNA translational control programs. *Biomolecules*, *5*, 1580–1599. https://doi.org/10.3390/biom5031580

Maharana, S., Wang, J., Papadopoulos, D. K., Richter, D., Pozniakovsky, A., Poser, I., Bickle, M., Rizk, S., Guillén-Boixet, J., Franzmann, T. M., Jahnel, M., Marrone, L., Chang, Y., Sterneckert, J., Tomancak, P., Hyman, A. A., and Alberti, S. (2018). RNA buffers the phase separation behavior of prion-like RNA binding proteins. Science, 360, 918-921. https://doi.org/10.1126/science.aar7366

Martin, K.C., and Ephrussi, A. (2009). mRNA localization: gene expression in the spatial dimension. *Cell*, *136*, 719–730. https://doi.org/10. 1016/j.cell.2009.01.044

Mateju, D., Franzmann, T. M., Patel, A., Kopach, A., Boczek, E. E., Maharana, S., Lee, H. O., Carra, S., Hyman, A. A., and Alberti, S. (2017). An aberrant phase transition of stress granules triggered by misfolded protein and prevented by chaperone function. *EMBO Journal*, *36*, 1669-1687. https://doi.org/10.15252/embj.201695957

Mateju, D., Eichenberger, B., Voigt, F., Eglinger, J., Roth, G., and Chao, J.A. (2020). Single-molecule imaging reveals translation of mRNAs localized to stress granules. *Cell*, *183*, 1801-1812. https://doi.org/10.1016/j.cell. 2020.11.010

Mayr, C. (2019). What Are 3' UTRs Doing? *Cold Spring Harbor Perspect Biology*, *11*,

a034728. https://doi.org/10.1101/cshperspect.a034728

Mayr, C. (2019). 3' UTRs Regulate Protein Functions by Providing a Nurturing Niche during Protein Synthesis. *Cold Spring Harbor Symposia on Quantitative Biology*, *84*, 95-104. https://doi.org/10.1101/sqb.2019.84.039206

Mayr, C., and Bartel, D. P. (2009). Widespread Shortening of 3′UTRs by Alternative Cleavage and Polyadenylation Activates Oncogenes in Cancer Cells. *Cell*, *138*, 673-684. https://doi.org/10.1016/j.cell.2009.06.016

McGrew, L. L., Dworkin-Rastl, E., Dworkin, M. B. and Richter, J. D. (1989). Poly(A) elongation during Xenopus oocyte maturation is required for translational recruitment and is mediated by a short sequence element. *Genes and Development*, *3*, 803-815. https://doi.org/10.1101/gad.3.6.803

Mendez, R., and Richter, J.D. (2001). Translational control by CPEB: a means to the end. *Nature Reviews Molecular Cell Biology*, *2*, 521–529. https://doi.org/10.1038/35080081

Mishima, Y., Fukao, A., Kishimoto, T., Sakamoto, H., Fujiwara, T., and Inoue, K. (2012). Translational inhibition by deadenylation-independent mechanisms is central to microRNA-mediated silencing in zebrafish. *PNAS*, *109*, 1104–1109. https://doi.org/10.1073/pnas. 1113350109

Mitschka, S., and Mayr, C. (2022). Context-specific regulation and function of mRNA alternative polyadenylation. Nature Reviews Molecular Cell Biology, 23, 779-796. https://doi.org/10.1038/s41580-022-00507-5

Mizutani, A., Fukuda, M., Ibata, K., Shiraishi, Y., and Mikoshiba, K. (2000). SYNCRIP, a cytoplasmic counterpart of heterogeneous nuclear ribonucleoprotein R, interacts with ubiquitous synaptotagmin isoforms. *Journal of Biological*

Chemistry, *275*, 9823-9831. https://doi.org/10.1074/jbc.275.13.9823

Moissoglu, K., Yasuda, K., Wang, T., Chrisafis, G., and Mili, S. (2019). Translational regulation of protrusion-localized RNAs involves silencing and clustering after transport. *eLife*, *8*, e44752. https:// doi.org/10.7554/elife.44752

Moon, S.L., Morisaki, T., Khong, A., Lyon, K., Parker, R., and Stasevich, T.J. (2019). Multicolour single-molecule tracking of mRNA interactions with RNP granules. *Nature Cell Biology*, *21*, 162–168. https://doi.org/10.1038/s41556-018-0263-4

Morales-Polanco, F., Bates, C., Lui, J., Casson, J., Solari, C.A., Pizzinga, M., Forte, G., Griffin, C., Garner, K.E., Burt, H.E., et al. (2021). Core Fermentation (CoFe) granules focus coordinated glycolytic mRNA localization and translation to fuel glucose fermentation. *iScience*, *24*, 102069. https://doi.org/10.1016/j.isci.2021.102069

Morohoshi, F., Ootsuka, Y., Arai, K., Ichikawa, H., Mitani, S., Munakata, N., and Ohki, M. (1998). Genomic structure of the human RBP56/hTAFII68 and FUS/TLS genes. *Gene*, *221*, 191-198. https://doi.org/10.1016/S0378-1119(98)00463-6

Nakayama, K., Ohashi, R., Shinoda, Y., Yamazaki, M., Abe, M., Fujikawa, A., Shigenobu, S., Futatsugi, A., Noda, M., Mikoshiba, K., Furuichi, T., Sakimura, K., and Shiina, N. (2017). RNG105/caprin1, an RNA granule protein for dendritic mRNA localization, is essential for long-term memory formation. eLife, 21, e29677. https://doi.org/10.7554/eLife.29677

Navarro, E., Mallén, A., and Hueso, M. (2021). Dynamic Variations of 3'UTR Length Reprogram the mRNA Regulatory Landscape. *Biomedicines*, *9*, 1560. https://doi.org/10.3390/biomedicines9111560

Nosella, M.L., and Forman-Kay, J.D. (2021). Phosphorylation-dependent regulation of

messenger RNA transcription, processing and translation within biomolecular condensates. *Current Opinion in Cell Biology*, *69*, 30–40. https://doi.org/10.1016/j.ceb.2020.12.007

Oldfield, C. J., and Dunker, A. D. (2014). Intrinsically Disordered Proteins and Intrinsically Disordered Protein Regions. *Annual Review of Biochemistry*, *83*, 553-584. https://doi.org/10.1146/annurev-biochem-072711-164947

Onichtchouk, D., Geier, F., Polok, B., Messerschmidt, M. D., Mössner, D., Wendik, B., Song, S., Taylor, V., and driver, W. (2010). Zebrafish Pou5f1-dependent transcriptional networks in temporal control of early development. *Molecular Systems Biology*, *6*, 354. https://doi.org/10.1038/msb.2010.9

Panasenko, O.O., Somasekharan, S.P., Villanyi, Z., Zagatti, M., Bezrukov, F., Rashpa, R., Cornut, J., Iqbal, J., Longis, M., Carl, S.H., Pena, C., Panse, V. G., and Collart, M. A. (2019). Cotranslational assembly of proteasome subunits in NOT1-containing assemblysomes. *Nature Structural and Molecular Biology*, *26*, 110–120. https://doi.org/10.1038/ s41594-018-0179-5

Passmore, L. A., and Coller, J. (2022). Roles of mRNA poly(A) tails in regulation of eukaryotic gene expression. *Nature Reviews Molecular Cell Biology*, *23*, 93-106. https://doi.org/10.1038/s41580-021-00417-y

Patel, A., Lee, H. O., Jawerth, L., Maharana, S., Jahnel, M.,Hein, M. Y., Stoynov, S., Mahamid, J., Saha, S., Franzmann, T. M., Pozniakovski, A., Poser, I., Maghelli, N., Royer, L. A., Weigert, M., Myers, E. W., Grill, S., Drechsel, D., and Hyman, A. A. (2015). A Liquid-to-Solid Phase Transition of the ALS Protein FUS Accelerated by Disease Mutation. *Cell*, *162*, 1066-1077. https://doi.org/10.1016/j.cell.2015.07.047

Perez-Camps, M., Tian, J., Chng, S. C., Sem, K. P., Sudhaharan, T., Teh, C., Wachsmuth, M., Korzh, V., Ahmed, S., and Reversade, B. (2016). Quantitative imaging reveals real-time Pou5f3–Nanog complexes driving dorsoventral mesendoderm patterning in zebrafish. *eLife*, *5*, e11475. https://doi.org/10.7554/eLife.11475

Pizzinga, M., Bates, C., Lui, J., Forte, G., MoralesPolanco, F., Linney, E., Knotkova, B., Wilson, B., Solari, C.A., Berchowitz, L.E., et al. (2019). Translation factor mRNA granules direct protein synthetic capacity to regions of polarized growth. *Journal of Cell Biology*, *218*, 1564–1581. https://doi.org/10.1083/jcb.201704019

Reim, G., and Brand, M. (2006). Maternal control of vertebrate dorsoventral axis formation and epiboly by the POU domain protein Spg/Pou2/ Oct4. *Development*, *133*, 2757–2770. https://doi. org/10.1242/dev.02391

Reim, G., Mizoguchi, T., Stainier, D.Y., Kikuchi, Y., and Brand, M. (2004). The POU domain protein spg (pou2/Oct4) is essential for endoderm formation in cooperation with the HMG domain protein casanova. *Developmental Cell*, *6*, 91–101. https://doi. org/10.1016/s1534-5807(03)00396-4

Ren, F., Lin, Q., Gong, G., Du, X., Dan, H., Qin, W., Miao, R., Xiong, Y., Xiao, R., Li, X., Gui, J., and Mei, J. (2020). Igf2bp3 maintains maternal RNA stability and ensures early embryo development in zebrafish. *Communications Biology*, *3*, 94. https://doi.org/10.1038/s42003-020-0827-2

Richter, J.D. (2007). CPEB: a life in translation. *Trends in Biochemical Sciences*, *32*, 279–285. https://doi. org/10.1016/j.tibs.2007.04.004

Richter, J.D., and Sonenberg, N. (2005). Regulation of cap-dependent translation by eIF4E inhibitory proteins. *Nature*, *433*, 477-480.

https://doi.org/10.1038/nature03205

Ripin, N., and Parker, R. (2023). Formation, function, and pathology of RNP granules. *Cell*, *186*, 4737-4756. https://doi.org/10.1016/j.cell.2023.09.006

Saitoh, A., Takada, Y., Horie, M., and Kotani, T. (2018). Pumilio1 phosphorylation precedes translational activation of its target mRNA in zebrafish oocytes. *Zygote*, *26*, 372–380. https://doi.org/10.1017/S0967199418000369

Scaramuzzino, C., Monaghan, J., Milioto, C., Lanson, N. A., Maltare, A., Aggarwal, T., Casci, I., Fackelmayer, F. O., Pennuto, m., and Pandey, U. B. (2013). Protein arginine methyltransferases 1 and 8 interact with FUS to modify its sub-cellular distribution and toxicity in vitro and in vivo. *PLOS ONE*, *8*, e61576. https://doi.org/10.1371/journal.pone.0061576

Schwartz, J. C., Cech, T. R., and Parker, R. R. (2015). Biochemical Properties and Biological Functions of FET Proteins. *Annal Review of Biochemistry*, *84*, 355-379. https://doi.org/10.1146/annurev-biochem-060614-034325

Shao, Y., Shu, X., Lu, Y., Zhu, W., Li, R., Fu, H., Li, C., Sun, W., Li, Z., Zhang, Y., Cao, X., Ye, X., Ajiboye, E., Zhao, B., Zhang, L., Wu, H., Feng, X., Yang, B., and Lu, H. (2023). A chaperone-like function of FUS ensures TAZ condensate dynamics and transcriptional activation. *Nature Cell Biology*, *26*, 86-99. https://doi.org/10.1038/s41556-023-01309-3

Sheets, M. D., Fox, C. A., Hunt, T., Vande Woude, and Wickens, M. (1994). The 3'-untranslated regions of c-mos and cyclin mRNAs stimulate translation by regulating cytoplasmic polyadenylation. *Genes and Development*, *8*, 926–938. https://doi.org/10.1101/gad.8.8.926

Shen, W., Gong, B., Xing, C., Zhang, L., Sun, J., Chen, Y., Yang, C., Yan, L., Chen, L.,

Yao, L., Li, G., Deng, H., Wu, X., and Meng, A. (2022). Comprehensive maturity of nuclear pore complexes regulates zygotic genome activation. *Cell*, *185*, 4954-4970. https://doi.org/10.1016/j.cell.2022.11.011

Shi, B., Zhang, J., Heng, J., Gong, J., Zhang, T., Li, P., Sun, B., Yang, Y., Zhang, N., Zhao, Y., Wang, H., Liu, F., Zhang, Q. C., and Yang, Y. (2020). RNA structural dynamics regulate early embryogenesis through controlling transcriptome fate and function. *Genome Biology*, *21*, 120. https://doi.org/10.1186/s13059-020-02022-2

Shi, B., Heng, J., Zhou, J., Yang, Y., Zhang, W., Kozoil, M, J., Zhao, Y., Li, P., Liu, F., and Yang, Y. (2020). Phase separation of Ddx3xb helicase regulates maternal-to-zygotic transition in zebrafish. *Cell Research*, *32*, 715-728. https://doi.org/10.1038/s41422-022-00655-5

Shiina, N. (2019). Liquid- and solid-like RNA granules form through specific scaffold proteins and combine into biphasic granules. *Journal of Biological Chemistry*, *294*, 3532–3548. https://doi.org/10.1074/ jbc.ra118.005423

Shin, Y., and Brangwynne, C.P. (2017). Liquid phase condensation in cell physiology and disease. *Science*, *357*, eaaf4382. https://doi.org/10.1126/science.aaf4382

Sorlien, E. L., Witucki, M. A., and Ogas, J. (2018). Efficient Production and Identification of CRISPR/Cas9-generated Gene Knockouts in the Model System *Danio rerio*. *Journal of Visualized Experiments, 138*, e56969. https://doi.org/10.3791/56969

Svitkin, Y. V., Yanagiya, A., Karetnikov, A. E., Alain, T., Fabian, M. R., Khoutorsky, A., Perreault, S., Topisirovic, I., and Sonenberg, N. (2013). Control of Translation and

miRNA-Dependent Repression by a Novel Poly(A) Binding Protein, hnRNP-Q. *PLOS Biology*, *11*, e1001564. https://doi.org/10.1371/journal.pbio.1001564

Swain, B, C., Sarkis, P., Ung, V., Rousseau, S., Fernandez, L., Meltonyan, A., Aho, V. E., Mercadante, D., Mackereth, C. D., and Aznauryan, M. (2024). Disordered regions of human eIF4B orchestrate a dynamic self-association landscape. *Nature Communications*, *15*, 8766. https://doi.org/10.1038/s41467-024-53136-1

Takeda, H., Matsuzaki, T., Oki, T., Miyagawa, T., and Amanuma, H. (1994). A novel POU domain gene, zebrafish pou2: expression and roles of two alternatively spliced twin products in early development. *Genes and Development*, *8*, 45–59. https://doi. org/10.1101/gad.8.1.45

Takada, Y., Fierro, L., Sato, K., Sanada, T., Ishii, A., Yamamoto, T., and Kotani, T. (2023). Mature mRNA processing that deletes 3' end sequences directs translational activation and embryonic development. Science Advances, 9, eadg6532. https://doi.org/doi/10.1126/sciadv.adg6532

Takei, N., Nakamura, T., Kawamura, S., Takada, Y., Satoh, Y., Kimura, A. P., and Kotani, T. (2018). High-Sensitivity and High-Resolution in Situ Hybridization of Coding and Long Non-coding RNAs in Vertebrate Ovaries and Testes. *Biological Procedures Online*, *20*, 1–14. https://doi.org/10.1186/s12575-018-0071-z

Takei, N., Sato, K., Takada, Y., Iyyappan, R., Susor, A., Yamamoto, T., and Kotani, T. (2021). Tdrd3 regulates the progression of meiosis II through translational control of Emi2 mRNA in mouse oocytes. *Current Research in Cell Biology*, *2*, 100009. https://doi.org/10.1016/j.crcbio.2021.100009

Takei, N., Takada, Y., Kawamura, S., Sato, K., Saitoh, A., Bormann, J., Yuen, W. S.,

Carroll, J., and Kotani, T. (2020). Changes in subcellular structures and states of pumilio 1 regulate the translation of target Mad2 and cyclin B1 mRNAs. *Journal of Cell Science*, *133*, jcs249128. https://doi.org/10.1242/jcs.249128

Tan, A. Y., and Manley, J. L. (2009). The TET family of proteins: functions and roles. *Journal of Molecular Cell Biology*, *1*, 82-92. https://doi.org/10.1093/jmcb/mjp025

Tauber, D., Tauber, G., and Parker, R. (2020). Mechanisms and Regulation of RNA Condensation in RNP Granule Formation. *Trends in Biochemical Sciences*, *45*, 764-778. https://doi.org/10.1016/j.tibs.2020.05.002

Tay, J., Hodgman, R. and Richter, J. D. (2000). The control of cyclin B1 mRNA translation during mouse oocyte maturation. *Developmental Biology*, *221*, 1-9. https://doi.org/10.1006/dbio.2000.9669

Thomas, M.G., Pascual, M.L., Maschi, D., Luchelli, L., and Boccaccio, G.L. (2014). Synaptic control of local translation: the plot thickens with new characters. *Cellular and Molecular Life Sciences*, *71*, 2219–2239. https://doi.org/10.1007/s00018-013-1506-y

tom Dieck, S., Kochen, L., Hanus, C., Heumuller, M., Bartnik, I., Nassim-Assir, B., Merk, K., Mosler, T., Garg, S., Bunse, S., Tirrell, D. A., and Schuman, E. M. (2015). Direct visualization of newly synthesized target proteins in situ. *Nature Methods*, *12*, 411–414. https://doi.org/10.1038/nmeth.3319

Tradewell, M., Yu, Z., Tibshirani, M., Boulanger, M., Durham, H. D., and Richard, S. (2012). Arginine methylation by PRMT1 regulates nuclear-cytoplasmic localization and toxicity of FUS/TLS harbouring ALS-linked mutations. *Human Molecular Genetics*, *1*, 136-149. https://doi.org/10.1093/hmg/ddr448

Trcek, T., Grosch, M., York, A., Shroff, H., Lionnet, T., and Lehmann, R. (2015). Drosophila germ granules are structured and contain homotypic mRNA clusters. *Nature Communication*, *6*, 7962. https:// doi.org/10.1038/ncomms8962

Trussina, I., Hartmann, A., Altamirano, C. D., Natarajan, J., Fischer, C. M., Aleksejczuk, M., Ausserwöger, H., Knowles, T., Schlierf, M., Franzmann, T. M., and Alberti, S. (2025). G3BP-driven RNP granules promote inhibitory RNA-RNA interactions resolved by DDX3X to regulate mRNA translatability. *Molecular Cell*, *85*, 1-17. https://doi.org/10.1016/j.molcel.2024.11.039

Updike, D.L., Hachey, S.J., Kreher, J., and Strome, S. (2011). P granules extend the nuclear pore complex environment in the C. elegans germ line. *Journal of Cell Biology*, *192*, 939–948. https://doi.org/10.1083/jcb.201010104

Veli, M., Yampolsky, L. Y., Grüning, B., and Onichtchouk, D. (2019). Pou5f3, SoxB1, and Nanog remodel chromatin on high nucleosome affinity regions at zygotic genome activation. *Genome Research*, *29*, 383-395. https://doi.org/10.1101/gr.240572.118

Vries, T., Novakovic, M., Ni, Y., Smok, I., Inghelram, C., Bikaki, M., Sarnowski, C. P., Han, Y., Emmanouilidis, L., Padroni, G., Leitner, A., and Allain, F. H. (2024). Specific protein-RNA interactions are mostly preserved in biomolecular condensates. *Science Advances*, *10*, eadm7435. https://doi.org/10.1126/sciadv.adm7435

Wadsworth, G. M., Zahurancik, W. J., Zeng, X., Pullara, P., Lai, L. B., Sidharthan, V., Pappu, R. V., Gopalan, V., and Banerjee, P. R. (2023). RNAs undergo phase transitions with lower critical solution temperatures. *Nature Chemistry*, *15*, 1693-

1704. https://doi.org/10.1038/s41557-023-01353-4

Wang, J., Choi, J., Holehouse, A. S., Lee, H. O., Zhang, X., Jahnel, M., Maharana, S., Lemaitre, R., Pozniakovsky, A., Drechsel, D., Poser, I., Pappu, R. V., Alberti, S., and Hyman, A. A. (2018). A Molecular Grammar Governing the Driving Forces for Phase Separation of Prion-like RNA Binding Proteins. *Cell*, *174*, 688-699. https://doi.org/10.1016/j.cell.2018.06.006

Wang, S., and Xu, Y. (2024). RNA structure promotes liquid-to-solid phase transition of short RNAs in neuronal dysfunction. *Communications Biology*, *7*, 137. https://doi.org/10.1038/s42003-024-05828-z

Wang, X., Leung, F., Bush, J. O, and Conti, M. (2024). Alternative cleavage and polyadenylation of the Ccnb1 mRNA defines accumulation of cyclin protein during the meiotic cell cycle. *Nucleic Acids Research*, *52*, 1258-1271. https://doi.org/10.1093/nar/gkad1151

Ward, J. J., Sodhi, J. S., McGuffin, L. J., Buxton, B. F., and Jones, D. T. (2004). Prediction and functional analysis of native disorder in proteins from the three kingdoms of life. *Journal of Molecular Biology*, *337*, 635–645. https://doi.org/10.1016/j.jmb.2004.02.002

Weil, T.T., Parton, R.M., Herpers, B., Soetaert, J., Veenendaal, T., Xanthakis, D., Dobbie, I.M., Halstead, J.M., Hayashi, R., Rabouille, C., and Davis, I. (2012). Drosophila patterning is established by differential association of mRNAs with P bodies. *Nature Cell Biology*, *14*, 1305–1313. https://doi.org/10.1038/ncb2627

Weill, L., Belloc, E., Bava, F. A., and Méndez, R. (2012). Translational control by changes in poly(A) tail length: Recycling mRNAs. *Nature Structural and*

Molecular Biology, *19*, 577–585. https://doi.org/10.1038/nsmb.2311

West, J.A., Mito, M., Kurosaka, S., Takumi, T., Tanegashima, C., Chujo, T., Yanaka, K., Kingston, R.E., Hirose, T., Bond, C., et al. (2016). Structural, super-resolution microscopy analysis of paraspeckle nuclear body organization. *Journal of Cell Biology*, *214*, 817–830. https://doi.org/10.1083/jcb. 201601071

Wiedner, H. J., and Giudice, J. (2021). It's not just a phase: function and characteristics of RNA-binding proteins in phase separation. Nature Structural and Molecular Biology, 28, 465-473. https://doi.org/10.1038/s41594-021-00601-w

Wilk, R., Hu, J., Blotsky, D., and Krause, H.M. (2016). Diverse and pervasive subcellular distributions for both coding and long noncoding RNAs. *Genes and Development*, *30*, 594–609. https://doi.org/ 10.1101/gad.276931.115

Winata, C. L., and Korzh, V. (2018). The translational regulation of maternal mRNAs in time and space. *FEBS Letters*, *592*, 3007-3023. https://doi.org/10.1002/1873-3468.13183

Winata, C. L., Łapiński, M., Pryszcz, L., Vaz, C., bin Ismail, M. H., Nama, S., Hajan, H. S., Lee, S. G. P., Korzh, V., Sampath, P., Tanavde, V., and Mathavan, S. (2018). Cytoplasmic polyadenylation-mediated translational control of maternal mRNAs directs maternal-to-zygotic transition. *Development*, *145*, dev159566. https://doi.org/10.1242/dev.159566

Woodland, H.R. (1974). Changes in the polysome content of developing Xenopus laevis embryos. *Developmental Biology*, *40*, 90–101. https://doi.org/10.1016/ 0012-1606(74)90111-0

Xiao, Y., Chen, J., Wan, Y., Gao, Q., Jing, N., Zheng, Y., and Zhu, X. (2019).

Regulation of zebrafish dorsoventral patterning by phase separation of RNA-binding protein Rbm14. *Cell Discovery*, *5*: 37. https://doi.org/10.1038/s41421-019-0106-x

Yang, G., Xin, Q., and Dean, J. (2024). Degradation and translation of maternal mRNA for embryogenesis. *Trends in Genetics*, *40*, 238-249. https://doi.org/10.1016/j.tig.2023.12.008

Yang, L., Chansky, H. A., and Hickstein, D. D. (2000). EWS.Fli-1 fusion protein interacts with hyperphosphorylated RNA polymerase II and interferes with serine-arginine protein-mediated RNA splicing. Journal of Biological Chemistry, 275, 37612–37618. https://doi.org/10.1074/jbc.M005739200

Yang, Y., Guo, L., Chen, L., Gong, B., Jia, D., and Sun, Q. (2023). Nuclear transport proteins: structure, function and disease relevance. *Signal Transduction and Targeted Therapy*, *8*, 425. https://doi.org/10.1038/s41392-023-01649-4

Yang, Y., Yang, C., Han, S. J., Daldello, E. M., Cho, A., Martins, J., Xia, G., and Conti, M. (2017). Maternal mRNAs with distinct 3' UTRs define the temporal pattern of Ccnb1 synthesis during mouse oocyte meiotic maturation. *Genes and Development*, *31*, 1302-1307. https://doi.org/10.1101/gad.296871.117

Yasuda, K., Zhang, H., Loiselle, D., Haystead, T., Macara, I.G., and Mili, S. (2013). The RNA-binding protein Fus directs translation of localized mRNAs in APC-RNP granules. *Journal of Cell Biology*, *203*, 737–746. https://doi.org/10.1083/jcb.201306058

Yokoi, S., Udagawa, T., Fujioka, Y., Honda, D., Okado, H., Watanabe, H., Katsuno, M., Ishigaki, S., and Sobue, G. (2017). 3' UTR Length-Dependent Control of

SynGAP Isoform α2 mRNA by FUS and ELAV-like Proteins Promotes Dendritic Spine Maturation and Cognitive Function. *Cell Reports*, *20*, 3071-3084. https://doi.org/10.1016/j.celrep.2017.08.100

Yoshizawa, T., Ali, R., Jiou, J., Fung, H., Burke, K. A., Kim, S. J., Lin, Y., Peeples, W. B., Saltzberg, D., Soniat, M., Baumhargt, J., M., Oldenboung, R., Sali, A., Fawzi, N. L., Rosen, M. K., and Chook, Y. M. (2018). Nuclear Import Receptor Inhibits Phase Separation of FUS through Binding to Multiple Sites. *Cell*, *173*, 693-705. https://doi.org/10.1016/j.cell.2018.03.003

Zaucker, A., Kumari, P., and Sampath, K. (2020). Zebrafish embryogenesis - a framework to study regulatory RNA elements in development and disease. *Developmental Biology*, *457*, 172–180. https://doi.org/10.1016/j.ydbio.2019.01.008

Zhang, C., Wang, M., Li, Y., and Zhang, Y. (2024). Profiling and functional characterization of maternal mRNA translation during mouse maternal-to-zygotic transition. *Science Advances*, *8*, eabj3967. https://doi.org/10.1126/sciadv.abj3967

Zhong, Q., Xiao, X., Qiu, Y., Xu, Z., Chen, C., Chong, B., Zhao, X., Hai, S., Li, S., An, Z., and Dai, L. (2023). Protein posttranslational modifications in health and diseases: Functions, regulatory mechanisms, and therapeutic implications. *MedComm*, *4*, e261. https://doi.org/10.1002/mco2.261

TABLES

Table 1. Oligonucleotide sequence

Primer	Sequence (5'→3')
For production of Pou5f3 antibody	
pou5f3-ORF-f1	ATGACGGAGAGAGCG
pou5f3-ORF-r1	ACCTCCTACGTCACTA
For RNA probe synthesis	
pou5f3-f1	ACATTTCCACACAGGCTGATAC
gfp-f1	CACATGAAGCAGCACGACTTCT
gfp-r1	ACGTTGTGGCTGTTGTAGTTGTAC
For cloning of *ewsr1b*	
ewsr1b-ORF-f1	GTTCTCCAACGGAAAGATGGCGTC
ewsr1b-ORF-r1	GCTTGATGCGTGAACTTAGTAGGG
ewsr1b-ORF-r2	AACTCAGCCATCTCTGGTAGAGTG
ewsr1b-ORF-r3	CAGCTACAGAGACATGTAAGACG
For IP/RT-PCR	
pou5f3-3' UTR-f1	GTCTCCATAACTTTGTAGTTTACTCG
pou5f3-3' UTR-r1	GCTACCTAAAAGTTATTGTAAGAG
α-tubulin-f1	ATTGCTGAGGCCTGGGCTCGTC
α-tubulin-r1	AGTGTCGCAAGGATTGACCTTTTAG
ewsr1b-ORF-f2	ATGGAAATGAGGGATCATCGTCAG
ewsr1b-ORF-r3	AGGCTGCTGGCTGTAGCCAGAATAG
ewsr1b-3' UTR-r1	CAGCTACAGAGACATGTAAGACG
For RT-PCR	
ewsr1a-ORF-f1	CAACAGTTACGGACAGGCTGGAAG
ewsr1a-ORF-r1	GTTTTCAGAGTCATCTTGCTCCTC
βactin-ORF-f1	AAATCGCTGCCCTGGTCGTT
β-actin-ORF-r1	GAAGCACTTCCTGTGGACGATG
For quantitative PCR	
ewsr1a-ORF-r2	GCTGTCCATAGGAAGACCCATATG
ewsr1b-ORF-r4	AGCAGAGGGCGCTGCCTGACTGTAG
For PAT assay	
P1 anchor primer	P-GGTCACCTTGATCTGAAGC-NH_2
P1' primer	GCTTCAGATCAAGGTGACCTTTTT
pou5f3-PAT-f1	TAGATGTACTCTTTGTCAGGGTGG
pou5f3-PAT-f2	TGGAGGTCATGTGCCTTATCTTTC
ewsr1b 3' UTR-Long-PAT-f1	CTGGTTTTAGTTAAACTCTTGTTGCG
ewsr1b 3' UTR-Long-PAT-f2	AATACTCAGTTGCCCTGTAGTC
ewsr1b 3' UTR-Short-PAT-f1	GAACTTCTCCTCCCTTTTCTCCAG
Morpholino oligo nucleotide	**Sequence (5' → 3')**
Pou5f3-ATG-MO	CTCTCTCCGTCATCTTTCCGCTAAA
Pou5f3-5mm-MO	CTCACTCCTTCATATTTCGGCTCAA
Ewsr1b-ATG-MO	TATAATTCGTGACTGACGCCATCTT
Ewsr1b-5mm-MO	TATATTTCCTGTCTCACGGCATCTT
Ewsr1b-3' UTR-MO	TGGAGGTGGAAAAGTTTATTTAAAA

Table 2. Proteins isolated in the immunoprecipitation of Syncrip

Protein Name	Gene Symbol	# PSMs	Exp. q-value
14-3-3 protein gamma-1	Ywhag1	2	0.022
26S proteasome non-ATPase regulatory subunit 11A	Psmd11a	6	0
45 kDa calcium-binding protein	Sdf4	1	0
4-trimethylaminobutyraldehyde dehydrogenase A	Aldh9a1a	13	0
Actin, cytoplasmic 1	Actba	237	0
Actin, cytoplasmic 2	Actbb	231	0
Actin-related protein 2-B	Actr2b	1	0
Aspartate aminotransferase, mitochondrial	Got2a	2	0
Atypical kinase COQ8A, mitochondrial	Coq8a	1	0.012
BOS complex subunit ncln	Ncln	2	0
Calumenin-B	Calub	1	0
Carnitine O-palmitoyltransferase 2, mitochondrial	Cpt2	2	0
Catalase	Cat	18	0
Catenin beta-1	Ctnnb1	1	0
CCR4-NOT transcription complex subunit 1	Cnot1	32	0
Citrate synthase, mitochondrial	Cs	1	0.02
Cytospin-A	Specc1la	1	0.022
Damage-control phosphatase ARMT1	Armt1	1	0
Desmoplakin-A	Dspa	3	0
Dolichyl-diphosphooligosaccharide--protein glycosyltransferase 48 kDa subunit	Ddost	9	0
Double-stranded RNA-binding protein Staufen homolog 2	Stau2	2	0
Dynamin-1-like protein	Dnm1l	1	0
Elongation factor 1-alpha	Eef1a	56	0
Elongation factor 1-gamma	Eef1g	24	0
Elongation factor 2b	Eef2b	28	0
Endoplasmic reticulum junction formation protein lunapark-A	Lnpka	2	0
Erlin-1	Erlin1	2	0.02
Eukaryotic translation initiation factor 2 subunit 3	Eif2s3	1	0
Eukaryotic translation initiation factor 2A	Eif2a	3	0
Eukaryotic translation initiation factor 3 subunit A	Eif3a	10	0
Eukaryotic translation initiation factor 3 subunit D	Eif3d	6	0
Eukaryotic translation initiation factor 3 subunit L	Eif3l	7	0
Fatty-acid amide hydrolase 2-B	Faah2b	8	0
G kinase-anchoring protein 1	Gkap1	2	0
Glyceraldehyde-3-phosphate dehydrogenase	Gapdh	21	0
Heat shock cognate 71 kDa protein	Hspa8	191	0
Heat shock protein HSP 90-beta	Hsp90ab1	32	0
Histone H2AX	H2ax	4	0.022
Histone-arginine methyltransferase CARM1	Carm1	4	0
Histone-binding protein RBBP4	Rbbp4	7	0
Hydroxysteroid dehydrogenase-like protein 2	Hsdl2	2	0
Hypoxia up-regulated protein 1	Hyou1	28	0
Inactive all-trans-retinol 13,14-reductase	Retsatl	77	0
Inosine-5'-monophosphate dehydrogenase 1a	Impdh1a	1	0
Inosine-5'-monophosphate dehydrogenase 2	Impdh2	2	0
Insulin-like growth factor 2 mRNA-binding protein 3	Igf2bp3	23	0
Keratin, type II cytoskeletal 8	Krt8	77	0
Large ribosomal subunit protein eL24	Rpl24	2	0
Large ribosomal subunit protein uL10	Rplp0	2	0
Large ribosomal subunit protein uL2	Rpl2	8	0
Lipase member H	Liph	2	0
L-lactate dehydrogenase B-A chain	Ldhba	14	0
Major vault protein	Mvp	1	0.021
Mini-chromosome maintenance complex-binding protein	Mcmbp	2	0
Nascent polypeptide-associated complex subunit alpha	Naca	4	0
NudC domain-containing protein 1	Nudcd1	4	0
Piwi-like protein 1	Piwil1	2	0
Polyadenylate-binding protein, cytoplamic 1A	Pabpc1a	4	0
Proliferating cell nuclear antigen	Pcna	1	0.021
Proteasomal ubiquitin receptor ADRM1	Adrm1	4	0
Protein RCC2 homolog	Rcc2	1	0.012

Protein Name	Gene Symbol	# PSMs	Exp. q-value
Protein transport protein Sec23A	Sec23a	5	0
Replication protein A 70 kDa DNA-binding subunit	Rpa1	24	0
Ribonucleoside-diphosphate reductase large subunit	Rrm1	8	0
RNA polymerase II-associated factor 1 homolog	Paf1	1	0.012
RuvB-like 1	Ruvbl1	1	0
RuvB-like 2	Ruvbl2	7	0
Septin-8-A	Sept8a	2	0
Serine--tRNA ligase, cytoplasmic	Sars1	3	0
Small ribosomal subunit protein eS1	Rps3a	3	0
Small ribosomal subunit protein eS4	Rps4x	4	0
Small ribosomal subunit protein eS8	Rps8a	4	0
Small ribosomal subunit protein mS39	Ptcd3	1	0.021
Small ribosomal subunit protein RACK1	Gnb2l1	2	0
Small ribosomal subunit protein uS2	Rps2a	12	0
Splicing factor 3B subunit 3	Sf3b3	2	0
Staphylococcal nuclease domain-containing protein 1	Snd1	1	0.011
Succinate dehydrogenase [ubiquinone] flavoprotein subunit, mitochondrial	Sdha	11	0
Synaptic vesicle membrane protein VAT-1 homolog	Vat1	9	0
Transcription elongation factor SPT6	Supt6h	2	0
Transitional endoplasmic reticulum ATPase	Vcp	26	0
Tripeptidyl-peptidase 1	Tpp1	2	0
Tyrosine--tRNA ligase, cytoplasmic	Yars1	3	0
Ubiquitin-like modifier-activating enzyme 5	Uba5	4	0
Unconventional myosin-Ic	Myo1c	3	0
V-type proton ATPase subunit d 1	Atp6v0d1	1	0.021
Y-box-binding protein 1	Ybx1	4	0

Proteins isolated in the immunoprecipittaion of Syncrip followed by mass spectrometry are listed. # PSMs, Number of Peptide Spectrum Match (PSM). PSM is a combination of a single spectrum and a candidate sequence predicted from that spectrum. Exp. q-value, the lower limit of false discovery rate (FDR) for which the PSM remains in this list.

FIGURES

Figure 1. **Zebrafish embryos accumulate Pou5f3 protein during the early stages of development.** (A) Domain structure of Pou5f3. Immunogen region is the target region of antibody. (B) Evaluation of mouse anti-Pou5f3 antibody specificity. (C) Time course of Pou5f3 accumulation in immature (Im) and mature (M) oocytes and in embryos at hours post fertilization (hpf). Ribosomal protein l11 (Rpl11) is a loading control. (D) Immunoblotting of Pou5f3 and Rpl11 in embryos not injected (-) and injected with Pou5f3-5mm-MO (5mm) and Pou5f3-ATG-MO (ATG) at 6 hpf. (E) Quantitative analysis of immunoblotting [means ± standard deviations (SD); n = 3]. *$p < 0.05$; **$p < 0.01$ (Tukey-Kramer test). (F) The intensities of both Pou5f3 bands in (C) were quantified and normalized with the intensities of Rpl11. (means ± SD; n = 7). NS, not significant; *$p < 0.05$, **$p < 0.01$ (Tukey-Kramer test).

A

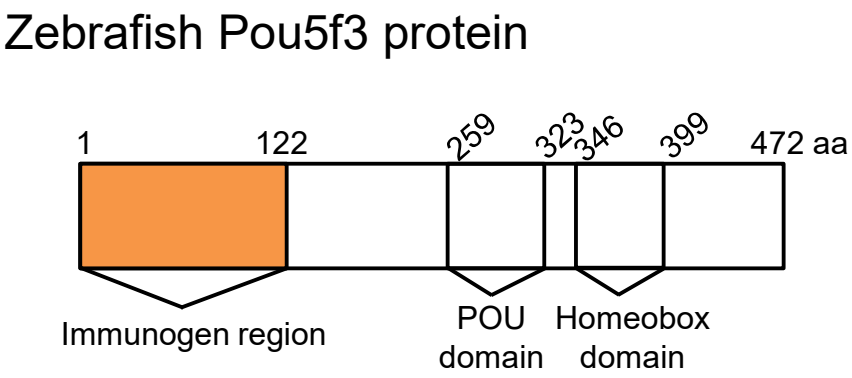
Zebrafish Pou5f3 protein
1
122
259
323
346
399
472 aa
Immunogen region
POU domain
Homeobox domain

B

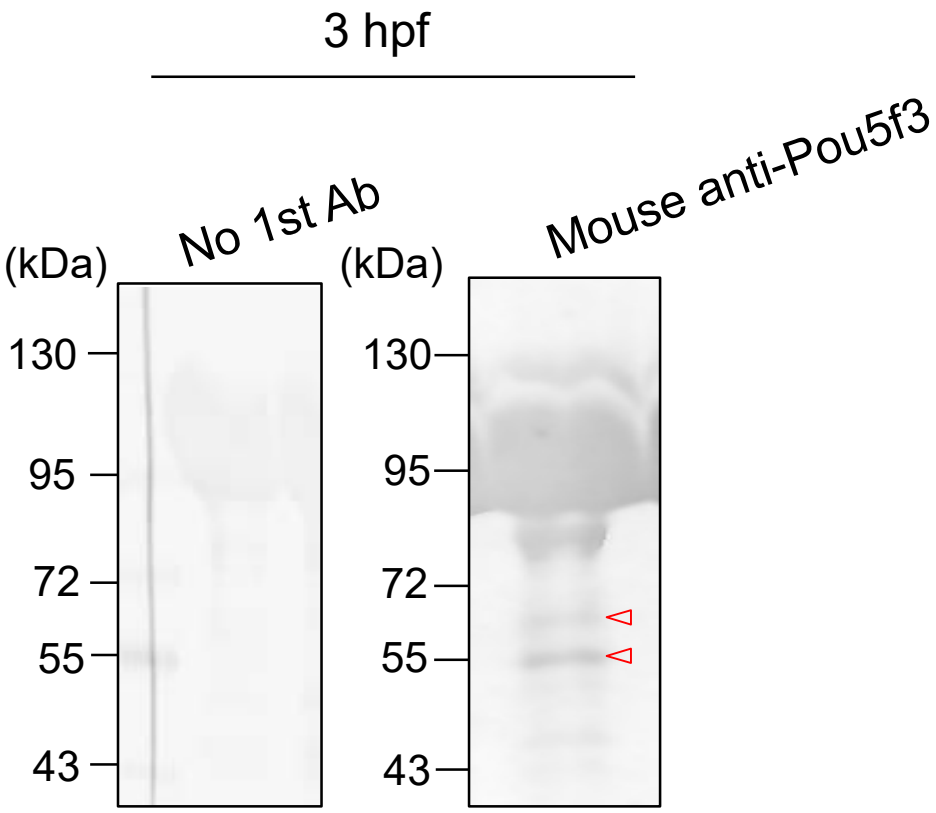
3 hpf
No 1st Ab
Mouse anti-Pou5f3
(kDa)
130
95
72
55
43
(kDa)
130
95
72
55
43

C

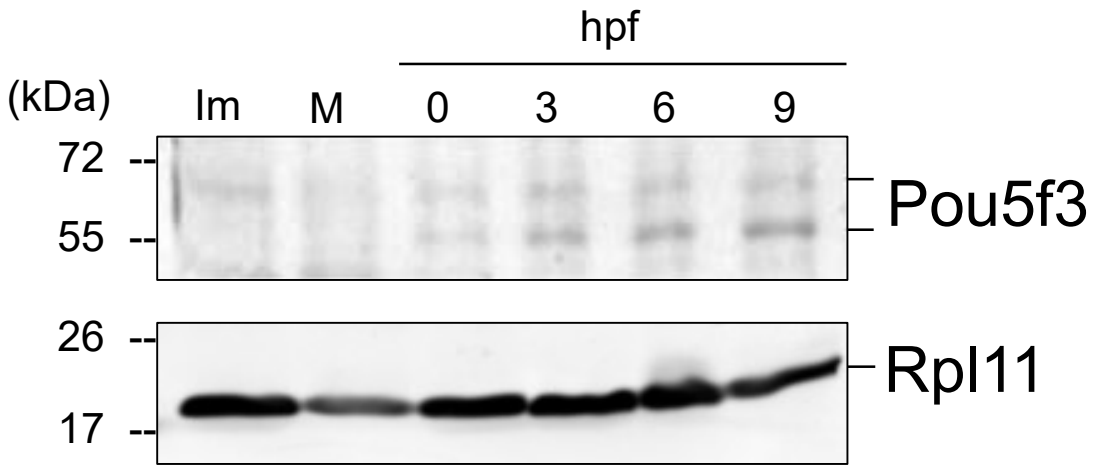
hpf
(kDa)
Im
M
0
3
6
9
72
55
26
17
Pou5f3
Rpl11

D

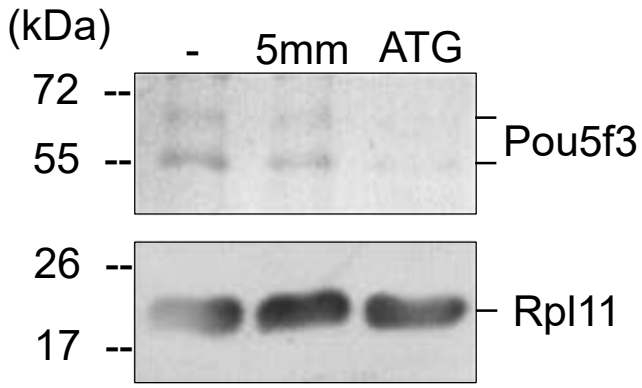
(kDa)
-
5mm
ATG
72
55
26
17
Pou5f3
Rpl11

E

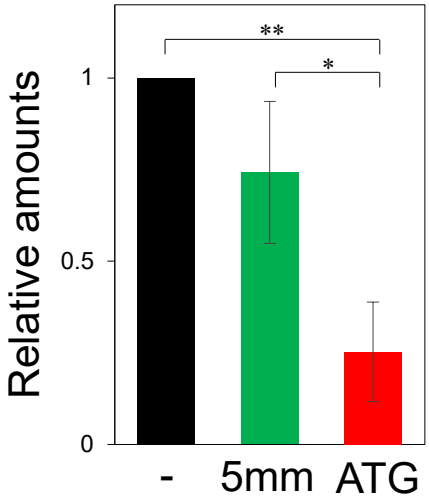
**
*
1
0.5
0
Relative amounts
-
5mm
ATG

F

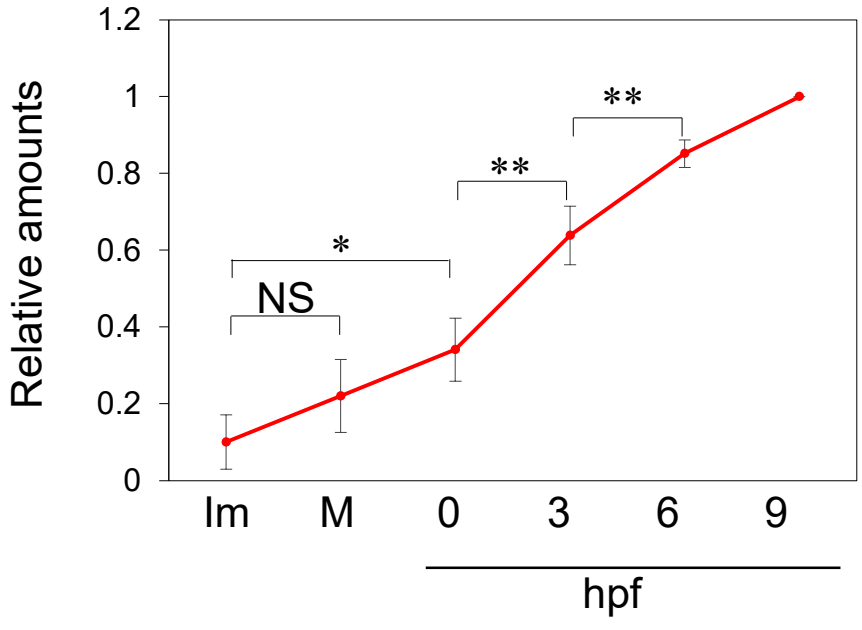
1.2
1
0.8
0.6
0.4
0.2
0
Relative amounts
NS
*
**
**
Im
M
0
3
6
9
hpf

Figure 2. **Zebrafish embryos assemble and maintain *pou5f3* mRNA as RNA granule during early development.**
(A) Whole mount *in situ* hybridization analyses of *pou5f3* mRNA (green) in embryos at 0, 3, and 6 hpf. Upper, high-resolution confocal images. Lower, enlarged views of the boxed regions in the upper images. DNA is shown in blue. Insets show bright-field views of live embryos. bd, blastodisc. Bars, upper, 20 μm; lower, 5 μm. (B) The number of granules per 100 μm^2 in embryos at 0, 3, and 6 hpf were counted (means ± SD; n=6). Similar results were obtained from three independent experiments. (C) Poly(A) test (PAT) assay for *pou5f3* mRNA in embryos at 0 and 3 hpf. Similar results were obtained from three independent experiments.

A

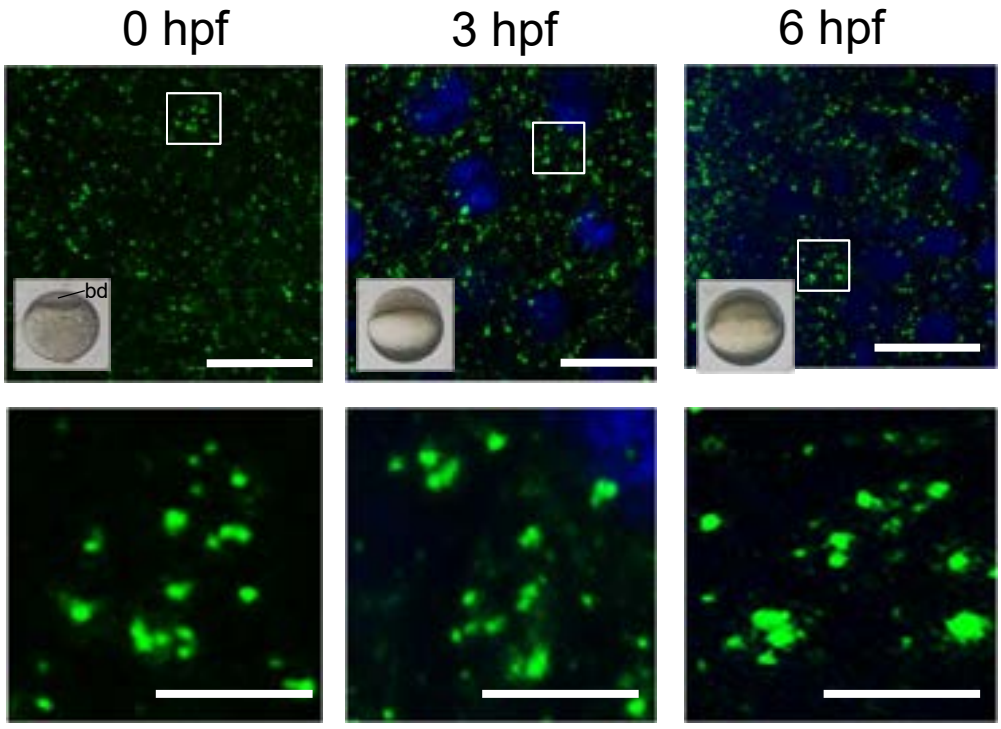
0 hpf
3 hpf
6 hpf
bd

B

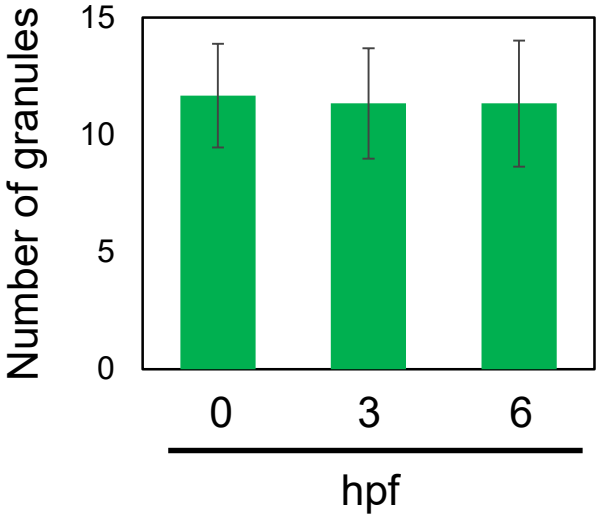
Number of granules
15
10
5
0
0
3
6
hpf

C

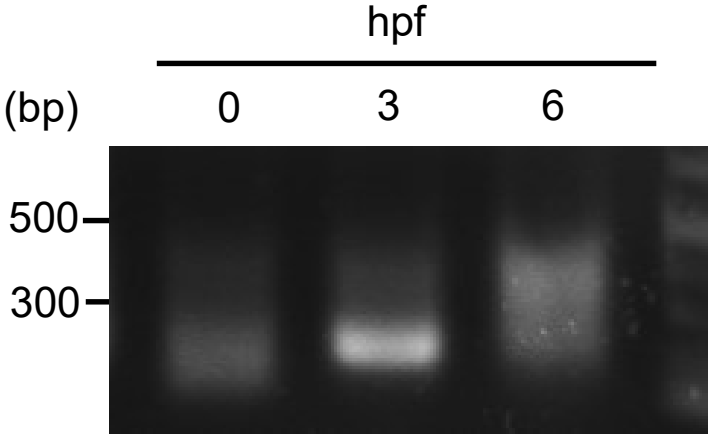
hpf
(bp)
0
3
6
500
300

Figure 3. **Visualization of translating sites during early development.**
(A) A schematic view for visualization of translating sites by ribopuromycylation. After pretreatment with CHX, embryos were stimulated with CHX and puromycin, which was detected by anti-puromycin antibody after washing out free puromycin. (B) Detection of translating sites (red) with anti-puromycin antibody in cleavage-stage embryos stimulated with (+) or without (-) CHX and puromycin (Puro). As a control, embryos were pretreated with anisomycin (Aniso) instead of CHX. DNA is shown in blue. (C) Detection of translating sites (red) in embryos at 0, 3 and 6 hpf. DNA is shown in blue. (D) The number of translating sites per 3,600 μm^2 in embryos at 0, 3 and 6 hpf was counted (means $\pm$ SD; n = 3). Similar results were obtained from three independent experiments. (E) Quantitative analysis of the areas of translation sites in embryos at 0, 3 and 6 hpf.

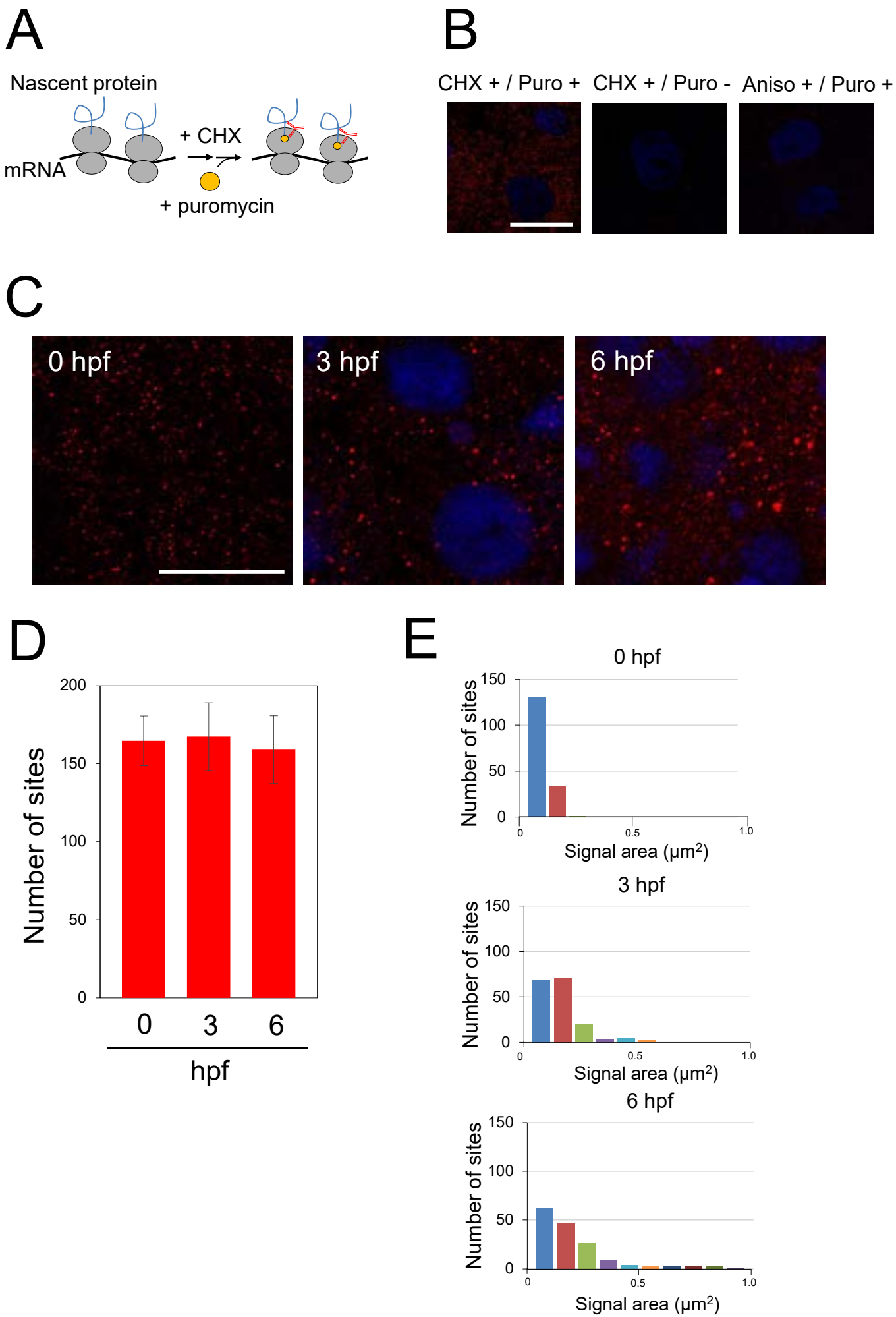
A
Nascent protein
mRNA
+ CHX
+ puromycin
B
CHX + / Puro +
CHX + / Puro -
Aniso + / Puro +
C
0 hpf
3 hpf
6 hpf
D
Number of sites
200
150
100
50
0
0
3
6
hpf
E
0 hpf
Number of sites
150
100
50
0
0
0.5
1.0
Signal area (μm²)
3 hpf
Number of sites
150
100
50
0
0
0.5
1.0
Signal area (μm²)
6 hpf
Number of sites
150
100
50
0
0
0.5
1.0
Signal area (μm²)

Figure 4. **Translating sites in embryos become colocalized with *pou5f3* RNA granules during early development.**
(A) 3D images of SIM for *pou5f3* mRNA (green) and translating sites (red) in embryos at 0 and 3 hpf. DNA is shown in blue. Insets show enlarged views of the boxed regions. Bars, 20 μm. (B) The numbers of *pou5f3* RNA granules (left) and translating sites (right) per 28,800 μm^3 in embryos at 0 and 3 hpf were counted (means ± SD; n = 3). (C) The number of colocalizations of *pou5f3* RNA granules and translating sites per 28,800 μm^3 in embryos at 0 and 3 hpf was counted (means ± SD; n = 3). Similar results were obtained from two independent experiments. **$p < 0.01$ (Student's *t*-test).

A

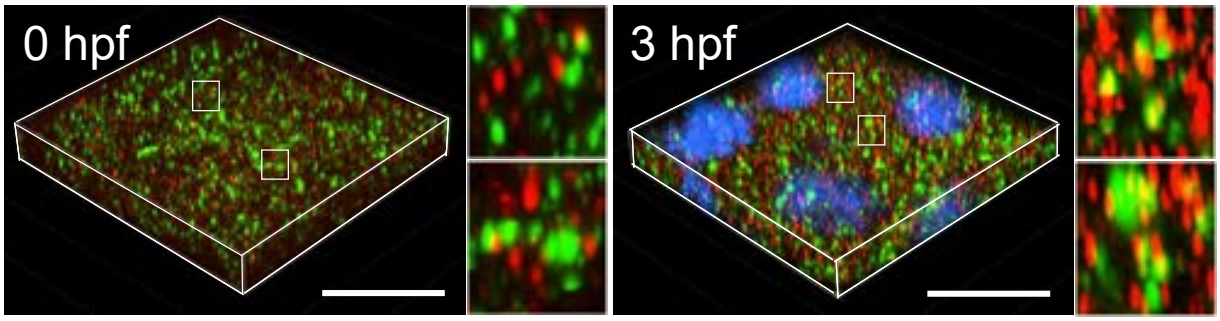
0 hpf
3 hpf

B

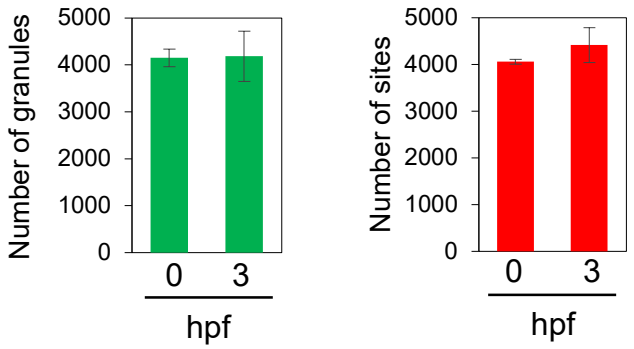
Number of granules
5000
4000
3000
2000
1000
0
0
3
hpf
Number of sites
5000
4000
3000
2000
1000
0
0
3
hpf

C

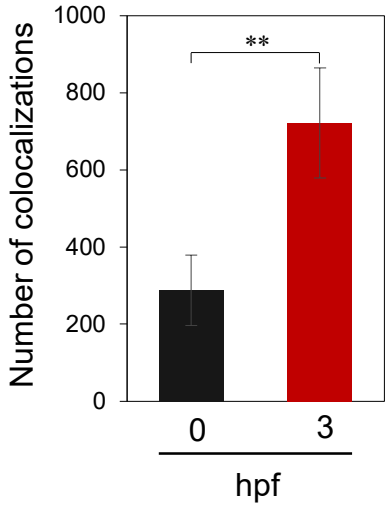
Number of colocalizations
1000
800
600
400
200
0
**
0
3
hpf

Figure 5. Visualization of *pou5f3*-translating sites during early development. (A) A schematic view for visualization of *pou5f3*-translating sites by Puro-PLA. (B) Evaluation of rabbit anti-Pou5f3 antibody specificity. (C) Detection of *pou5f3*-translating sites in embryos at 0 and 3 hpf stimulated with (+) or without (-) puromycin (Puro). After fixation, embryos were incubated with (+) and without (-) anti-puromycin antibody (Primary Ab). DNA is shown in blue. (C) The number of *pou5f3*-translating sites per 10,000 μm^2 in embryos at 0 and 3 hpf was counted (means $\pm$ SD; n = 6). Similar results were obtained from two independent experiments. **$p < 0.01$ (Tukey-Kramer test).

A

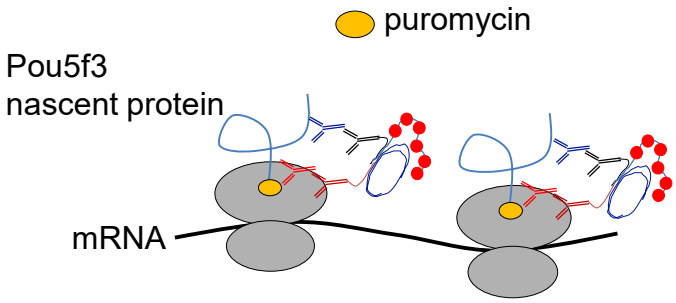
puromycin
Pou5f3
nascent protein
mRNA

B

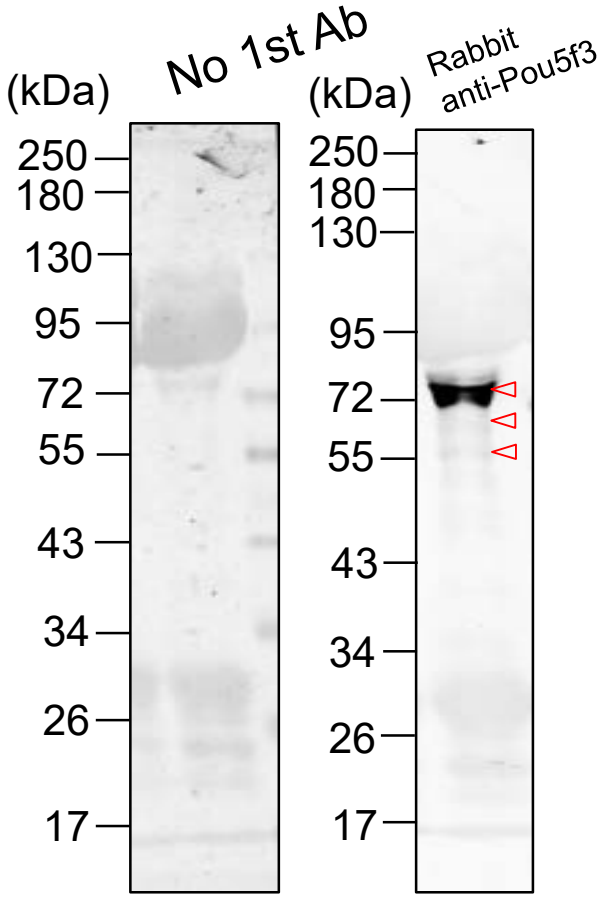
3 hpf
No 1st Ab
Rabbit
anti-Pou5f3
(kDa)
250
180
130
95
72
55
43
34
26
17
(kDa)
250
180
130
95
72
55
43
34
26
17

C

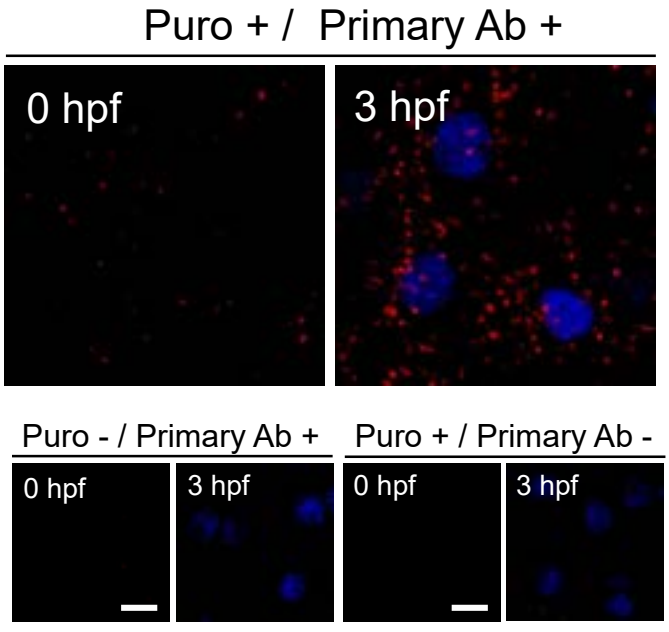
Puro + / Primary Ab +
0 hpf
3 hpf
Puro - / Primary Ab +
Puro + / Primary Ab -
0 hpf
3 hpf
0 hpf
3 hpf

D

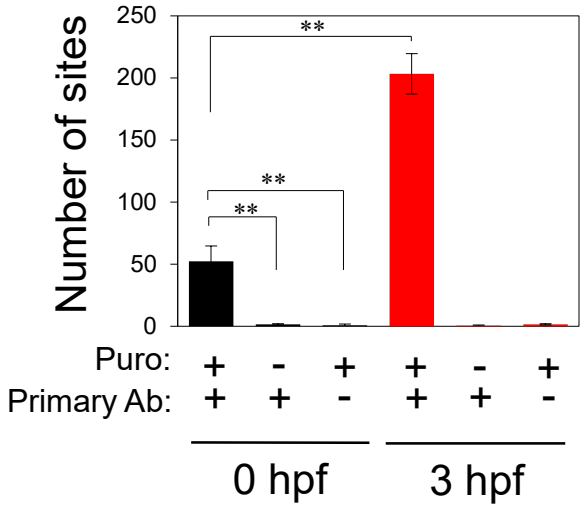
Number of sites
250
200
150
100
50
0
**
**
**
Puro:
Primary Ab:
+ - + + - +
+ + - + + -
0 hpf
3 hpf

Figure 6. **Embryos start to translate *pou5f3* mRNAs at the sites of granules, termed embryonic RNA granules, during the mitotic cleavage stage.** (A) 3D images of SIM for *pou5f3* mRNA (green) and *pou5f3*-translating sites (red) in embryos at 0 and 3 hpf. DNA is shown in blue. (B) The number of colocalizations of *pou5f3* RNA granules and *pou5f3*-translating sites per 14,400 μm^3 in embryos at 0 and 3 hpf was counted (means $\pm$ SD; n = 4). Similar results were obtained from two independent experiments. **$p < 0.01$ (Student's *t*-test). (C) Enlarged views of *pou5f3* RNA granules and *pou5f3*-translating sites in the boxed regions in (A). Intensity profiles along the dashed lines are shown in the graphs. Bars, 20 μm.

A

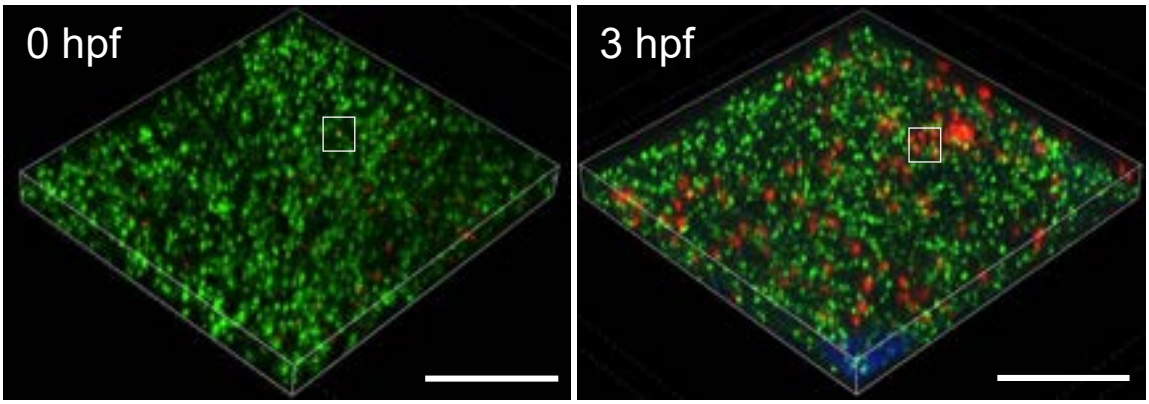
0 hpf
3 hpf

B

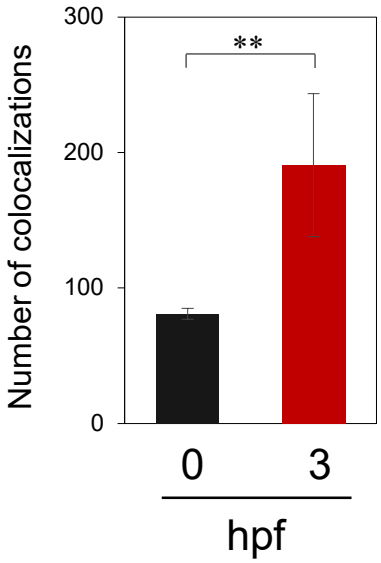
300
200
100
0
**
Number of colocalizations
0
3
hpf

C

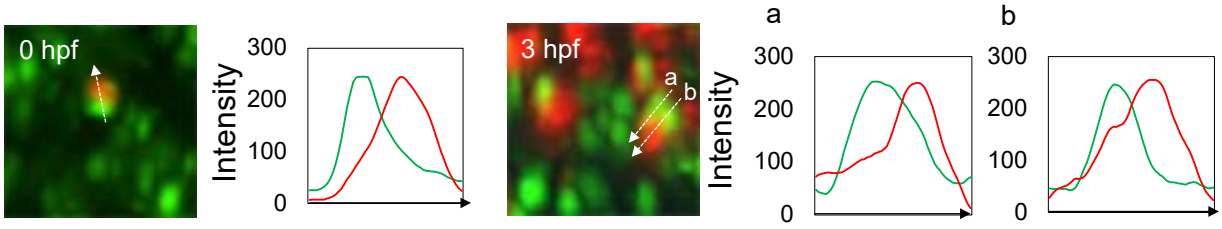
0 hpf
Intensity
300
200
100
0
3 hpf
a
b
a
b

Figure 7. **Embryos start to translate *pou5f3* mRNAs within embryonic RNA granules during the mitotic cleavage stage.** (A) A schematic view for visualization of *pou5f3*-translating sites by Rpl11-Pou5f3 PLA. Rpl11 is located at the surface of large subunits of ribosomes. (B) Detection of Rpl11-Pou5f3 PLA in embryos at 0 and 3 hpf. DNA is shown in blue. (C) The number of Rpl11-Pou5f3 PLA sites per 3,600 μm^2 in embryos at 0 and 3 hpf was counted (means $\pm$ SD; n = 6). Similar results were obtained from two independent experiments. ***p < 0.001 (Student's *t*-test). (D) 3D images of SIM for *pou5f3* mRNA (green) and Rpl11-Pou5f3 PLA sites (red) in embryos at 0 and 3 hpf. (E) The number of colocalizations of *pou5f3* RNA granules and Rpl11-Pou5f3 PLA sites per 14,400 μm^3 in embryos at 0 and 3 hpf were counted (means $\pm$ SD; n = 6). Similar results were obtained from two independent experiments. **p < 0.01 (Student's *t*-test). Bars, 20 μm.

A

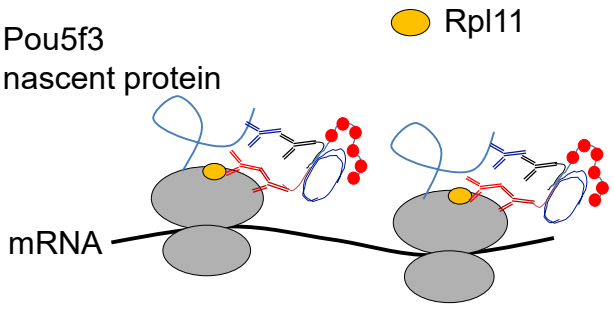
Rpl11
Pou5f3
nascent protein
mRNA

B

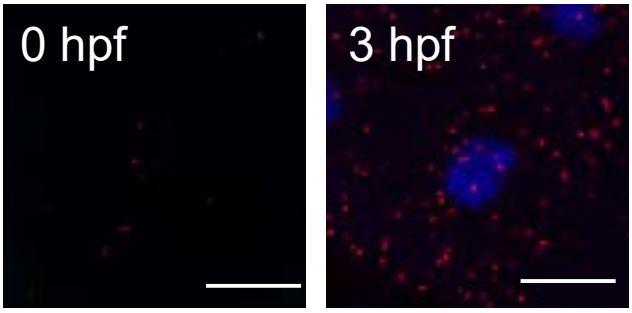
0 hpf
3 hpf

C

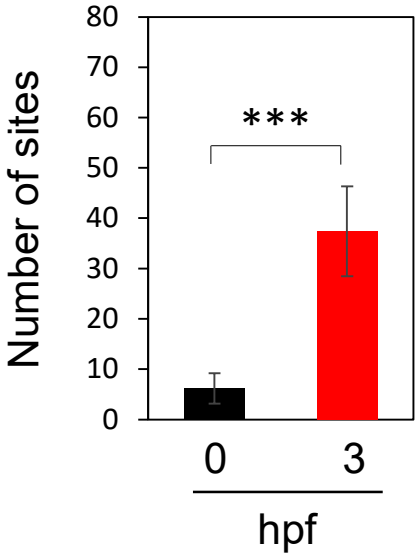
Number of sites
80
70
60
50
40
30
20
10
0
***
0
3
hpf

D

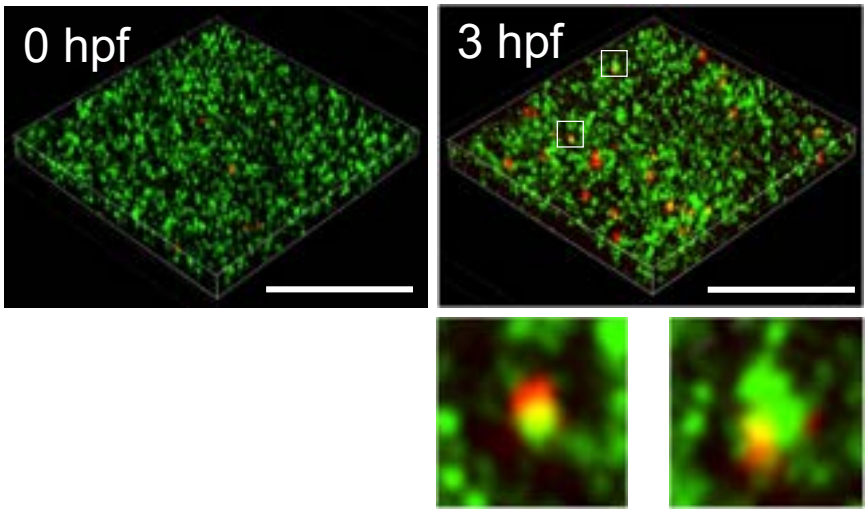
0 hpf
3 hpf

E

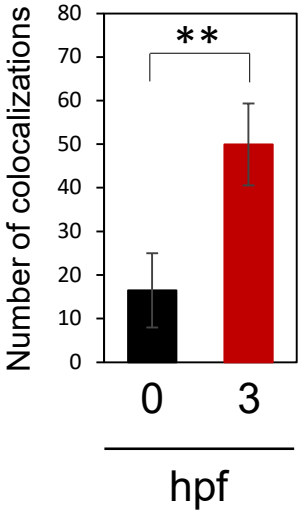
Number of colocalizations
80
70
60
50
40
30
20
10
0
**
0
3
hpf

Figure 8. **The state of embryonic RNA granules is changed from solid-like to liquid-like during early stages of development.**
(A) Quantitative analysis of the volumes of *pou5f3* RNA granules in embryos at 0 and 3 hpf. (B) Quantitative analysis of the average volumes of *pou5f3* RNA granules in embryos at 0 and 3 hpf (means ± SD; n = 3). *p < 0.05 (Student's *t*-test). (C-F) FISH analysis of *pou5f3* mRNA (green) in embryos at 0 hpf (C) and 3 hpf (E) without (Control) and with hexanediol (Hexanediol) or hexanetriol (Hexanetriol). DNA is shown in blue. The number of *pou5f3* RNA granules per 3,600 μm^2 in the embryos at 0 hpf (D) and 3 hpf (F) treated without (-) and with hexanediol (HD) or hexanetriol (HT) was counted (means ± SD; n = 4). Similar results were obtained from two independent experiments. **p < 0.01, ***p < 0.001 (Tukey-Kramer test). (G) Immunoblotting of puromycylated peptides with anti-puromycin antibody in embryos at 3 hpf treated with (+) or without (−) puromycin (Puro) and hexanediol (HD). (H) Puro-PLA of *pou5f3*-translating sites (red) in embryos at 3 hpf without (Control) and with hexanediol (Hexanediol) or hexanetriol (Hexanetriol). DNA is shown in blue. (I) The number of *pou5f3*-translating sites per 3,600 μm^2 in the embryos treated without (-) and with hexanediol (HD) or hexanetriol (HT) was counted (means ± SD; n = 6). Similar results were obtained from two independent experiments. ***p < 0.001, ****p < 0.0001 (Tukey-Kramer test). Bars, 20 μm.

A

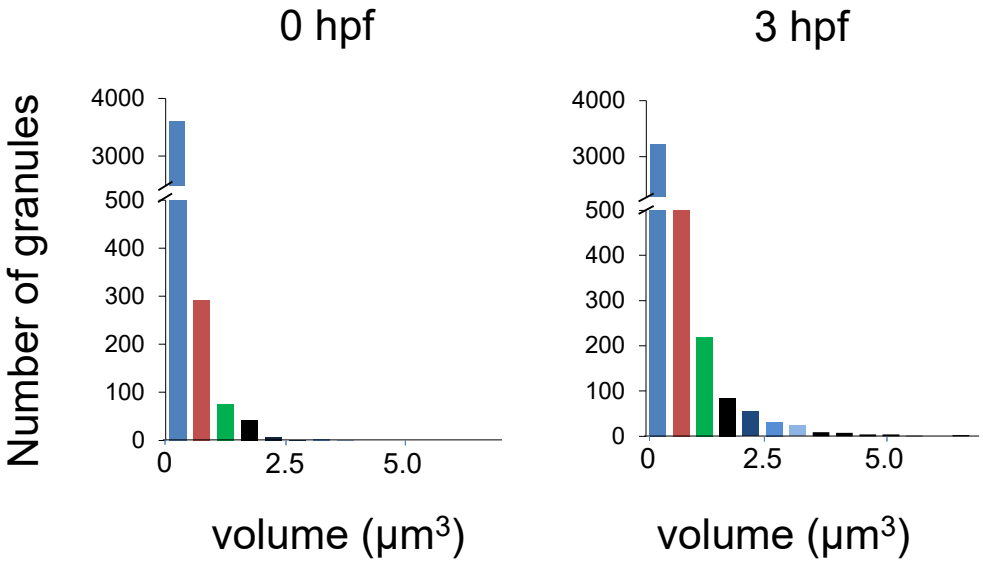
0 hpf
3 hpf
Number of granules
4000
3000
500
400
300
200
100
0
0
2.5
5.0
volume (μm3)
volume (μm3)

B

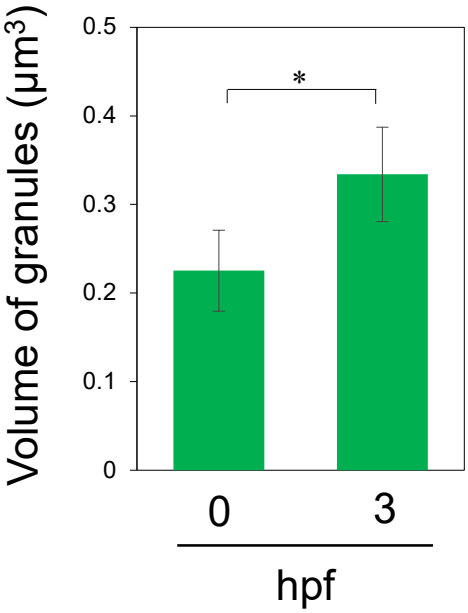
Volume of granules (μm3)
0.5
0.4
0.3
0.2
0.1
0
*
0
3
hpf

C

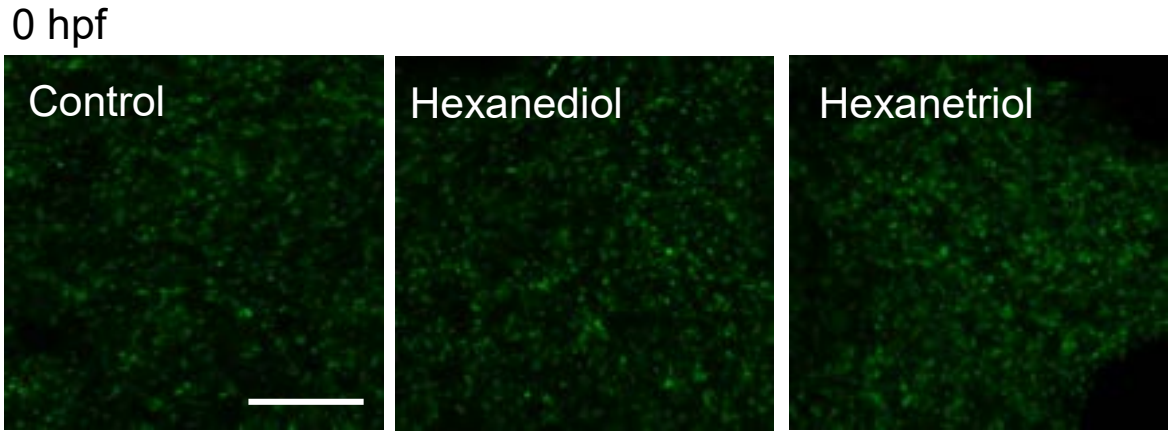
0 hpf
Control
Hexanediol
Hexanetriol

D

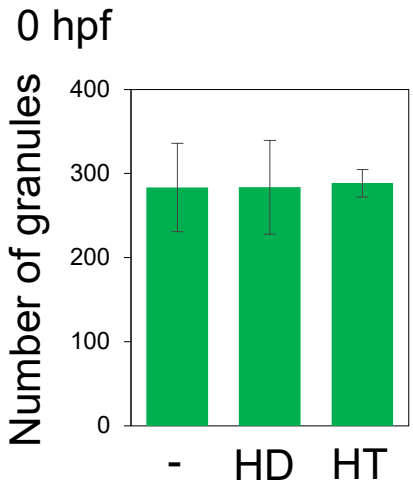
0 hpf
Number of granules
400
300
200
100
0
-
HD
HT

E

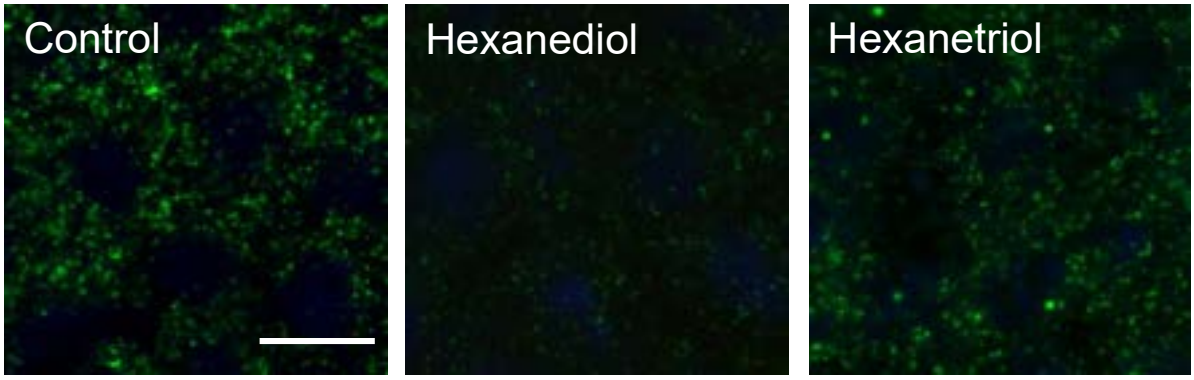
3 hpf
Control
Hexanediol
Hexanetriol

F

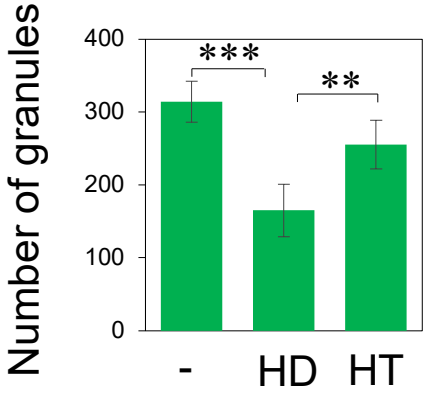
3 hpf
Number of granules
400
300
200
100
0
***
**
-
HD
HT

G

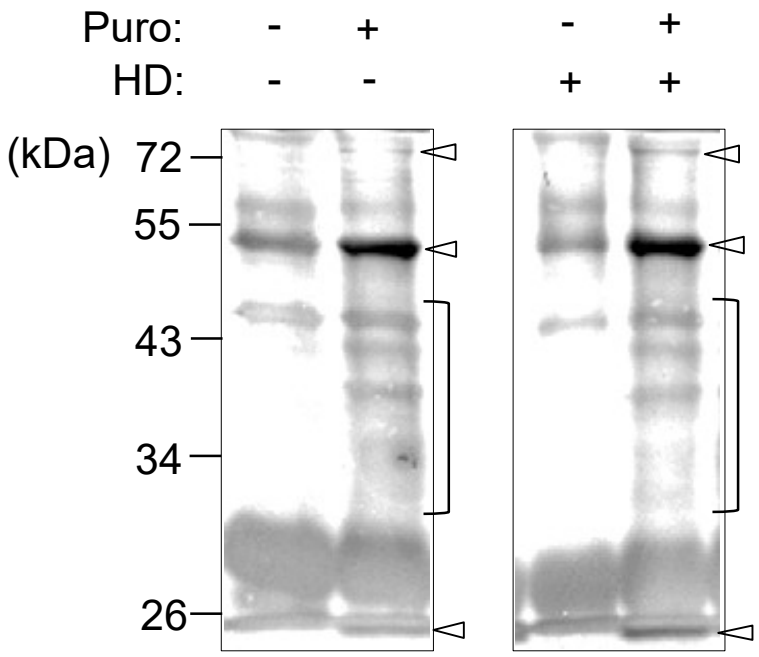
Puro: - + - +
HD: - - + +
(kDa)
72
55
43
34
26

H

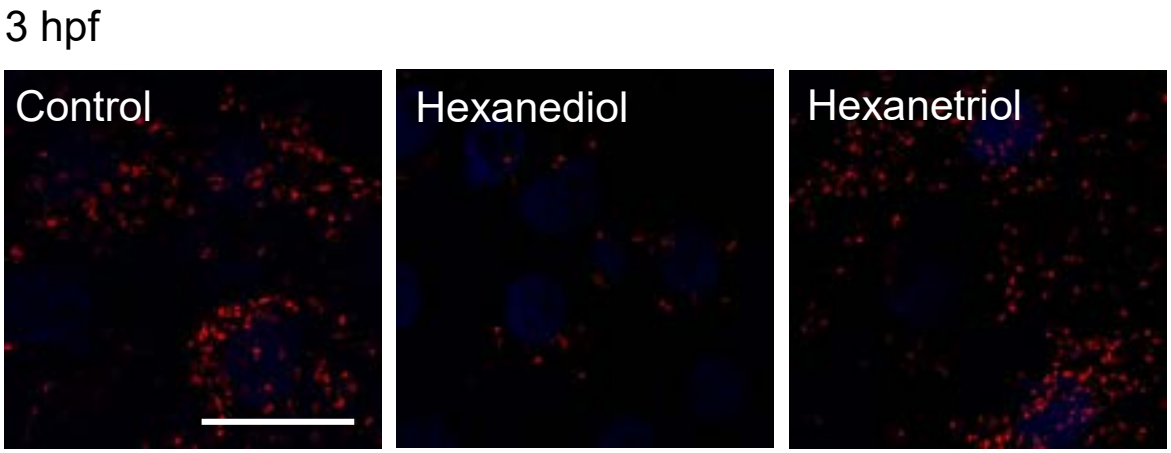
3 hpf
Control
Hexanediol
Hexanetriol

I

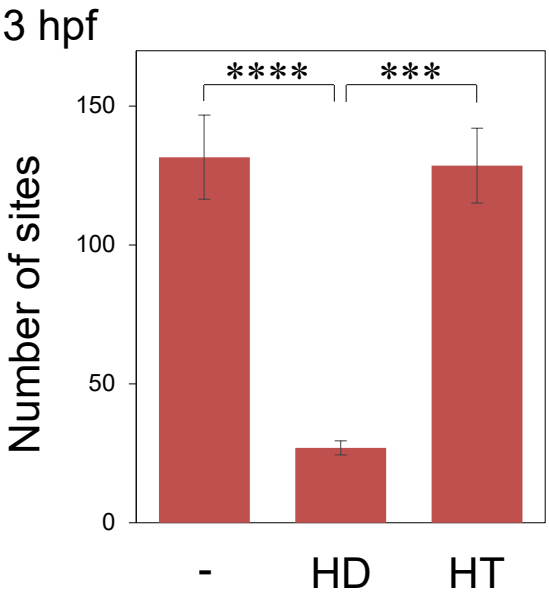
3 hpf
****
***
Number of sites
150
100
50
0
-
HD
HT

Figure 9. **The amount of Syncrip is decreased during the early stages of zebrafish development.** (A) Domain structure of zebrafish Syncrip. RBD, RNA-binding domain. (B) Evaluation of mouse and rabbit anti-Syncrip antibody specificity. The upper band (indicated with *) may be non-specific signal. (C) Time course analysis of the amount of Syncrip in embryos at hours post fertilization (hpf). Rpl11 is a loading control. (D) Relative amounts of Syncrip (means ± SD; n = 5). NS, not significant; *p < 0.05; **p<0.01 (Tukey-Kramer test). (E) Immunofluorescence of Syncrip in embryos at 0, 3, and 6 hpf. No 1st Ab at 0 hpf is the image as negative control. DNA is shown in blue. Scale bars, 20 μm.

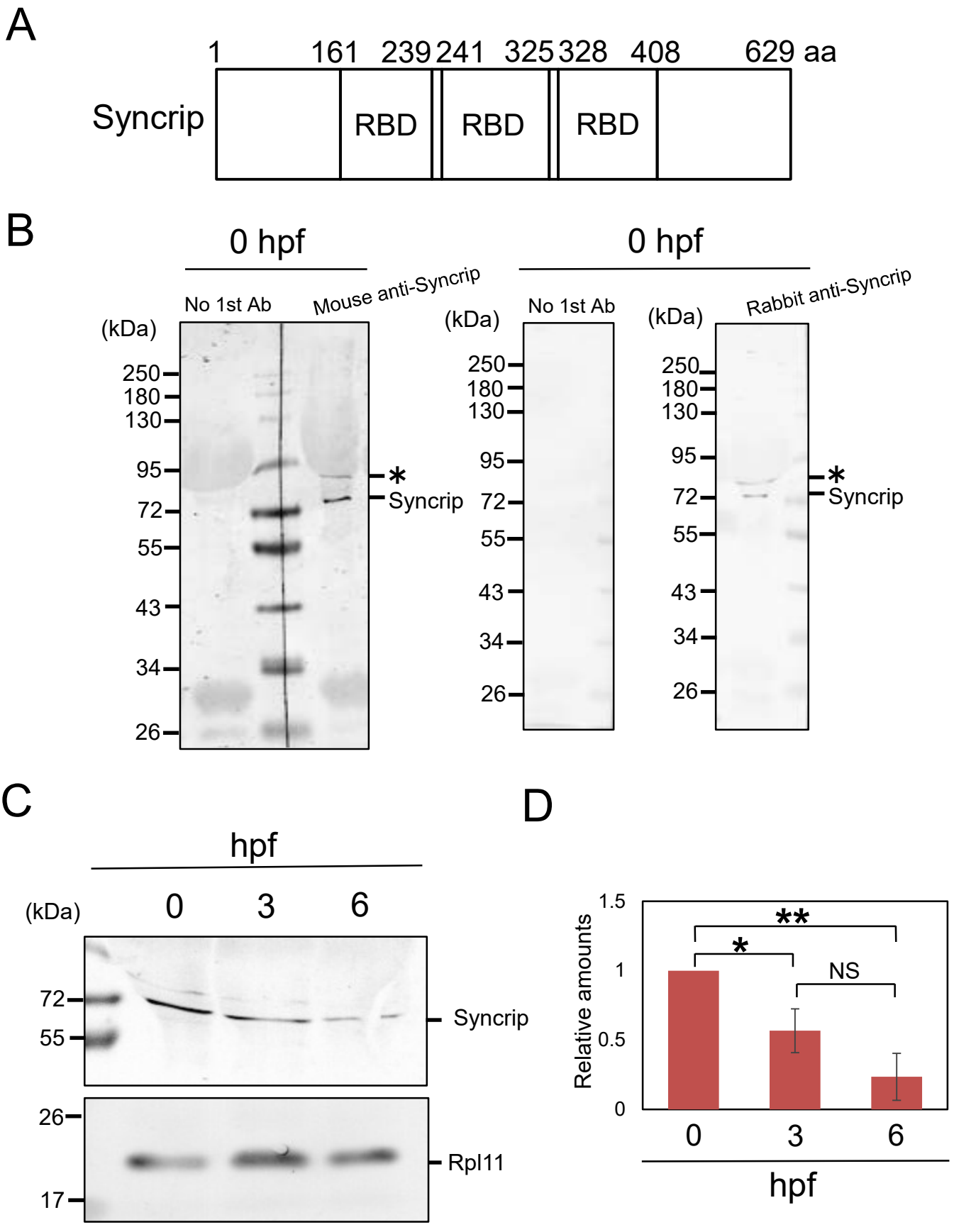
A
1
161
239
241
325
328
408
629 aa
Syncrip
RBD
RBD
RBD
B
0 hpf
0 hpf
No 1st Ab
Mouse anti-Syncrip
No 1st Ab
Rabbit anti-Syncrip
(kDa)
(kDa)
(kDa)
250
180
130
95
72
55
43
34
26
*
Syncrip
C
hpf
(kDa)
0
3
6
72
55
26
17
Syncrip
Rpl11
D
Relative amounts
1.5
1
0.5
0
**
*
NS
0
3
6
hpf

E

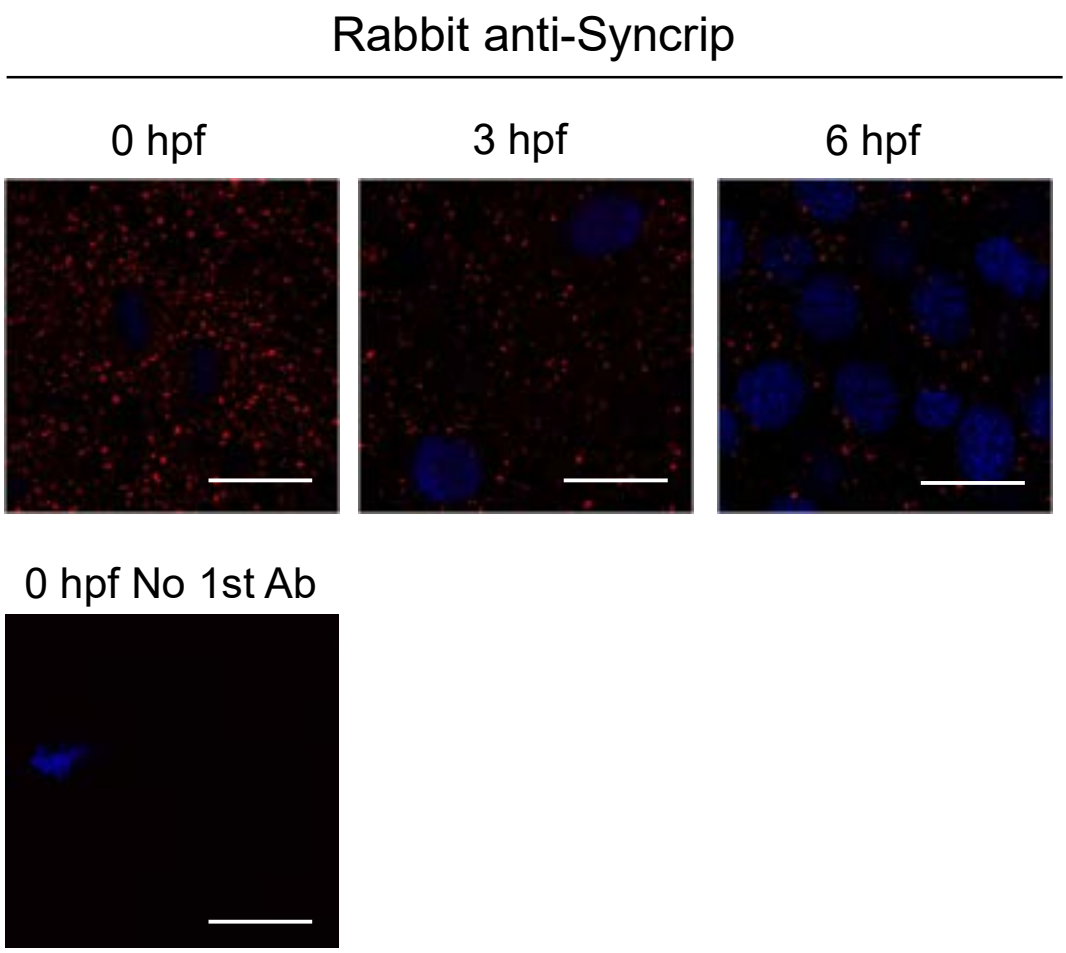

Figure 10. Syncrip binds to *pou5f3* mRNA in embryos. (A) Double staining of *pou5f3* mRNA (green) and Syncrip (red) in embryos at 0 and 3 hpf. DNA is shown in blue. Left, high-resolution confocal images. Right, enlarged views of the boxed regions in the left images. Bars, 20 μm. (B) The number of colocalizations of *pou5f3* RNA granules and Syncrip per 100 μm^2 in embryos at 0 and 3 hpf were counted (means ±SD; n=8). Similar results were obtained from two independent experiments. ******$p < 0.000001$ (Student's *t* test). (C) Immunoblotting of embryo extracts at 0 hpf before IP (Initial) and IP with control IgG (IgG) or anti-Syncrip (α-Syncrip) antibody and RT-PCR for *pou5f3* and *α-tubulin* mRNA. Similar results were obtained from two independent experiments.

A

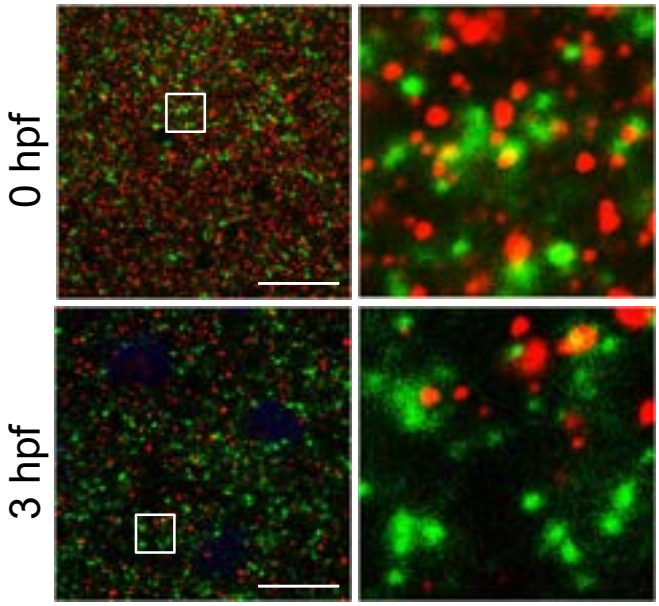
0 hpf
3 hpf

B

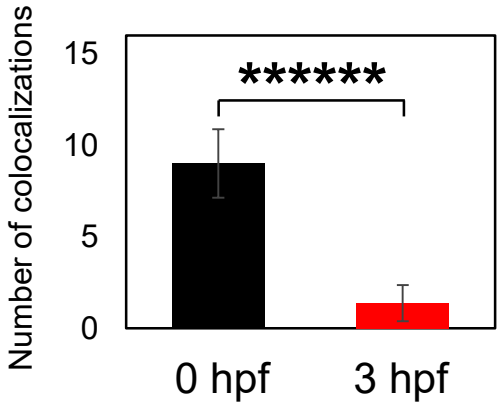
Number of colocalizations
15
10
5
0
******
0 hpf
3 hpf

C

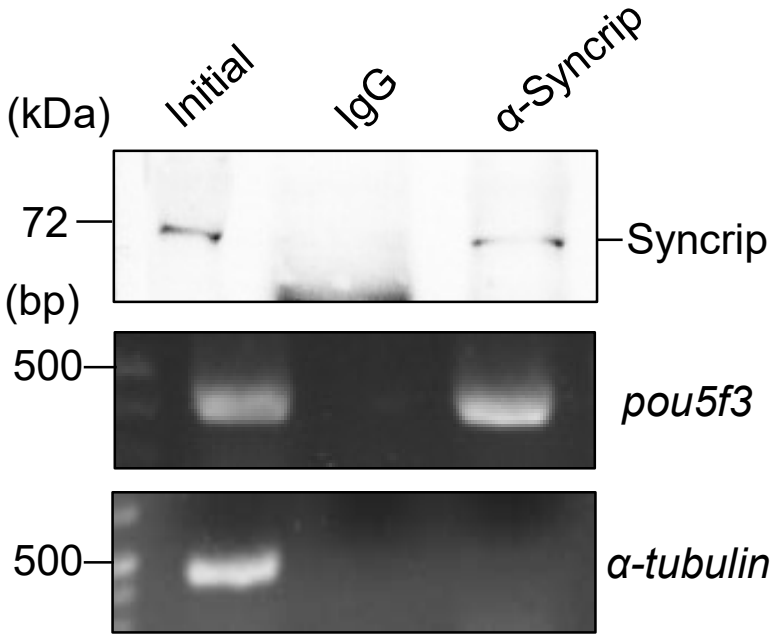
(kDa)
Initial
IgG
α-Syncrip
72
Syncrip
(bp)
500
pou5f3
500
α-tubulin

Figure 11. Over-expression of Syncrip represses *pou5f3* mRNA translation.

(A) Immunoblotting of Pou5f3, GFP-Syncrip, GFP, and Rpl11 in embryos not injected (-) and injected with GFP (GFP) or GFP-Syncrip (GFP-Syncrip) at 6 hpf. The band indicated by the arrow is GFP-Syncrip. ＊ indicates the egg yolk. Rpl11 is a loading control. (B) Relative amounts of Pou5f3 in embryos not injected (-) and injected with GFP (GFP) or GFP-Syncrip (GFP-Syncrip) at 6 hpf (means ±SD; n=3). Similar results were obtained from three independent experiments. *$p < 0.05$; **$p<0.01$ (Tukey-Kramer test). (C) Double immunofluorescence of GFP (green) and Pou5f3 (red) in embryos not injected (-) and injected with GFP (GFP) or GFP-Syncrip (GFP-Syncrip) at 6 hpf. Bars, 20 μm. (D) PAT assay for *pou5f3* mRNA in embryos not injected (-) and injected with GFP (GFP) or GFP-Syncrip (GFP-Syncrip) at 6 hpf. Similar results were obtained from two independent experiments. (E) IP/RT-PCR analysis of GFP and GFP-Syncrip with *pou5f3* mRNA. Left: Immunoblotting of IP with control IgG (IgG) and anti-GFP (α-GFP) or anti-GFP Syncrip (α-GFP Syncrip) antibody using embryo extracts at 6 hpf. Right: RT-PCR for *pou5f3* mRNA. Similar results were obtained from two independent experiments.

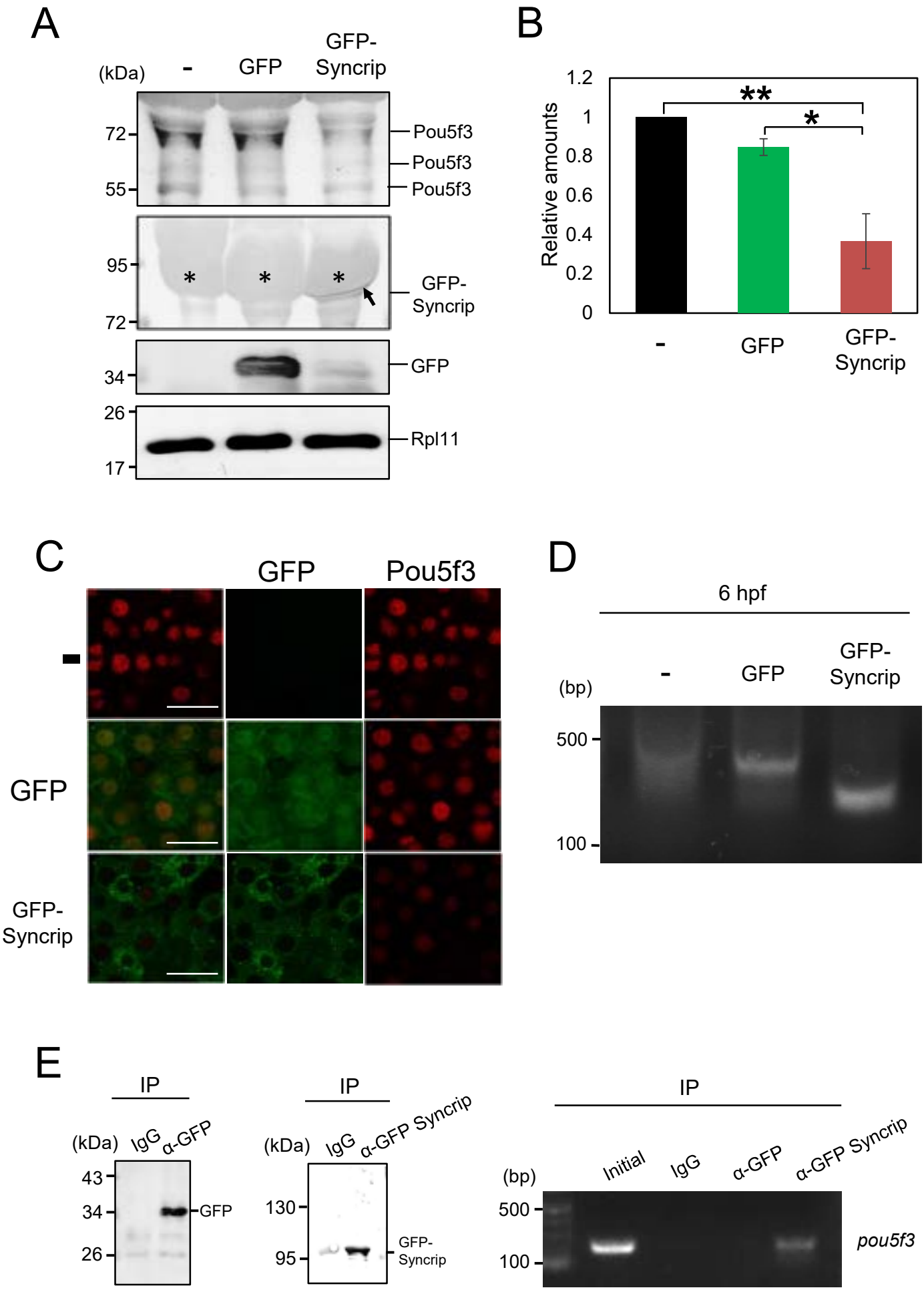
A
(kDa)
-
GFP
GFP-Syncrip
72
55
95
72
34
26
17
Pou5f3
Pou5f3
Pou5f3
GFP-Syncrip
GFP
Rpl11
B
Relative amounts
1.2
1
0.8
0.6
0.4
0.2
0
**
*
-
GFP
GFP-Syncrip
C
GFP
Pou5f3
-
GFP
GFP-Syncrip
D
6 hpf
-
GFP
GFP-Syncrip
(bp)
500
100
E
IP
(kDa)
IgG
α-GFP
43
34
26
GFP
IP
(kDa)
IgG
α-GFP Syncrip
130
95
GFP-Syncrip
IP
(bp)
Initial
IgG
α-GFP
α-GFP Syncrip
500
100
pou5f3

Figure 12. Syncrip interacts with proteins involved in translational regulation.
(A) Immunoblotting of embryo extracts at 0 hpf before IP (Initial) and IP with control IgG (IgG) or anti-Syncrip (α-Syncrip) antibody. (B) Silver staining of proteins immunoprecipitated with IgG or anti-Syncrip (α-Syncrip) antibody. The arrow heads indicate bands specifically detected in α-Syncrip. (C) Gene ontology analysis (molecular function) of proteins isolated as proteins interacting with Syncrip (Table. 2). (D) Representations of proteins isolated in mass spectrometry and involved in translation.

A

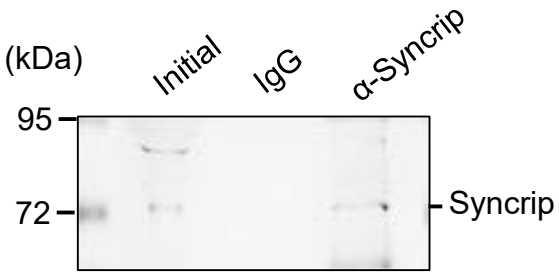

B

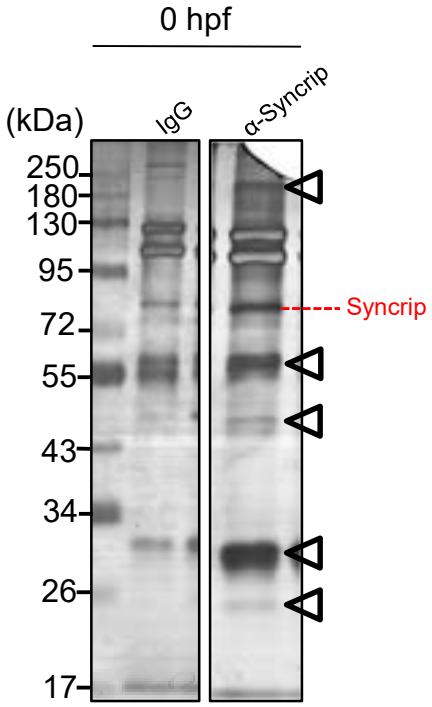

C

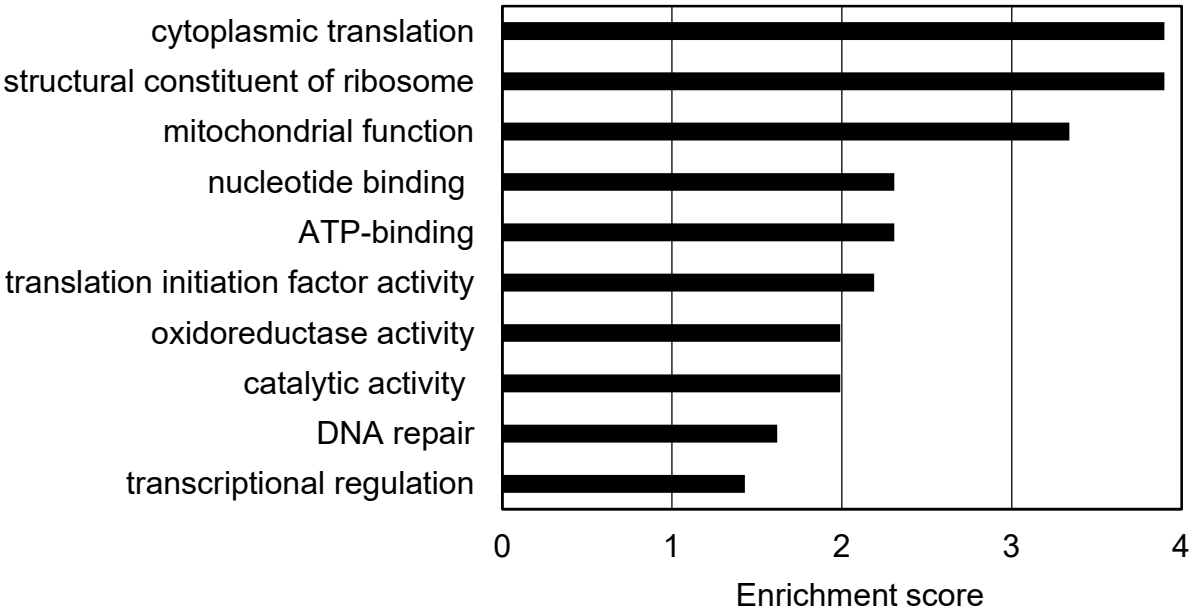

D

Cnot1	Igf2bp3
Stau2	Piwil1
Eif2s3	Pabpc1a
Eif2a	Paf1
Eif3a	Sf3b3
Eif3d	Spt6
Eif3l	Ybx1

Figure 13. Ewsr1b is increased during the early stages of development and localized in the nucleus and cytoplasm. (A) Top: Domain structure of zebrafish Ewsr1a and Ewsr1b. SYGQ-rich, serine-tyrosine-glycine-glutamine-rich domain; RGG, arginine-glycine-glycine-rich domain; RRM, RNA recognition domain; ZnF, zinc finger domain; NLS, nuclear localization signal. Bottom: Comparison of amino acid sequences between Ewsr1a and Ewsr1b. Light blue; SYGQ-rich domain, Orange; RGG domain, Green; RRM domain, Purple; ZnF domain, Black; NLS. Amino acids highlighted in yellow are common to the two proteins (Total: 396). (B) RT-PCR for *ewsr1a*, *ewsr1b*, and *β-actin* mRNAs in oocytes and embryos at 6 hpf. (C) Quantitative RT-PCR for *ewsr1a* and *ewsr1b* mRNAs in oocytes (left) and embryos at 6 hpf (right) (means ±SD; n = 3). ******$p < 0.000001$; *******$p < 0.0000001$ (Student's *t* test). (D) Evaluation of mouse anti-Ewsr1b antibody specificity. (E) Time courses of Ewsr1b accumulation in embryos at 0, 3, and 6 hpf. Rpl11 is a loading control. (F) Relative amounts of Ewsr1b (means ±SD; n = 3). NS; not significant, **$p < 0.01$ (Tukey-Kramer test). (G) Immunofluorescence of Ewsr1b at 0, 1, 3, and 6 hpf. DNA is shown in blue. Upper, high-resolution confocal images. Lower, enlarged views of the boxed regions in the upper images. No 1st Ab at 6 hpf is the image as negative control. Similar results were obtained from three independent experiments. Bars, 20 μm.

A

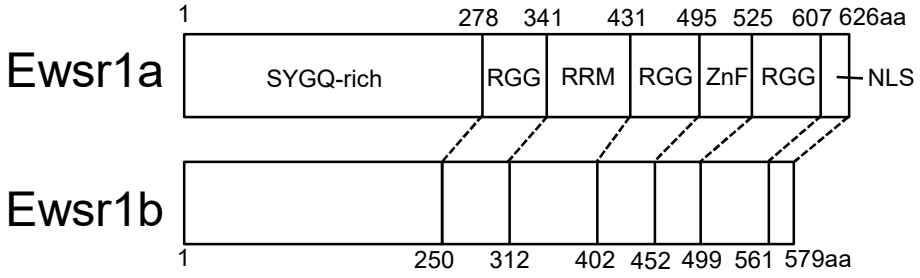
1
278
341
431
495
525
607
626aa
Ewsr1a
SYGQ-rich
RGG
RRM
RGG
ZnF
RGG
NLS
Ewsr1b
1
250
312
402
452
499
561
579aa

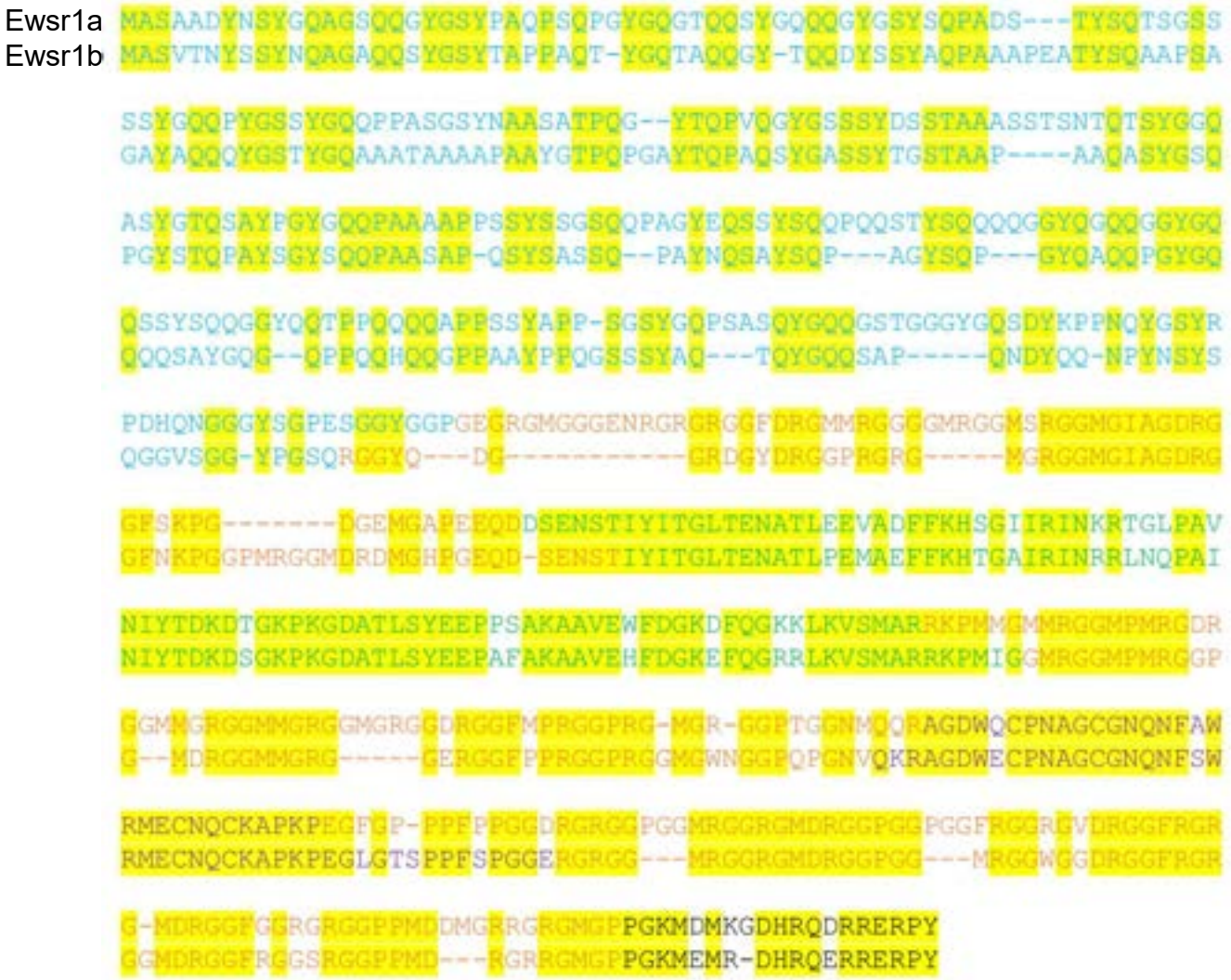
Ewsr1a
Ewsr1b

B

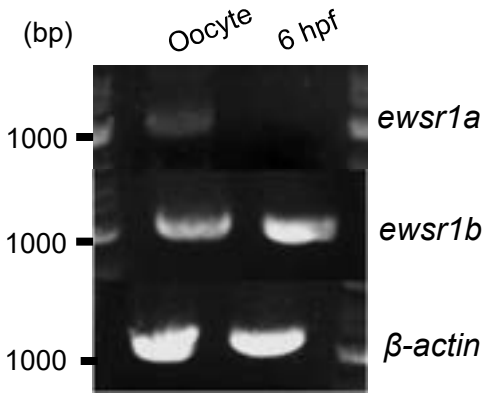
(bp)
Oocyte
6 hpf
1000
1000
1000
ewsr1a
ewsr1b
β-actin

C

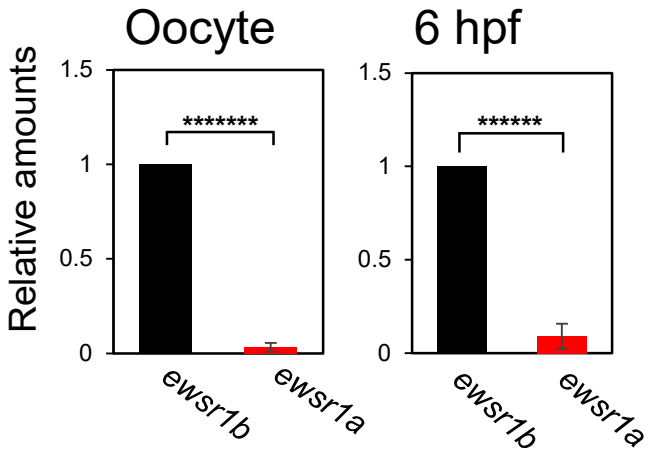
Oocyte
6 hpf
Relative amounts
1.5
1
0.5
0
****
******
ewsr1b
ewsr1a
ewsr1b
ewsr1a

D

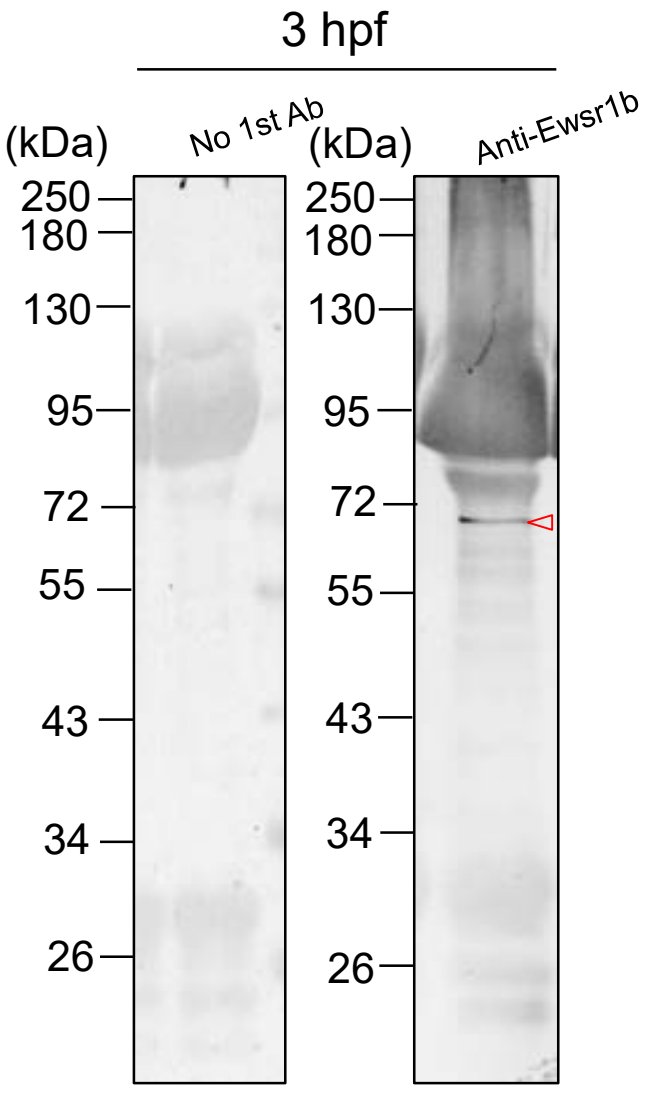
3 hpf
(kDa)
No 1st Ab
(kDa)
Anti-Ewsr1b
250
180
130
95
72
55
43
34
26
250
180
130
95
72
55
43
34
26

E

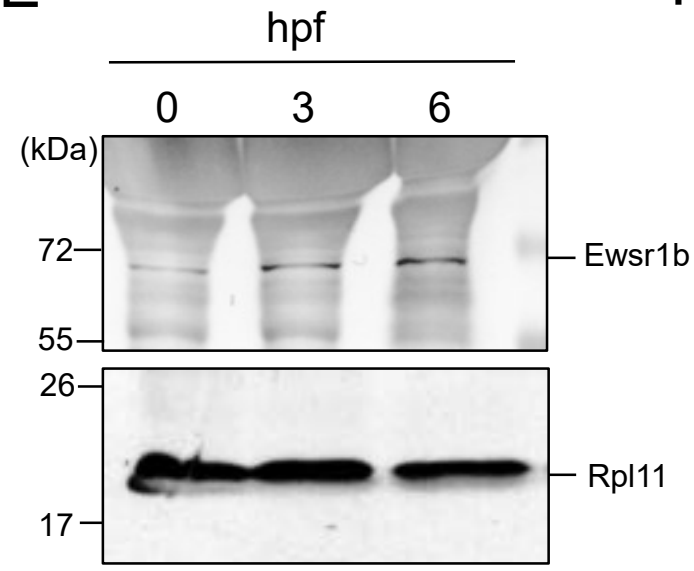
hpf
0
3
6
(kDa)
72
55
26
17
Ewsr1b
Rpl11

F

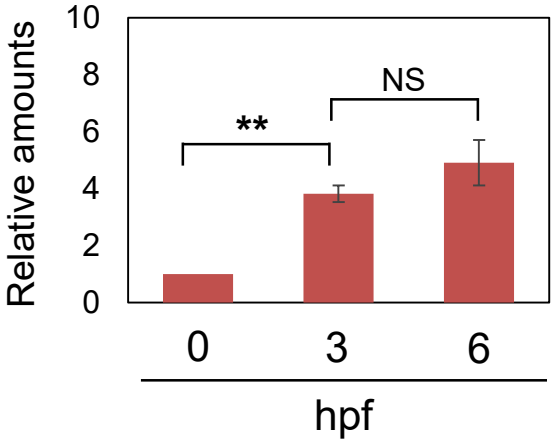
Relative amounts
10
8
6
4
2
0
**
NS
0
3
6
hpf

G

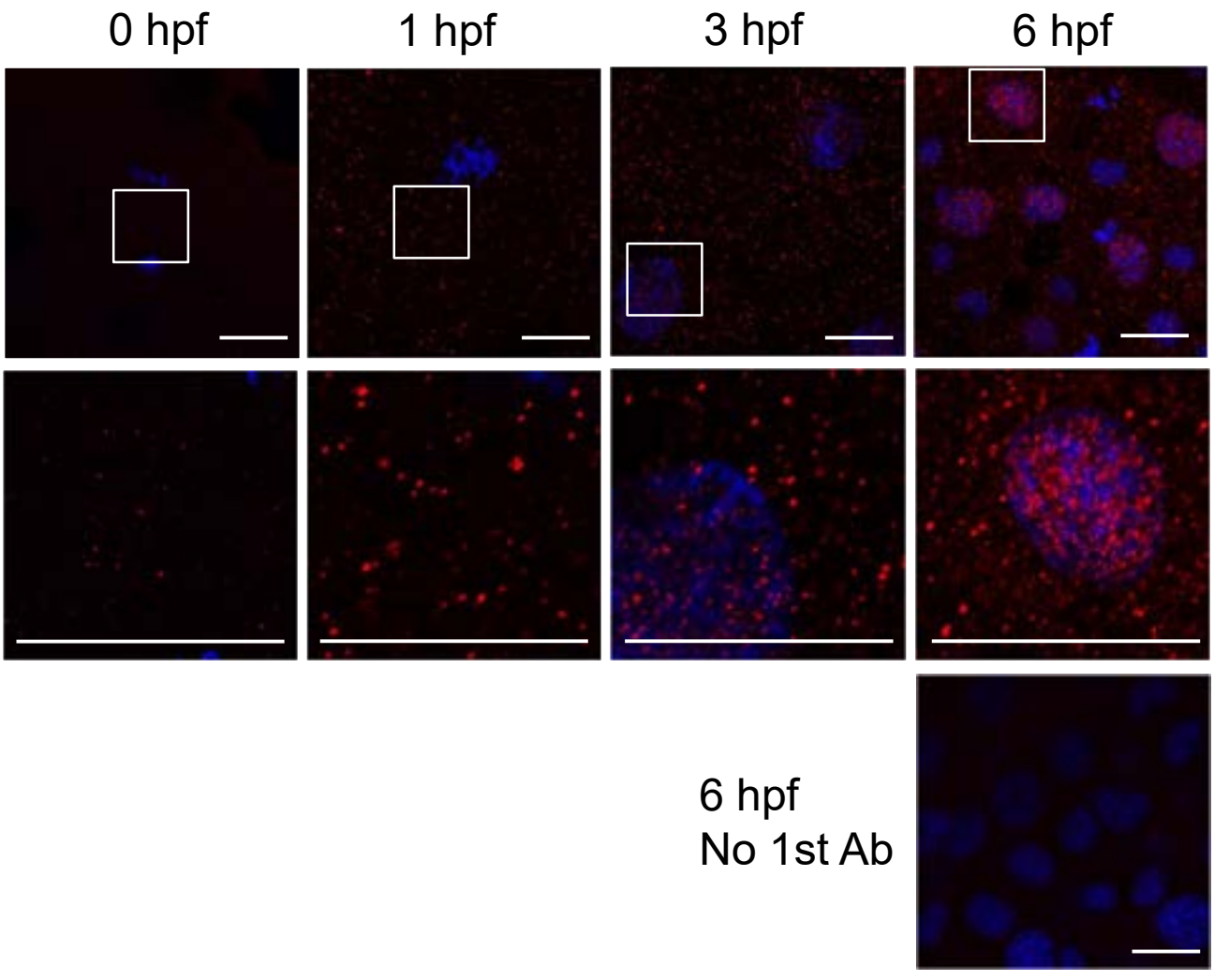
0 hpf
1 hpf
3 hpf
6 hpf
6 hpf
No 1st Ab

Figure 14. Ewsr1b would regulate *pou5f3* mRNA translation and Pou5f3 protein function.
(A) Time course analysis of Ewsr1b and Pou5f3 accumulation in embryos at 0, 1, 2, and 3 hpf. Rpl11 is a loading control. (B) Relative amounts of Ewsr1b and Pou5f3 at 0, 1, 2, and 3 hpf (means ± SD; n = 3). NS, not significant; *p < 0.05; **p < 0.01; ***p < 0.001 (Tukey-Kramer test). (C) Double staining of *pou5f3* mRNA (green) and Ewsr1b (red) at 0 and 3 hpf. DNA is shown in blue. Left, high-resolution confocal images. Right, enlarged views of the boxed regions in the left images.(D) The number of colocalizations of *pou5f3* mRNA and Ewsr1b per 100 μm^2 in embryos at 0 and 3 hpf were counted (means ± SD; n = 3). Similar results were obtained from three independent experiments. *****p < 0.00001 (Student's *t* test). (E) Staining of *pou5f3* mRNA (green), Pou5f3 (red), and Ewsr1b (magenta) at 3 hpf embryo. Left, a high-resolution confocal image. Right, enlarged views of the boxed regions in the left image. (F) Double staining of Ewsr1b (green) and Pou5f3 (red) in embryos at 3 hpf. DNA is shown in blue. Left, a high-resolution confocal image. Middle, enlarged view of the boxed region in the left image. Right, enlarged views of the boxed regions in the middle image. Similar results were obtained from three independent experiments. (G) Proximity ligation assay (PLA) of Ewsr1b and Pou5f3 in embryos at 0, 1, 2, and 3 hpf. DNA is shown in blue. (H) The number of PLA signals in embryos at 0, 1, 2, and 3 hpf per 400 μm^2 were counted (means ± SD; n = 6). *******p < 0.0000001 (Tukey-Kramer test). Bars, 20 μm.

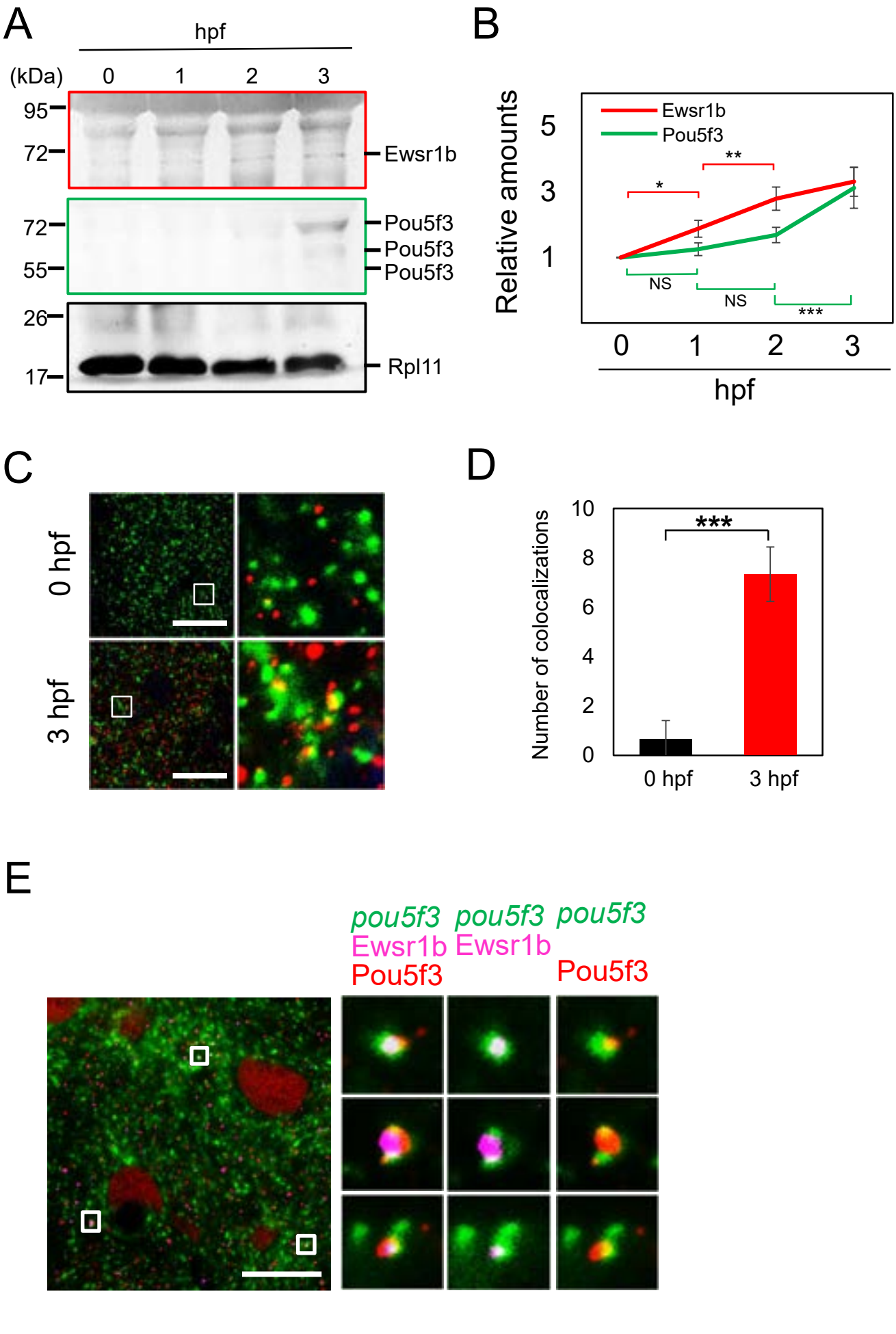
A
hpf
(kDa)
0
1
2
3
95
72
Ewsr1b
72
55
Pou5f3
Pou5f3
Pou5f3
26
17
Rpl11
B
Relative amounts
5
3
1
Ewsr1b
Pou5f3
*
**
NS
NS
***
0
1
2
3
hpf
C
0 hpf
3 hpf
D
Number of colocalizations
10
8
6
4
2
0
***
0 hpf
3 hpf
E
pou5f3
Ewsr1b
Pou5f3
pou5f3
Ewsr1b
pou5f3
Pou5f3

F

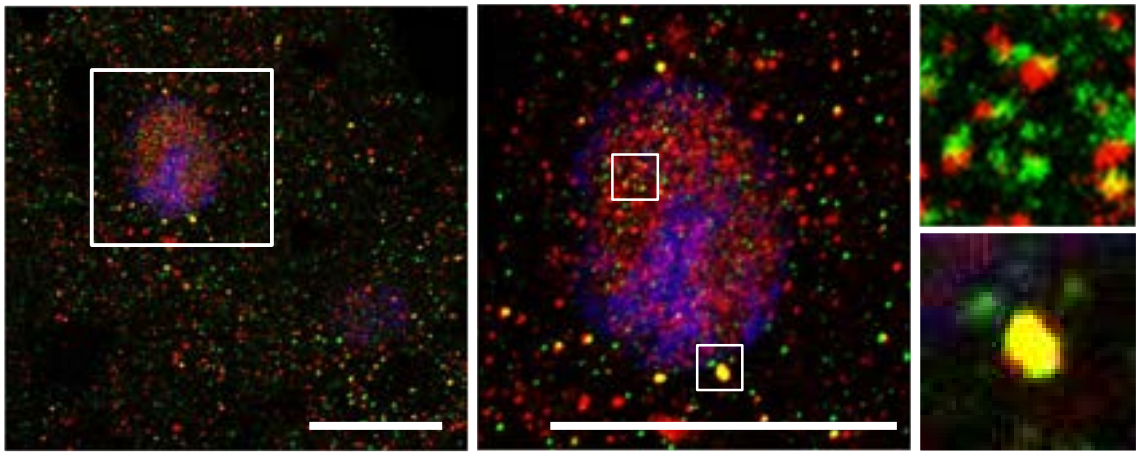

G

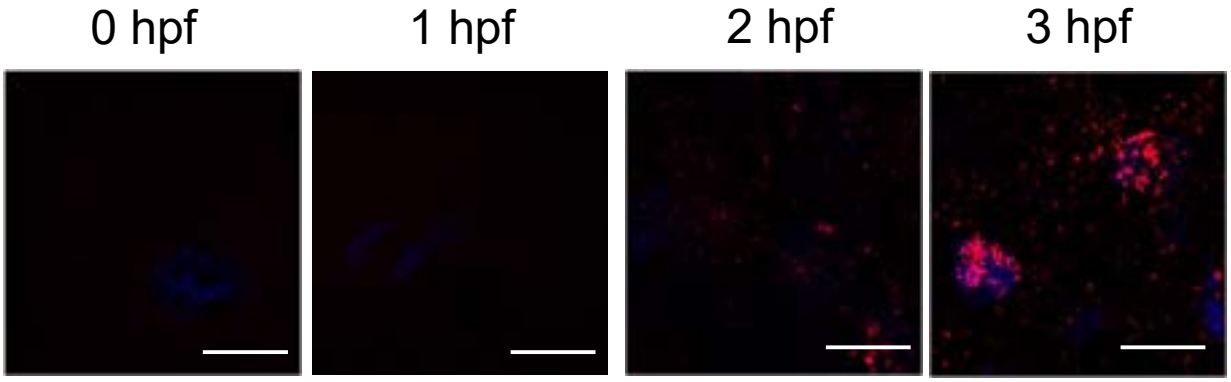
0 hpf
1 hpf
2 hpf
3 hpf

H

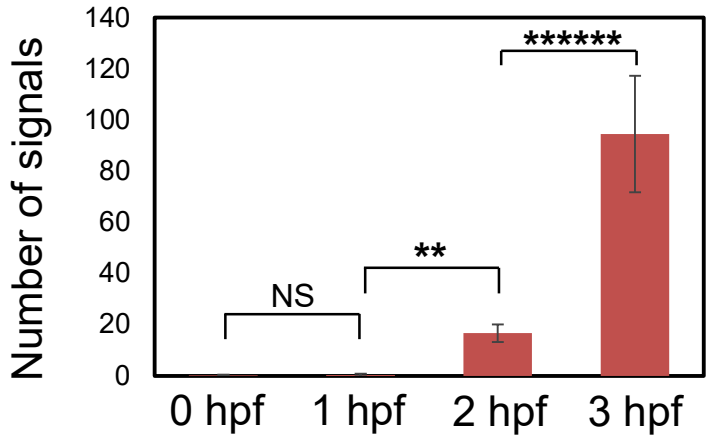
Number of signals
140
120
100
80
60
40
20
0
NS
**
******
0 hpf
1 hpf
2 hpf
3 hpf

Figure 15. Ewsr1b is required for the progression of early zebrafish development.
(A) Immunoblotting of Ewsr1b, Pou5f3 and Rpl11 in embryos not injected (-) and injected with Ewsr1b-ATG-MO (ATG-MO) and Ewsr1b-5mm-MO (5mm-MO) at 6 hpf. Rpl11 is a loading control. (B) Quantitative analysis of immunoblotting (means ± SD; n = 3). *p<0.05; **p < 0.01; ***p<0.001 (Tukey-Kramer test). (C) Lateral views of WT embryos and embryos injected with ATG-MO (ATG-MO) and 5mm-MO (5mm-MO) at 4, 6, 8, and 24 hpf. Bars, 300 μm. Similar results were obtained from six independent experiments. (D) The percentage of embryos with developmental abnormalities (means ± SD; n = 6). ********p<0.00000001 (Student's *t* test).

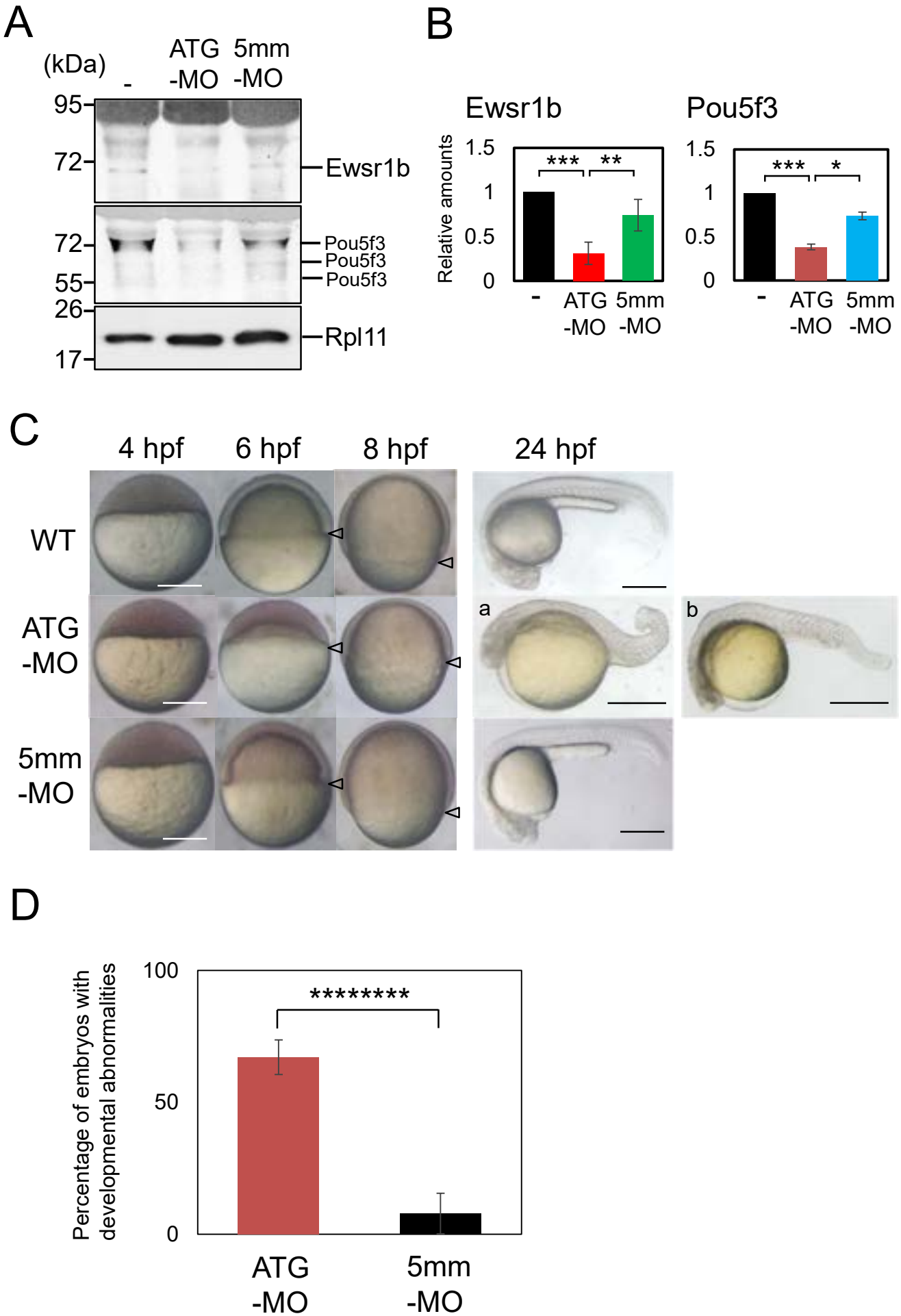
A
(kDa)
-
ATG -MO
5mm -MO
95
72
72
55
26
17
Ewsr1b
Pou5f3
Pou5f3
Pou5f3
Rpl11
B
Ewsr1b
Pou5f3
Relative amounts
1.5
1
0.5
0
***
**
*
-
ATG -MO
5mm -MO
C
4 hpf
6 hpf
8 hpf
24 hpf
WT
ATG -MO
5mm -MO
a
b
D
Percentage of embryos with developmental abnormalities
100
50
0
****
ATG -MO
5mm -MO

Figure 16. Two transcript variants of *ewsr1b* mRNA are expressed in zebrafish embryo.
(A) A schematic diagram of Long and Short sequences of *ewsr1b* mRNA 3' UTR. Light blue, stop codon; Green, poly(A) signal. (B) PAT assay for *ewsr1b* 3' UTR-Long (3' UTR-Long) and Short (3' UTR-Short) mRNA in embryos at 0, 1, 2, and 3 hpf. Similar results were obtained from three independent experiments. (C) IP/RT-PCR analysis of Rpl11 with *ewsr1b* mRNA in embryos at 1 and 3 hpf. Top: Immunoblotting of embryo extracts at 1 and 3 hpf before IP (Initial) and IP with control IgG (IgG) and anti-Rpl11 (α-Rpl11) antibody. ＊: Non-specific bands. Bottom: RT-PCR for *ewsr1b* mRNA ORF (*ewsr1b*-ORF), *ewsr1b* mRNA 3' UTR (*ewsr1b*-3' UTR) and *pou5f3* mRNA. Similar results were obtained from two independent experiments. (D) A schematic diagram of double *in situ* hybridization for identifying *ewsr1b* 3' UTR-Long and Short mRNA. (E) Double *in situ* hybridization of *ewsr1b* mRNA ORF (green) and 3' UTR (red) in embryos at 0 and 3 hpf. DNA is shown in blue. Left, high-resolution confocal images. Right, enlarged views of the boxed regions in the left images. Signals surrounded by line circles indicate 3' UTR-Long mRNAs, and signals surrounded by dotted circles indicate 3' UTR-Short mRNAs.(F) Measurement of the distance from the center of the nucleus to 3' UTR-Long (white lines) and Short mRNA (light blue dotted lines) at 3 hpf embryo. DNA is shown in blue. (G) The distance from the center of the nucleus (means ± SD; n = 60) to signals of 3' UTR-Long and Short mRNAs (means ± SD; n = 80). . Similar results were obtained from three independent experiments. **$p < 0.01$ (Student's *t* test). Bars, 20 μm.

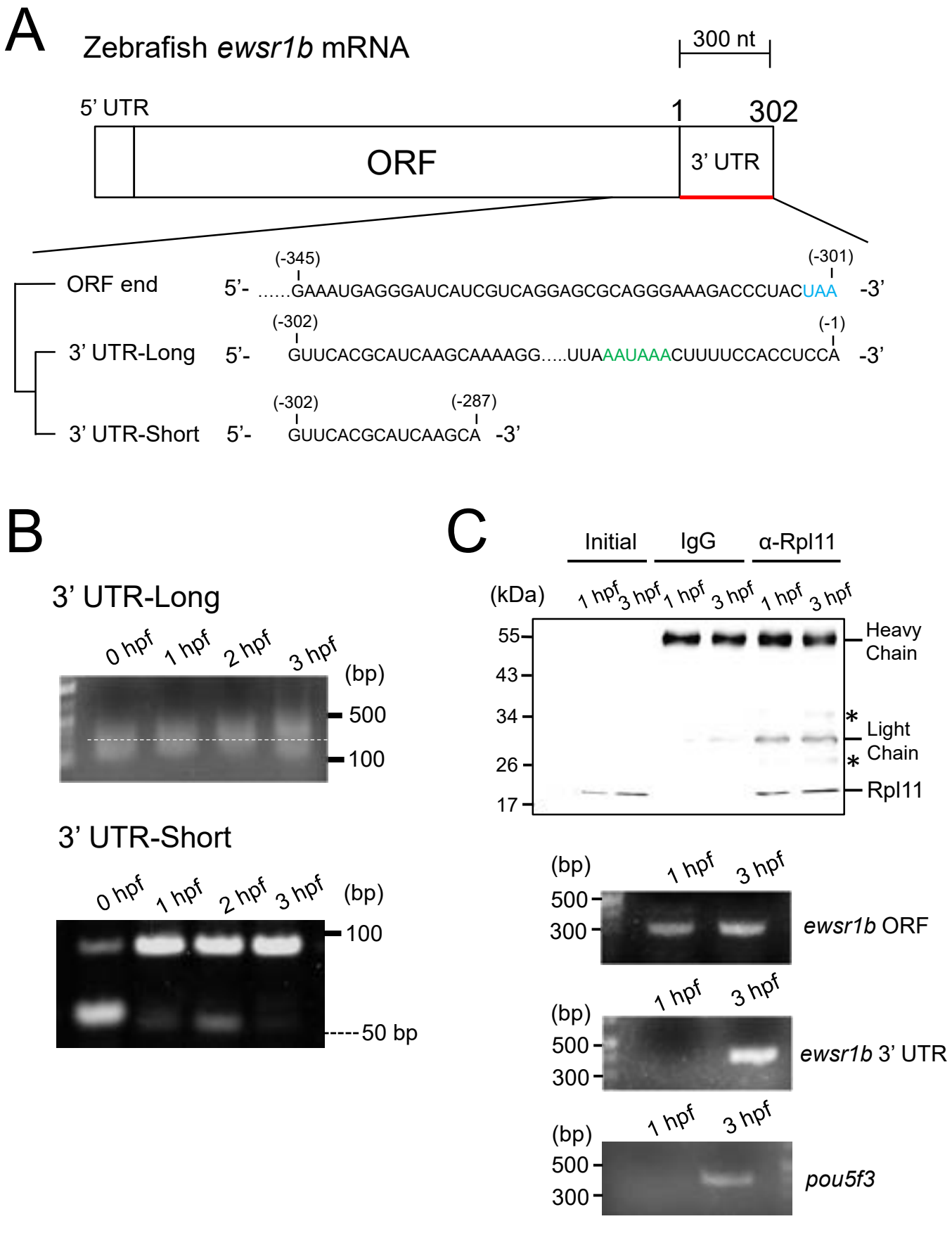
A
Zebrafish ewsr1b mRNA
300 nt
5' UTR
1
302
ORF
3' UTR
(-345)
(-301)
ORF end
5'- .....GAAAUGAGGGAUCAUCGUCAGGAGCGCAGGGAAAGACCCUACUAA -3'
(-302)
(-1)
3' UTR-Long
5'- GUUCACGCAUCAAGCAAAAGG.....UUAAAUAAACUUUUCCACCUCCA -3'
(-302)
(-287)
3' UTR-Short
5'- GUUCACGCAUCAAGCA -3'
B
3' UTR-Long
0 hpf
1 hpf
2 hpf
3 hpf
(bp)
500
100
3' UTR-Short
0 hpf
1 hpf
2 hpf
3 hpf
(bp)
100
50 bp
C
Initial
IgG
α-Rpl11
(kDa)
1 hpf
3 hpf
1 hpf
3 hpf
1 hpf
3 hpf
55
43
34
26
17
Heavy Chain
Light Chain
Rpl11
(bp)
1 hpf
3 hpf
500
300
ewsr1b ORF
(bp)
1 hpf
3 hpf
500
300
ewsr1b 3' UTR
(bp)
1 hpf
3 hpf
500
300
pou5f3

D

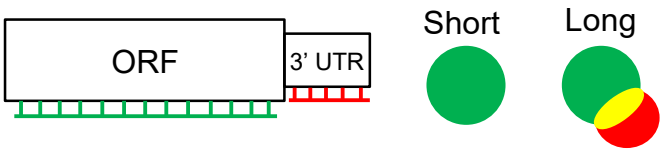
ORF
3' UTR
Short
Long

E

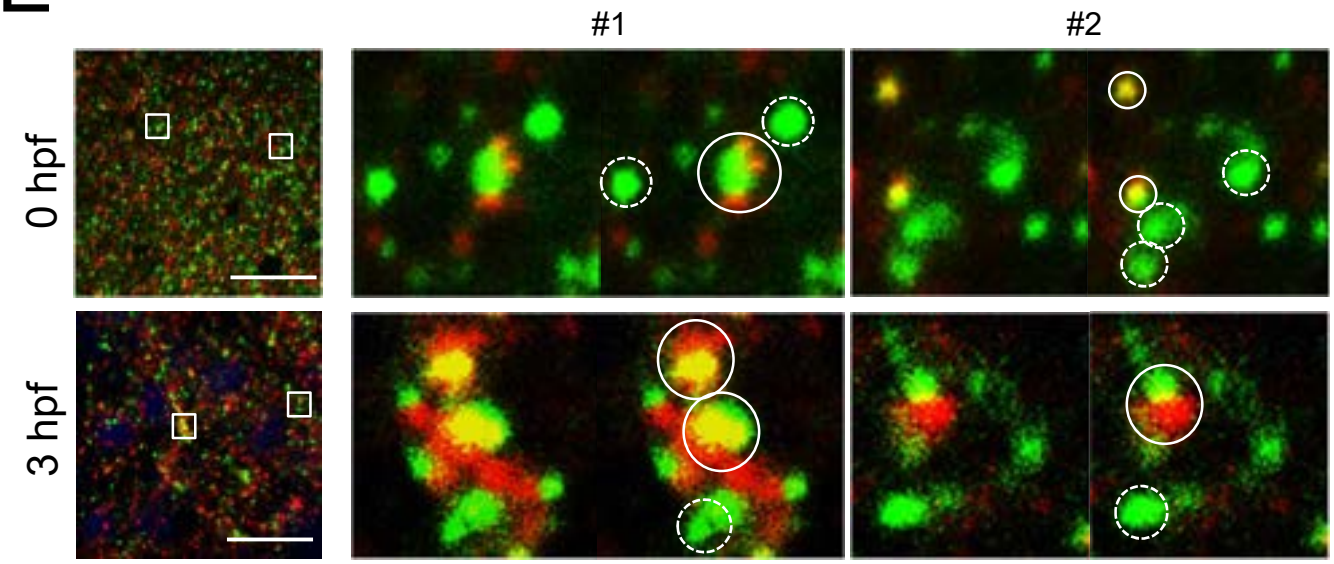
#1
#2
0 hpf
3 hpf

F

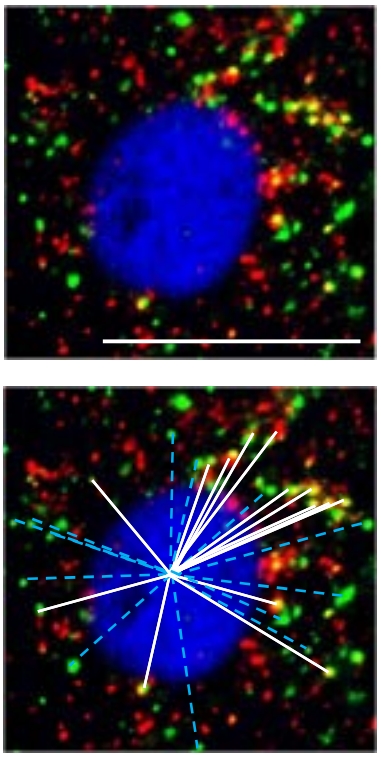

G

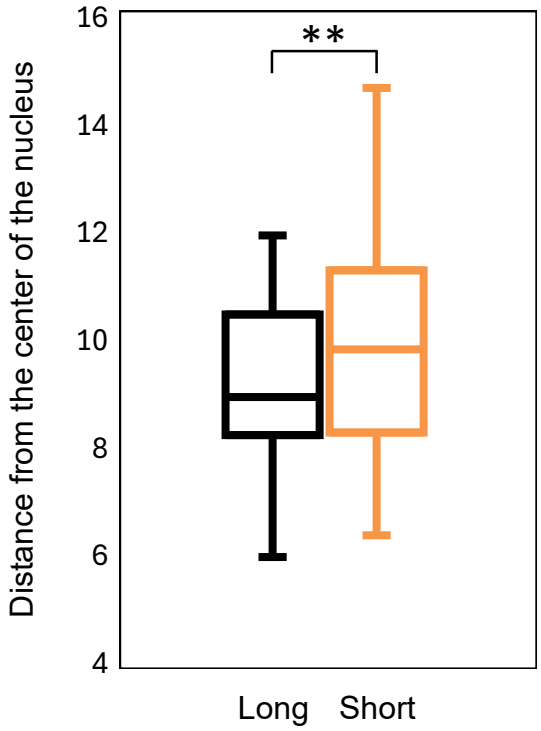
**
16
14
12
10
8
6
4
Distance from the center of the nucleus
Long
Short

Figure 17. The lengths of *ewsr1b* mRNA 3' UTR determine the protein localization and function.
(A) A schematic diagram of GFP-Ewsr1b 3' UTR-Long mRNA and GFP-Ewsr1b 3' UTR-Short mRNA. (B) Expression analysis of GFP-Ewsr1b 3' UTR-Long (Long) and GFP-Ewsr1b 3' UTR-Short (Short) in embryos at 6 hpf. Similar results were obtained from three independent experiments. Bars, 20 μm. (C) Co-immunoprecipitation and IP/RT-PCR analyses of GFP-Ewsr1b 3' UTR-Long and GFP-Ewsr1b 3' UTR-Short with Pou5f3 or *pou5f3* mRNA. Top: IP of embryo extracts at 6 hpf in embryos not injected (-) and injected with GFP-Ewsr1b 3' UTR-Long mRNA (Long) and Short mRNA (Short) with anti-GFP (α-GFP) antibody. Middle: Immunoblotting of Pou5f3. Bottom: RT-PCR for *pou5f3* mRNA. Similar results were obtained from two independent experiments. (D) Left; distribution of GFP-Ewsr1b 3' UTR-Short in embryos at 6 hpf. Right, time-lapse images of the boxed region in the left image showing fusion of two protein droplets (arrows) into a larger drop. Similar results were obtained from three independent experiments. Bars, 10 μm. (E) A schematic diagram of simultaneous detection of injected GFP-tagged mRNA and synthesized protein. (F) Double staining of GFP (green) and *gfp* mRNA (red) in embryos at 4 hpf injected with GFP-Ewsr1b 3' UTR-Long mRNA (Long) and Short mRNA (Short). Bars, 20 μm. (G) The distance from the center of the nucleus to signals of GFP-Ewsr1b 3' UTR-Long mRNA (Long) and Short mRNA (Short) (means ± SD; n = 80). Similar results were obtained from two independent experiments. **********$p < 0.0000000001$ (Student's *t* test).

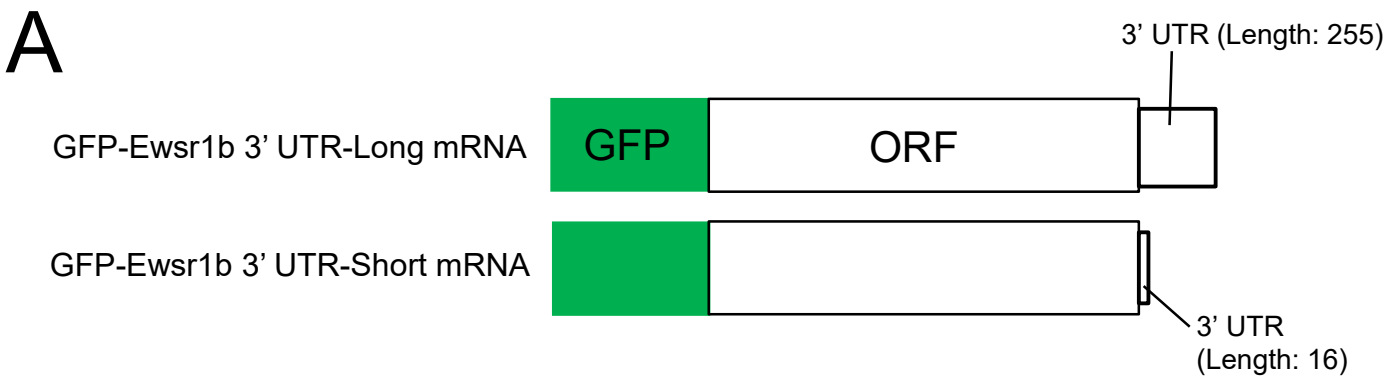
A
3' UTR (Length: 255)
GFP-Ewsr1b 3' UTR-Long mRNA
GFP
ORF
GFP-Ewsr1b 3' UTR-Short mRNA
3' UTR
(Length: 16)

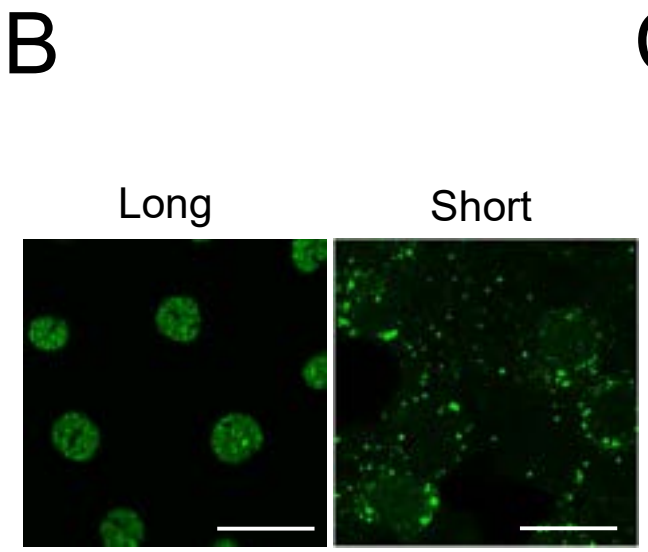
B
Long
Short

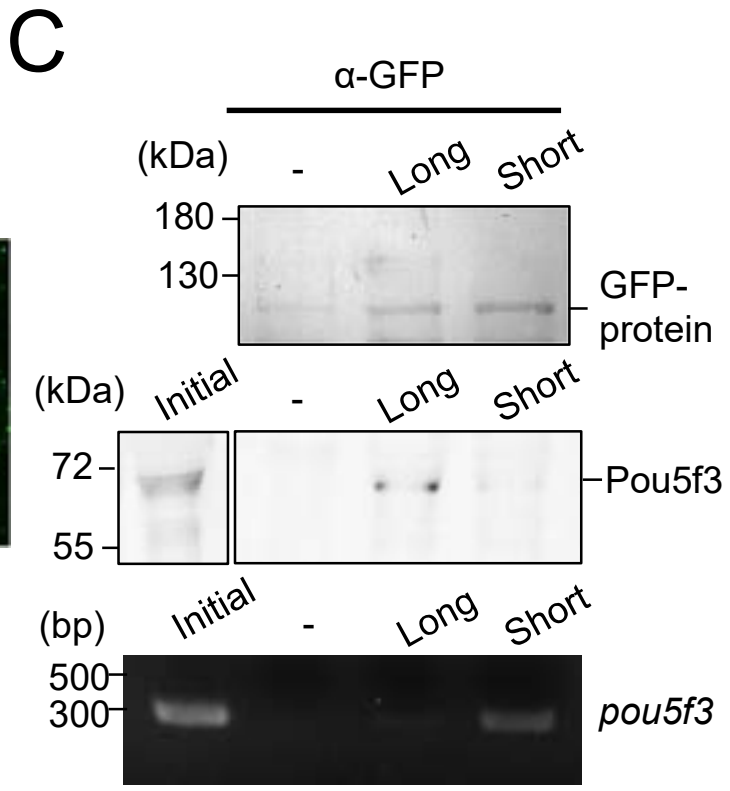
C
α-GFP
(kDa)
-
Long
Short
180
130
GFP-
protein
(kDa)
Initial
-
Long
Short
72
55
Pou5f3
(bp)
Initial
-
Long
Short
500
300
pou5f3

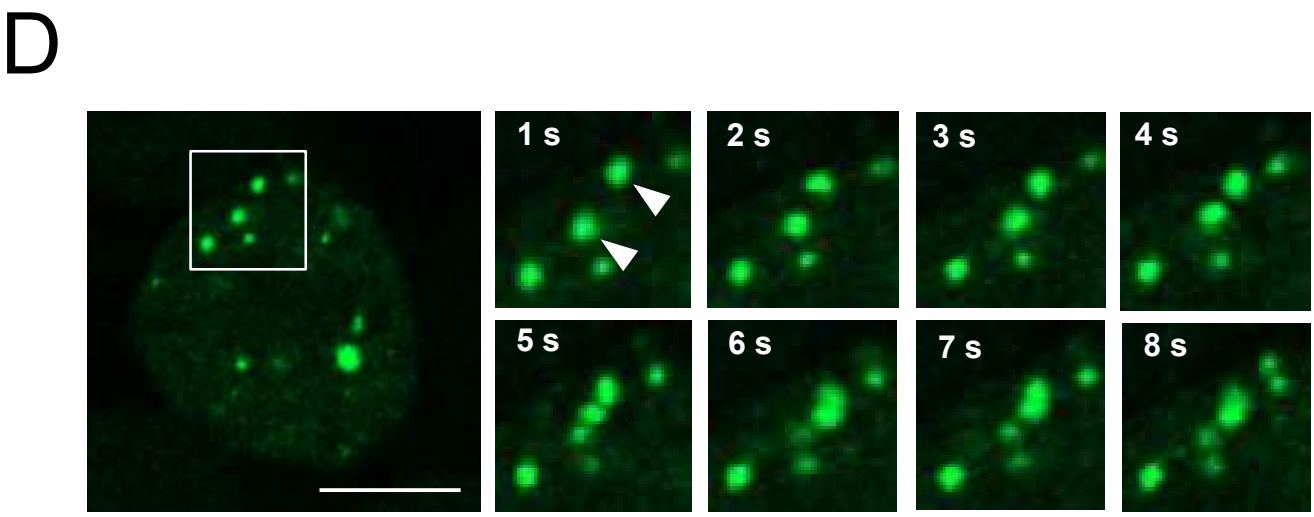
D
1 s
2 s
3 s
4 s
5 s
6 s
7 s
8 s

E

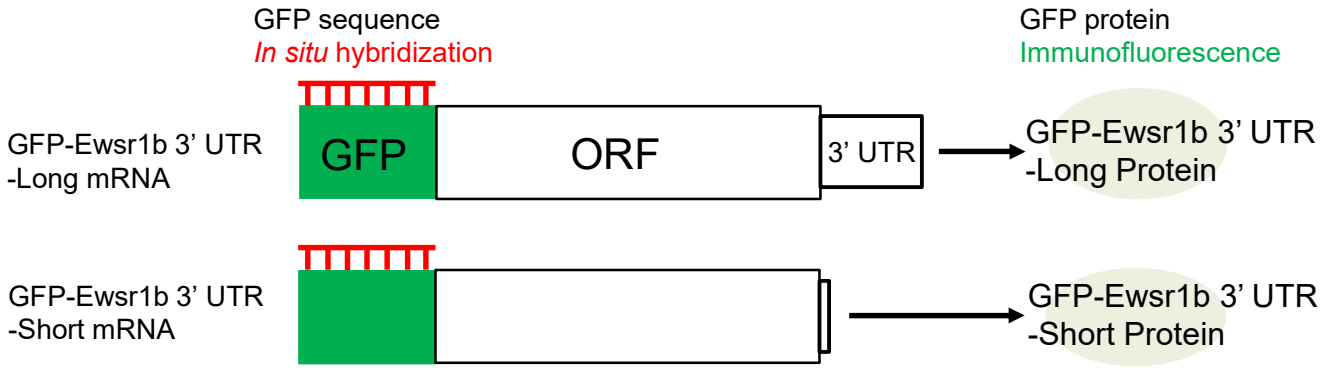
GFP sequence
In situ hybridization
GFP protein
Immunofluorescence
GFP-Ewsr1b 3' UTR
-Long mRNA
GFP
ORF
3' UTR
GFP-Ewsr1b 3' UTR
-Long Protein
GFP-Ewsr1b 3' UTR
-Short mRNA
GFP-Ewsr1b 3' UTR
-Short Protein

F

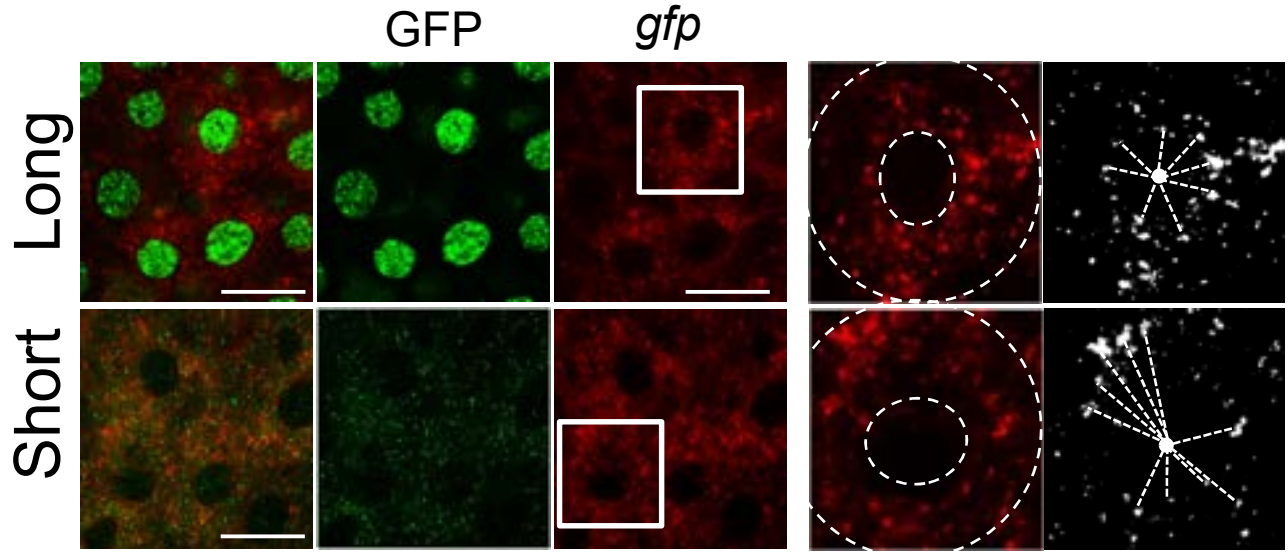
GFP
gfp
Long
Short

G

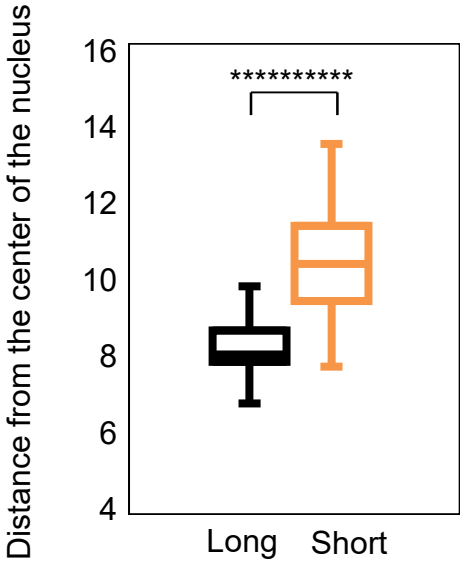
Distance from the center of the nucleus
16
14
12
10
8
6
4
****
Long
Short

Figure 18. Ewsr1b synthesized from 3' UTR-Long mRNA is important for proper protein localization in the nucleus.

(A) The 3' UTR sequences of *ewsr1b* mRNA that are targeted by Ewsr1b-3' UTR-MO (3' UTR-MO). (B) Double immunofluorescence of Ewsr1b (green) and Pou5f3 (red) in embryos not injected (-) and injected with Ewsr1b-ATG-MO (ATG-MO) and Ewsr1b-3' UTR-MO (3' UTR-MO) at 4 hpf. Bars, 20 μm. (B) Quantitative analysis of Ewsr1b and Pou5f3 in the nucleus and cytoplasm. Top: Intensities of signals of Ewsr1b and Pou5f3 in the nucleus (means ± SD; n = 18) Bottom: The number of signals of Ewsr1b and Pou5f3 in the cytoplasm per 100 μm^2 (means ± SD; n = 18). NS, not significant; *****p<0.00001; ****:p<0.0001; ***p<0.001; *p < 0.05 (Tukey-Kramer test). Similar results were obtained from two independent experiments. (D) Immunoblotting of Ewsr1b and Pou5f3 in embryos not injected (-) and injected with Ewsr1b-ATG-MO (ATG-MO) and Ewsr1b-3' UTR-MO (3' UTR-MO) at 4 hpf. Rpl11 is a loading control. (E) Quantitative analysis of immunoblotting (means ± SD; n = 3). NS, not significant; ***p<0.001; **p<0.01; *p < 0.05 (Tukey-Kramer test). Similar results were obtained from three independent experiments.

A

ewsr1b mRNA 3' UTR end

5'- AATTTTTTTTTAAATAAACTTTTCCACCTCCA -3'

3' UTR-MO 3'- AAAATTTATTTGAAAAGGTGGAGGT -5'

B

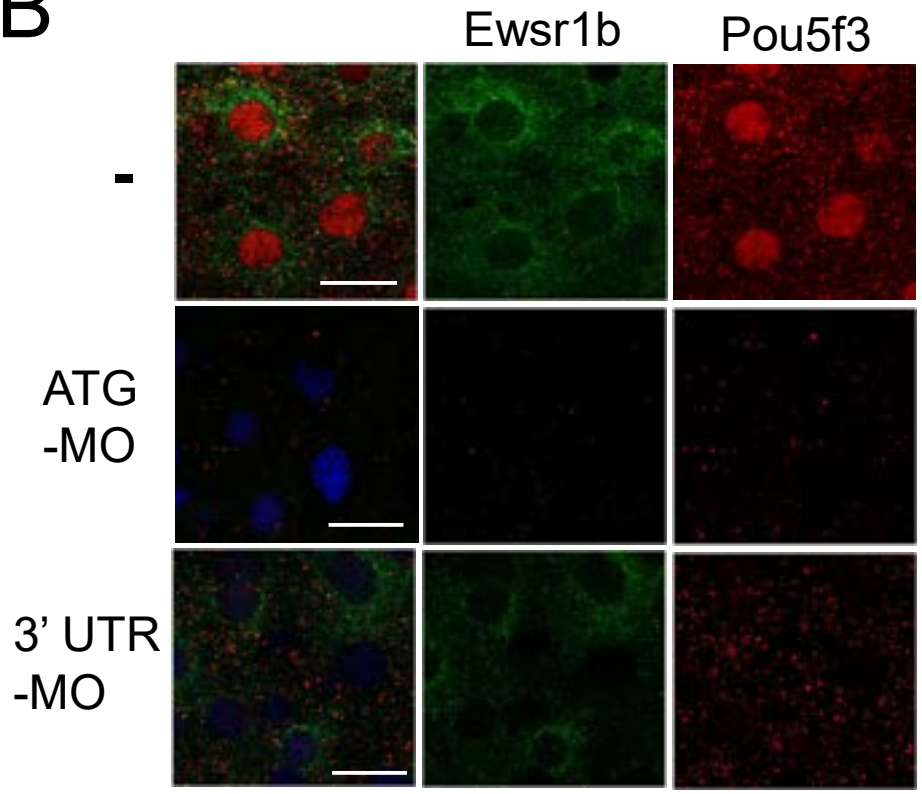

C

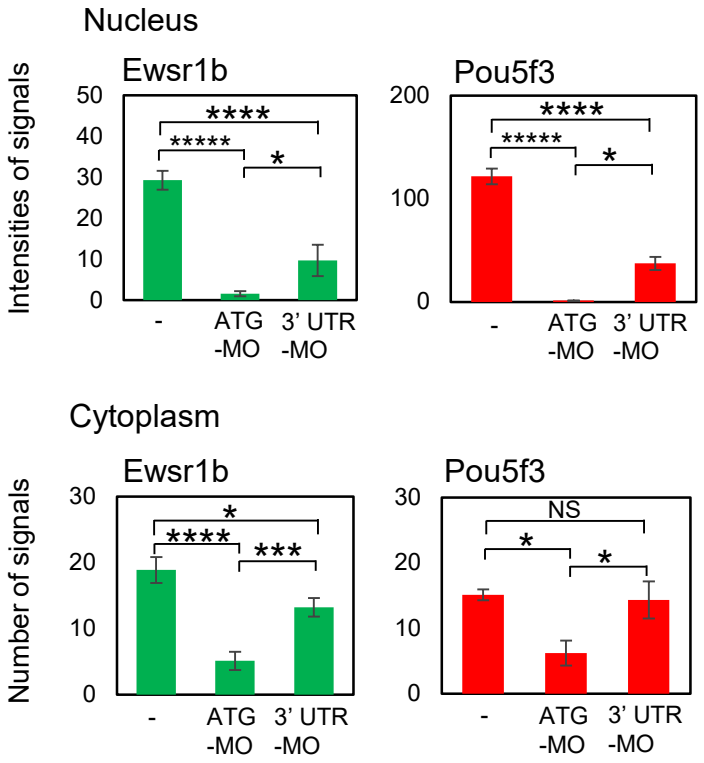

D

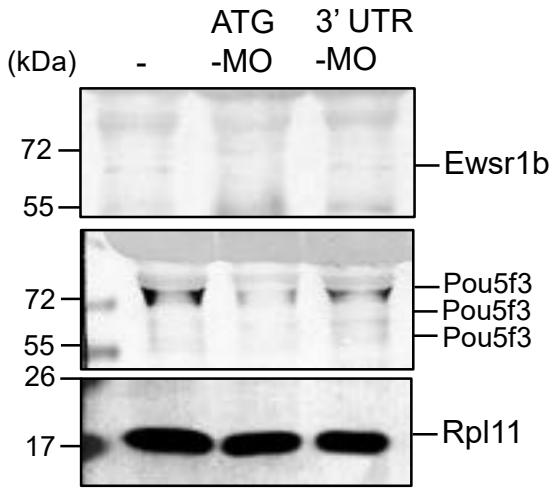
(kDa)
-
ATG
-MO
3' UTR
-MO
72
55
Ewsr1b
72
55
26
Pou5f3
Pou5f3
Pou5f3
17
Rpl11

E

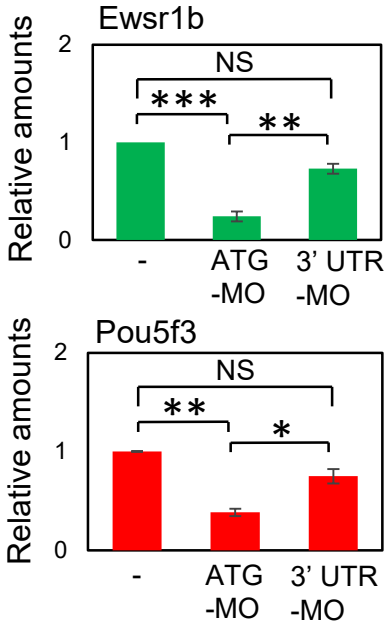
Ewsr1b
Relative amounts
2
1
0
NS
***
**
-
ATG
-MO
3' UTR
-MO
Pou5f3
Relative amounts
2
1
0
NS
**
*
-
ATG
-MO
3' UTR
-MO

Figure 19. Importin beta-1 binds to *ewsr1b* mRNA 3' UTR and transports Ewsr1b to the nucleus.
(A) Immunofluorescence of Importin beta-1 in embryos at 3 hpf. (B) Immunoblotting of embryo extracts at 3 hpf after IP with control IgG (IgG) or anti-Importin beta-1 (α-Importin beta-1) antibody and RT-PCR for *ewsr1b* mRNA and α-tubulin mRNA. Similar results were obtained from two independent experiments. (C) Double staining of *ewsr1b* mRNA 3' UTR (green) and Importin beta-1 (red) in embryos at 3 hpf. Left, high-resolution confocal image. Right, enlarged views of the boxed regions in the left image. Similar results were obtained from two independent experiments. (D) PLA of Ewsr1b and Importin beta-1 in embryos at 3 and 6 hpf . Left: Confocal image not added with Ewsr1b 1st antibody (No Ewsr1b 1st Ab) as a negative control. Medium: Confocal image in embryos at 3 hpf. Light: Confocal image in embryos at 6 hpf. Similar results were obtained from two independent experiments. Bars, 20 μm

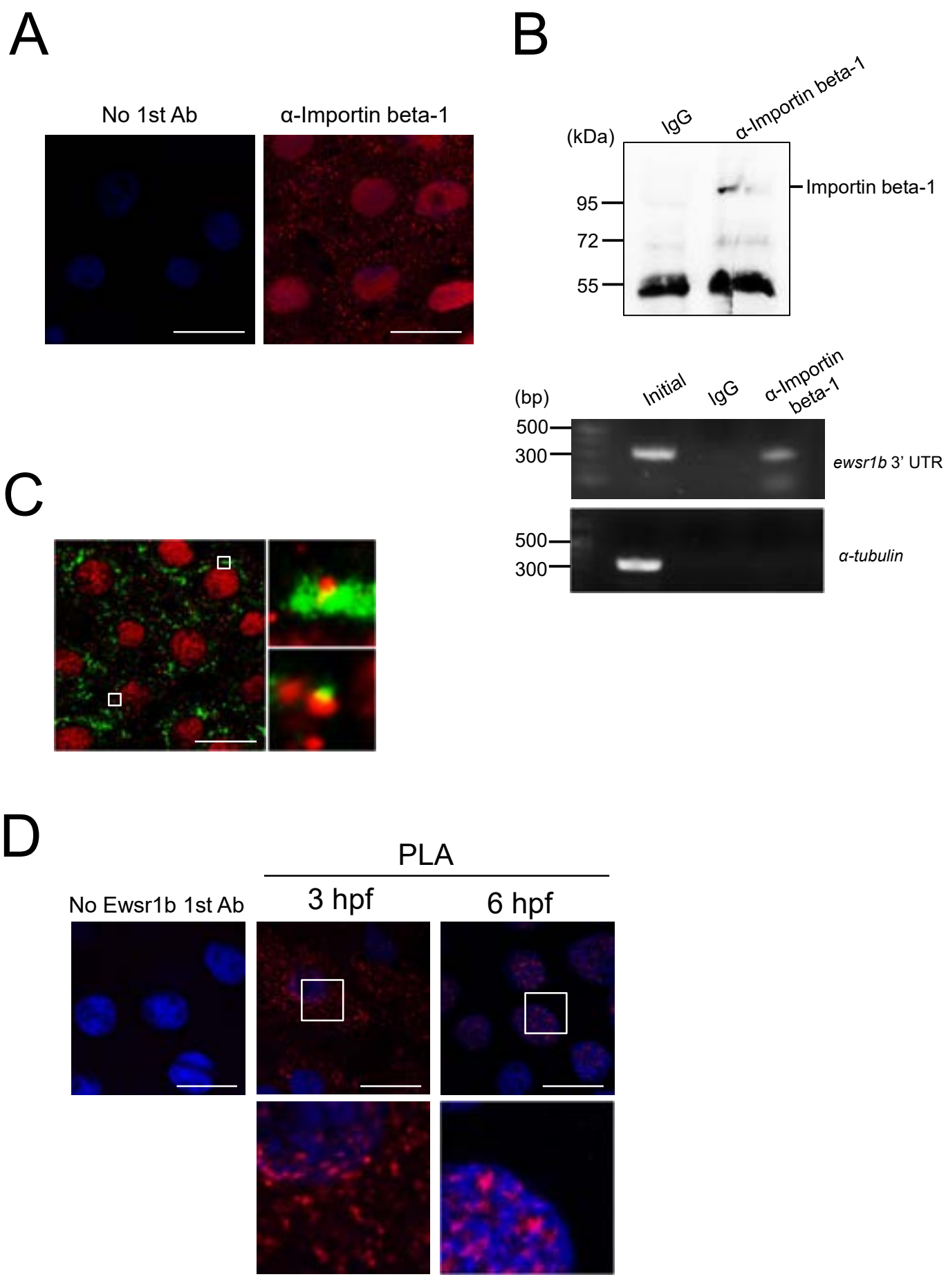
A
No 1st Ab
α-Importin beta-1
B
IgG
α-Importin beta-1
(kDa)
95
72
55
Importin beta-1
Initial
IgG
α-Importin beta-1
(bp)
500
300
ewsr1b 3' UTR
500
300
α-tubulin
C
D
PLA
No Ewsr1b 1st Ab
3 hpf
6 hpf

Figure 20. Protein degradation after fertilization is important for translational regulation.
(A) Lateral views of WT embryos and embryos injected with MG132 at 2 and 5 hpf. Bars, 300 μm. Similar results were obtained from two independent experiments. (B) Immunoblotting of Ewsr1b and Rpl11 in embryos not injected (-) and injected with DMSO or MG132 at 1 hpf. Rpl11 is a loading control. (C) Relative amounts of Ewsr1b in embryos not injected (-) and injected with DMSO or MG132 at 1 hpf (means ±SD; n=3). Similar results were obtained from three independent experiments. *$p < 0.05$; **$p<0.01$ (Tukey-Kramer test). (D) Immunofluorescence of Ewsr1b in embryos not injected (-) and injected with DMSO (DMSO) or MG132 (MG132) at 1 hpf. Bars, 20 μm. (E) PAT assay for *ewsr1b* 3' UTR-Short mRNA in embryos not injected (-) at 0 and 1 hpf and injected with DMSO (DMSO) or MG132 (MG132) at 1 hpf. Similar results were obtained from two independent experiments.

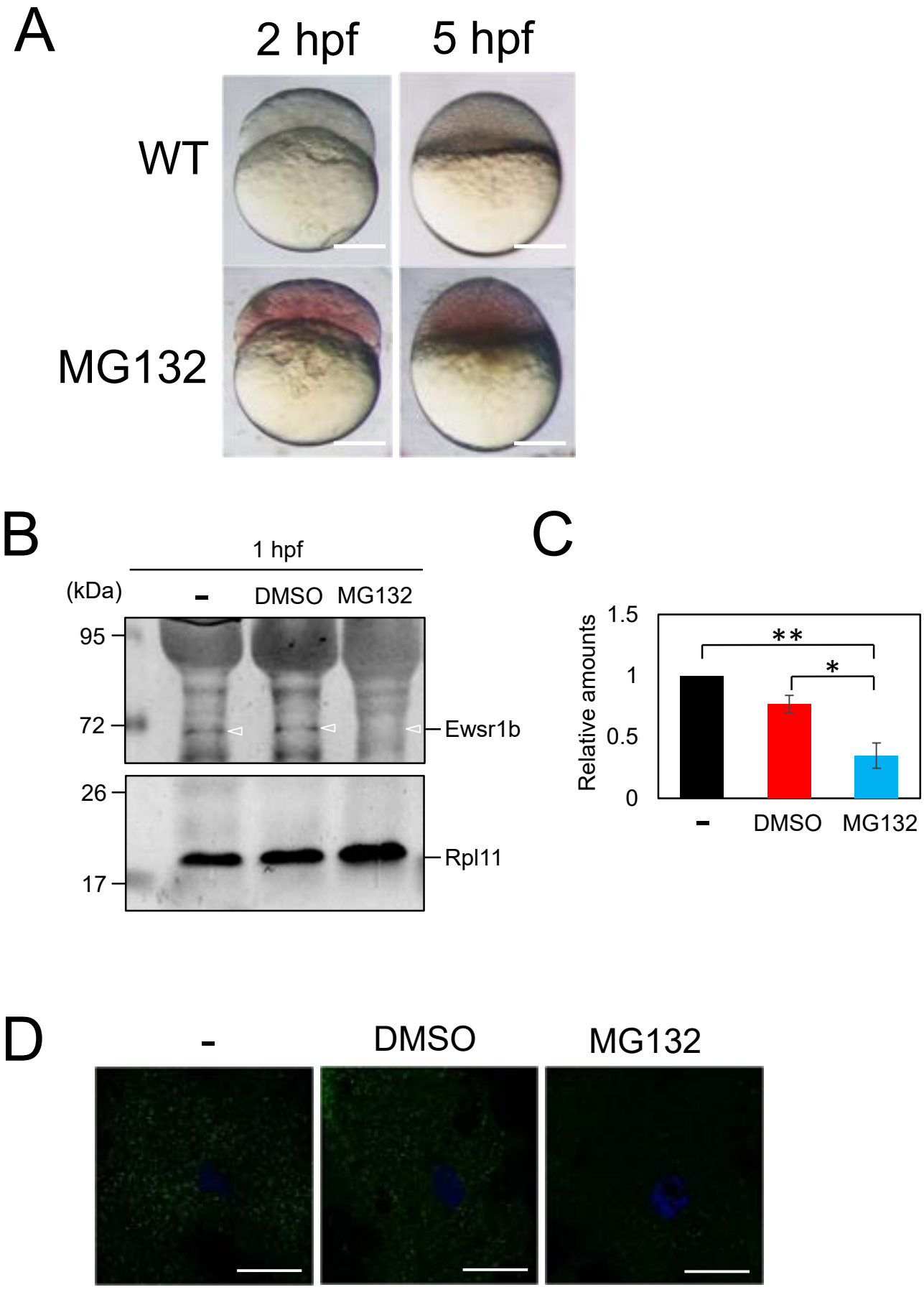
A
2 hpf
5 hpf
WT
MG132
B
1 hpf
(kDa)
-
DMSO
MG132
95
72
Ewsr1b
26
17
Rpl11
C
Relative amounts
1.5
1
0.5
0
**
*
-
DMSO
MG132
D
-
DMSO
MG132

E

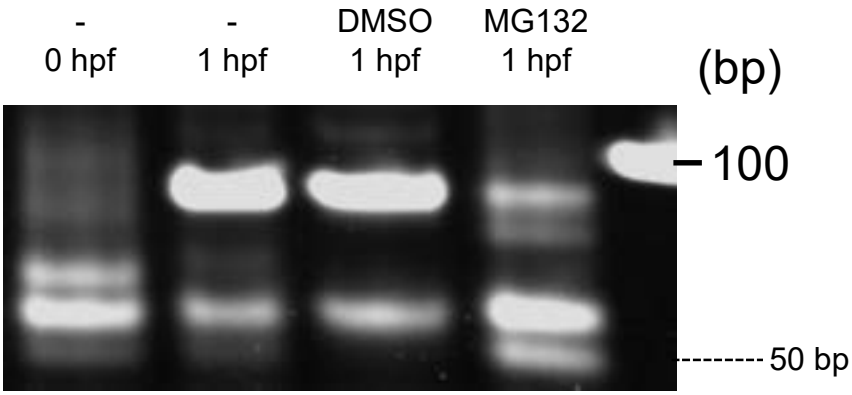

Figure 21. The state of Syncrip and Ewsr1b is different. (A) IDRs of Syncrip and Ewsr1b analyzed by IUPred3. The score > 0.5 indicates the IDR. (B) Left; distribution of GFP-Syncrip and GFP-Ewsr1b in embryos at 6 hpf. Right, time-lapse images of the boxed region in the left image showing dynamics of two protein droplets (arrows). Similar results were obtained from three independent experiments. (C) Representative images of the FRAP experiment from pre-bleach to 3 seconds of post-bleach conducted in GFP-Syncrip and GFP-Ewsr1b. Similar results were obtained from three independent experiments. (D) Fluorescence recovery curves in GFP-Syncrip (n=3) and GFP-Ewsr1b (means ± SD; n = 3). Similar results were obtained from three independent experiments. Bars, 10 μm.

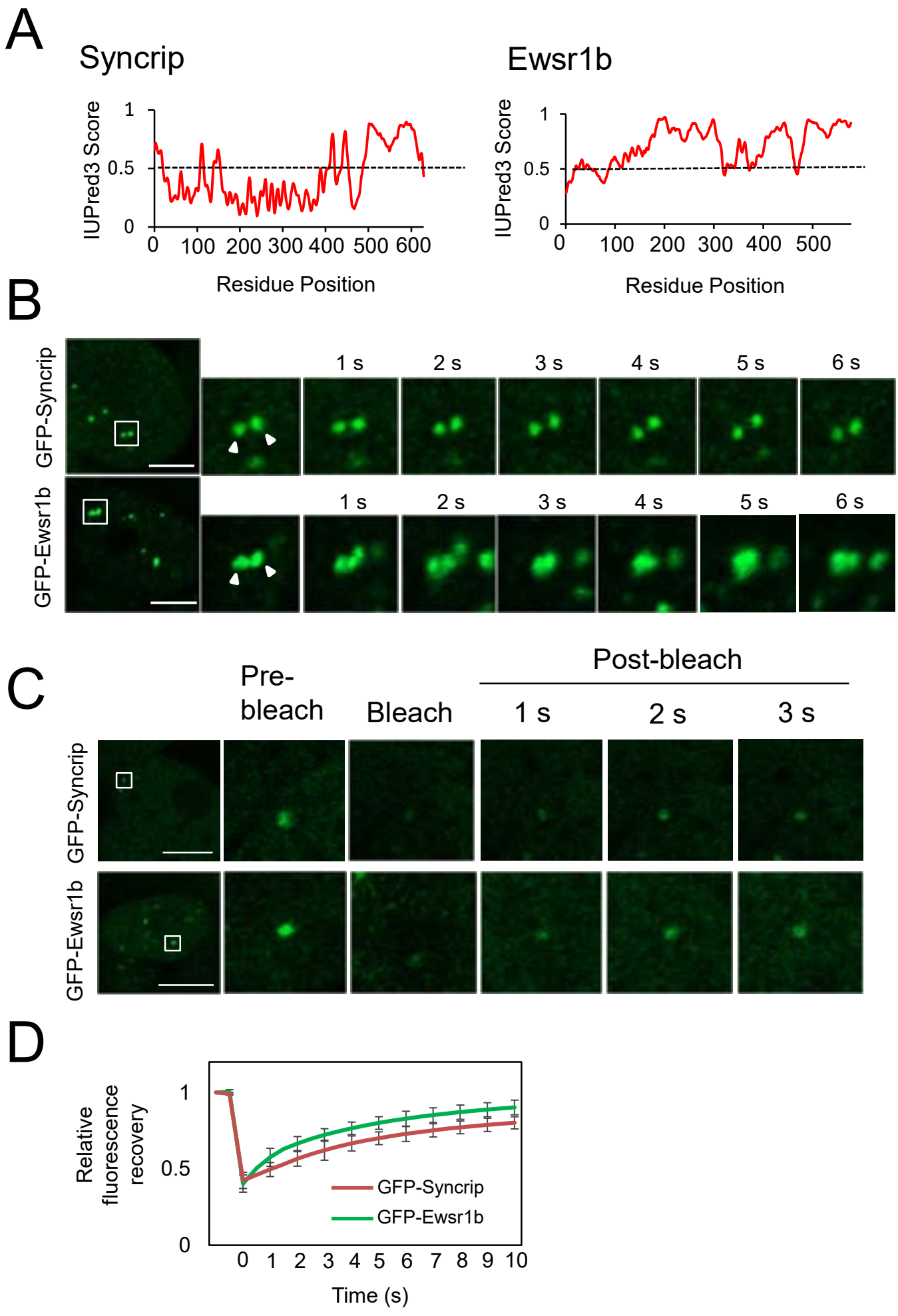
A
Syncrip
IUPred3 Score
1
0.5
0
0 100 200 300 400 500 600
Residue Position
Ewsr1b
IUPred3 Score
1
0.5
0
0 100 200 300 400 500
Residue Position
B
GFP-Syncrip
1 s
2 s
3 s
4 s
5 s
6 s
GFP-Ewsr1b
1 s
2 s
3 s
4 s
5 s
6 s
C
Pre-bleach
Bleach
Post-bleach
1 s
2 s
3 s
GFP-Syncrip
GFP-Ewsr1b
D
Relative fluorescence recovery
1
0.5
0
GFP-Syncrip
GFP-Ewsr1b
0 1 2 3 4 5 6 7 8 9 10
Time (s)

Figure 22. Schematic diagrams of summaries in this study.

pou5f3 mRNA forms granular structures and its translation is activated while maintaining RNA granules. The state of RNA granules changes from solid-like to liquid-like when translation is activated. Syncrip is involved in translational repression and Ewsr1b is involved in translational activation of *pou5f3* mRNA. Translational control that depends on the length of 3' UTR regulates synthesized protein localization and function.

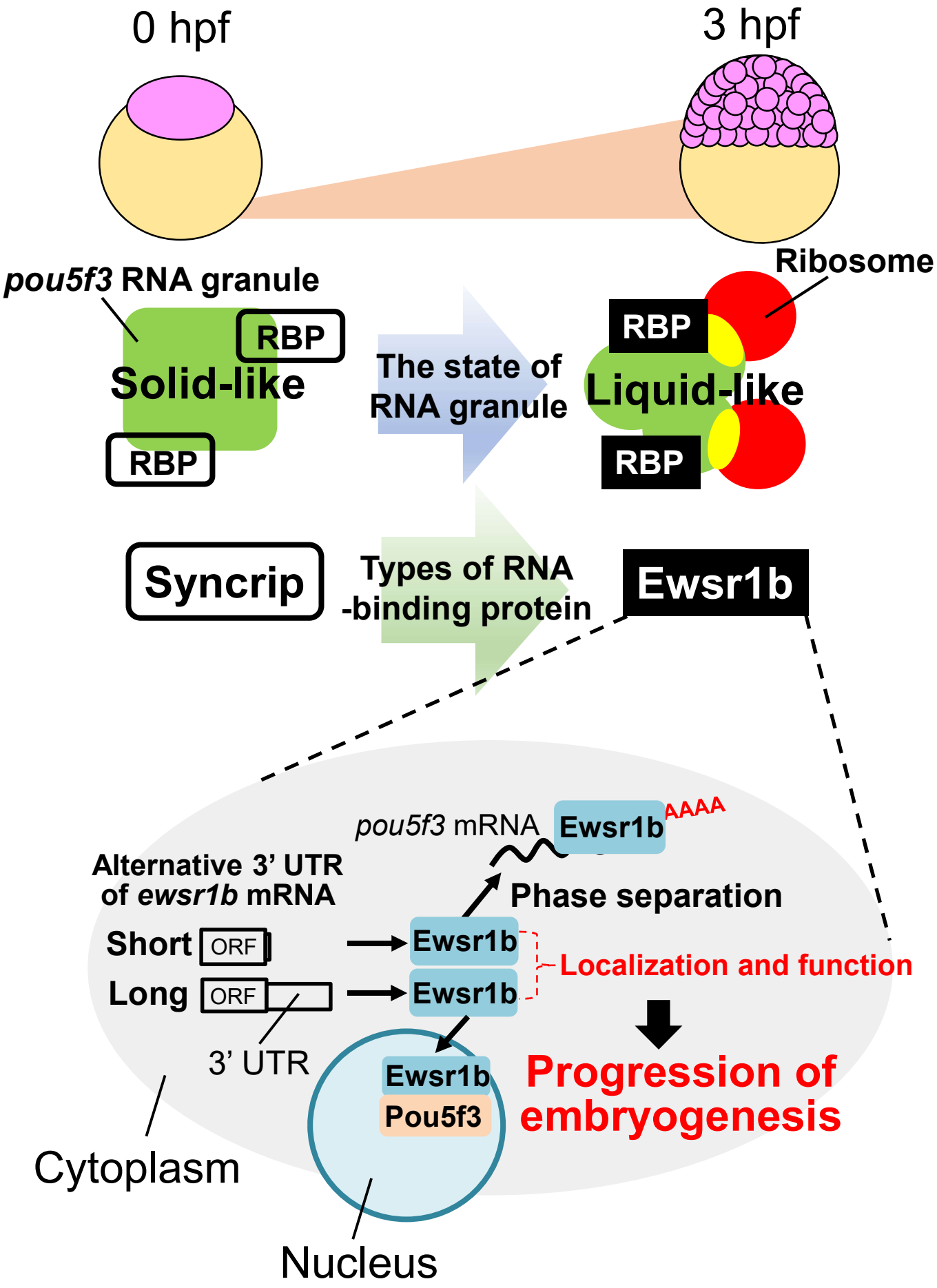
0 hpf
3 hpf
pou5f3 RNA granule
RBP
Solid-like
RBP
The state of
RNA granule
Ribosome
RBP
Liquid-like
RBP
Syncrip
Types of RNA
-binding protein
Ewsr1b
pou5f3 mRNA
Ewsr1b
AAAA
Alternative 3' UTR
of ewsr1b mRNA
Phase separation
Short
ORF
Long
ORF
Ewsr1b
Ewsr1b
Localization and function
3' UTR
Ewsr1b
Pou5f3
Progression of
embryogenesis
Cytoplasm
Nucleus